Titre: Title:	Steel fibers reinforced carbon bonded alumina-magnesia castables
Auteur: Author:	Balamurugan Kumarasami
Date:	2005
Type:	Mémoire ou thèse / Dissertation or Thesis
Référence: Citation:	Kumarasami, B. (2005). Steel fibers reinforced carbon bonded alumina-magnesia castables [Master's thesis, École Polytechnique de Montréal]. PolyPublie. https://publications.polymtl.ca/7400/

UNIVERSITÉ DE MONTRÉAL

STEEL FIBERS REINFORCED CARBON BONDED ALUMINA-MAGNESIA CASTABLES

KUMARASAMI BALAMURUGAN

PROGRAMME DE GÉNIE MÉTALLURGIQUE

ÉCOLE POLYTECHNIQUE DE MONTRÉAL

MÉMOIRE PRÉSENTÉ EN VUE DE L'OBTENTION D'UN DIPLÔME DE

MAîTRISE ÈS SCIENCES APPLIQUÉES (M.Sc.A)

(GÉNIE MÉTALLURGIQUE)

AVRIL 2005

Your file Votre référence
ISBN: 0-494-01346-X
Our file Notre référence
ISBN: 0-494-01346-X

UNIVERSITÉ DE MONTRÉAL

ÉCOLE POLYTECHNIQUE DE MONTRÉAL

Ce mémoire intitulé

STEEL FIBERS REINFORCED CARBON BONDED ALUMINA-MAGNESIA CASTABLES

présenté par : KUMARASAMI Balamurugan

en vue d'obtention du diplôme de : Maîtrise ès Sciences Appliquées

a été dûment accepté par le jury d'examen constitué de :

M. SAVADOGO, Oumarou, directeur d'état, président

M. RIGAUD, Michel, D.Sc.A., membre et directeur de recherche

M. TURENNE, Sylvain, Ph.D., membre

ACKNOWLEDGMENTS

First of all, I am greatly indebted to my supervisor Prof. Michel Rigaud for his guidance and parental care throughout this work, especially at the finishing stage. He has been a constant source of encouragement and support during the entire programme of study. Whatever I learned from him will definitely help me through out my future-professional career and in that aspect I am truly grateful to him. I dedicate this thesis to him.

I extend my heartiest thanks to my friend Dr. K. Sankaranaraynanae (Research Associate, CIREP) for his encouragement, suggestions, help and support during the complete period of my research work.

I express thankful to Dr. Stefan Palco, Dr. E. Divry, Dr. E. Paransky, Dr. R. Pelletier, and Dr. Huiqing He for their help, valuable assistance and suggestions.

Words are indeed insufficient to express my heartful gratitude to my friends Dr. Xianxin Zhou, Mr. P. A. Anctil and Mr. Hashami for their constant support during the last tenure of my work.

I would also thank Mrs. Theresa Crisson and Ariagnee Miro for their secretarial help and assistance.

RÉSUMÉ

La présente étude a été effectuée en considérant la simplicité d'installation et les coûts avantageux, résultant de la substitution des briques de magnesie-carbone par des bétons réfractaires contenant du carbone, dans les poches de coulée d'aciers, à la zone de laitier. Le remplacement des briques par des bétons requiert que ces bétons carbonés possèdent des propriétés thermo-chimiques et thermo-mécaniques au mois équivalentes. Le projet se situe donc dans le prolongement des travaux entrepris au CIREP sur l'évaluation de ces matériaux en terme de résistance à la corrosion, à l'oxydation et aux contraintes thermiques et mécaniques. Ce projet porte plus particulièrement sur l'amélioration des propriétés thermomécaniques, et notamment l'augmentation de l'énergie de rupture des bétons carbonés à températures intermediares (800 à 1100°C). Pour ce faire l'effet du renforcement par des fibres d'acier sera dûment évalué, et ceci constitue l'objet principal de ce mémoire.

Dans ce travail les efforts ont été concentrés sur des bétons d'alumine-magnésie-carbone. Le carbone, sous forme de graphite a été incorporé sous forme de microboulettes extrudées selon la technique mise au point au CIREP. Les bétons contenaient comme composition de base 6% poids de microboulettes de graphite, 6% poids de fines de magnésie, 4% poids de ciment alumineux à 70% poids d'alumine fondue en grains de différentes tailles. Deux types de fibres métalliques ont été testés : en acier au carbone et en acier inoxydable, avec 3 catégories de longueur : 19, 25 et

50mm, à des niveaux variables en poids : 0, 2, 4 et 6% poids – Au total 24 compositions différentes.

Les mesures rhéologiques ont été effectuées pour évaluer l'ouvrabilité de ces bétons avec fibres. Par la suite des échantillons ont été coulés, séchés puis cuits sous atmosphère réductrice et recouvert de coke pour éviter l'oxydation, puis caractérisés à différentes températures –

Les échantillons de bétons cuits ont été évalués selon la méthode de l'essai-coin, sous argon, à température ambiante et à 1100°C. Les courbes d'effort-deformation obtenues ont permis de calculer l'énergie de rupture, le module d'élasticité et la ténacité des bétons-renforcés ou non. D'autres échantillons de bétons carbonés ont été testés de la même façon mais cette fois non cuits, seulement séchés et ce pour des fins de comparaison. La porosité apparente, la densité et le changement linéaire permanent (PLC) sur tous échantillons, après séchage et après cuisson ont été mesurés. La résistance mécanique en flexion de plusieurs bétons carbonés renforcés a aussi été mesurée sous argon à 800 et à 1100°C.

Finalement des observations sous microscopie optique et sous microscopie à balayage ont été faites pour mieux interpréter les résultats.

À la suite de tous ces travaux, les principaux points à retenir seront maintenant énumérés.

L'addition des fibres d'acier a pour effet de décroître la coulabilité des bétons. Cette décroissance est directement fonction de la quantité de fibres utilisée et aussi de leur longueur.

L'addition de fibres d'acier (au carbone ou inoxydable) influence drastiquement les propriétés rheologiques des bétons, mais le comportement général demeure le même que celui du béton sans fibre. Au total tous ces bétons se comportent comme des fluides Bingham, sans être dilatant, même pour les bétons contenant jusqu'à 4% poids de fibres, quelque soit la longueur (19, 25 ou 50mm) et jusqu'à 6% poids pour les longueurs de 19 et 25mm.

Il a été possible de déterminer les conditions optimales de pompage pour la plupart des bétons carbonés avec fibres, en termes de seuil d'écoulement et viscosité.

Quant aux considérations portant sur les caractéristiques thermomécaniques, il faudra retenir les points suivants :

- L'énergie de rupture des bétons AMC avec fibre, est plus élevée que l'énergie de rupture du même béton sans fibre. Ceci représente aussi un avantage pour la résistance aux chocs thermiques–

- L'ajout de fibres d'acier inoxydable ne s'est pas avéré avantageux par rapport à l'ajout de fibres d'acier ordinaire.
- La déformation des fibres lors du mélange cause une variabilité dans les résultats qui croit avec la longueur et la quantité de fibres utilisées.
- La quantité optimale de fibres à utiliser se limite à 2% poids, avec préférablement des fibres de 19mm de long. Il est toutefois possible de produire des bétons AMC avec 6% poids de fibres, ayant une longueur de 50 mm.
- Après cuisson, il est clair que l'effet bénéfique des fibres est moindre lorsqu'on utilise 6 et même 4% poids de fibres.
- Les valeurs de modules de rupture à chaud sont grandement influencées par la température et la dégradation des fibres à 800 et à 1100°C.
- Les valeurs calculées des modules d'élasticité sont, pour tous les bétons avec fibres, les mêmes, indépendamment de leur longueur, de leur quantité ou de leur nature (inoxydable ou non), mais sont fonction de l'histoire thermique des échantillons. Ces valeurs décroissent grandement lorsque les échantillons ont été portés à hautes températures.
- Les valeurs calculées de K_{IC} sont fonction de l'endommagement des bétons, qui croît avec la dégradation des fibres. L'ampleur est fonction de la quantité de fibres utilisée. Ceci est substancié par des observations micrographiques, qui illustrent l'importance des microfissures et des décohésions fibres-matrice.

Au total, suite à ce travail de type expérimental il est possible d'avancer que oui, l'objectif d'augmenter la résistance à la propagation des fissures de bétons carbonés, de type AMC, peut être atteint. Il faut toutefois admettre que de porter les échantillons jusqu'à 1100°C est néfaste, car la stabilité des fibres à cette température est insuffisante, même si elles sont incorporées dans des bétons carbonés, qui a priori devraient maintenir des conditions réductrices, de façon plus marqué, dans l'intérieur des échantillons -

ABSTRACT

The current investigation has been carried out considering the simplicity in placement and cost benefits of replacing MgO-C brick by carbon containing castables in slag line of steel ladles. The replacement of brick by castables demands the similar or even superior properties for carbon based castables than existing MgO-C bricks in terms of corrosion, penetration and oxidation resistance with excellent thermo mechanical properties. This work is a continuation of CIREP's long time project on carbon containing castables and the evaluation of such material for corrosion, oxidation and other properties have been successfully completed with positive conclusions. The improvement of thermo-mechanical properties, especially the work of fracture is another area to be filled out with the present investigation. Reinforcing castables with steel fibres for intermediate temperature application is one of the viable solutions to improve the thermo-mechanical properties and is the core objective for the present work.

Alumina-Magnesia-Carbon based self-flow castable system has been chosen for this work. The dispersibility problem due to introduction of carbon has been overcome by the pelletizing them through extrusion process (CIREP's original development) and introducing them into castables. The improvement of penetration resistance due to in-situ spinel formation is exploited by choosing proper composition containing MgO in the fine matrix. The chosen castables contains 6 wt% extruded graphite pellets, 6 wt% fine magnesia, 4 wt% 70 % alumina cement, 6.5 wt% calcined alumina, 6 wt%

reactive alumina and the remaining being coarse white fused alumina with various size distribution. In this basic composition, two different steel fibres namely carbon and stainless steel fibres are added in different amount (0, 2, 4, 6 wt %) and length (19, 25, 50 mm).

Rheological measurements on fibre containing castables are made using a rheometer with different type, amount and length of fibres to verify their suitability for placement even with fibre content. Samples of required dimensions have been cast and pre-fired in reducing atmosphere (coke covered) to avoid oxidation of carbon in the structure, the tested at different temperatures.

The pre-fired samples are evaluated for force-displacement behaviour in inert atmosphere (Argon) using wedge splitting technique at room temperature as well as at 1100°C, which gives the way to calculate work of fracture, modulus of elasticity and fracture toughness of the castables at the test temperature. The wedge splitting tests on unfired - dried samples are also carried out for evaluation and comparison purposes. Apparent porosity, bulk density and permanent linear change measurements are made on dried, fired and tested samples at room and high temperatures. The hot strength of pre-fired castables are also measured in argon atmosphere at 800 and 1100°C with different type, length and amount of steel fibres. Optical and SEM analysis are also made on samples to understand the fracture surface, interface structure and chemistry. With this work, the following points are emphasized:

The addition of steel fibre decreases self-flowability in general. The magnitude of flow reduction has been enhanced with increasing either amount or length of fibre. The fibres acts as needle shaped lengthy grain and impeding the flow of castable.
The addition of fibres drastically influence of rheology of castables. Still, the castables with fibre addition behaves in a similar way as that of base castable rheologically. This means castables with or with out fibre addition behaves as Bingham fluid and dilatancy is not observed even with 6 wt% of 19 and 25 mm and up to 4 wt% of 50 mm fibres.

With this result, it is emphasized that the castable is pumpable with 2 wt% of fibre of either 19 or 25 mm length. Addition of 50 mm fibre is deleterious in all respects and the flow decay is enhanced.

The pumping box plot using calculated values of rheological constants, flow resistance (G) and torque viscosity (H) prescribe the domain for composition selection for better pumpability.

After considering rheology and suitability of castable for placement the most important judgements are made with respect to the performance of castables through various tests at room as well as at high temperature:

- The work of fracture, which is the prime factor that quantifies the sustainability of castable under given thermo mechanical conditions, has shown definite

improvement with fibre addition at high temperature. This improvement is going to definitely improve the thermal shock resistance of castables under the imposed thermal strain.

- An important point to be noted is that the castables containing SS406 does not show any improvement when compared with carbon steel fibres at high temperature.

- Bending effect of fibres during mixing stage results in scattering of work of fracture values with respect to amount and length.

- Although the maximum value for work of fracture is observed with 50 mm length of Alumina-Magnesia-carbon (AMC) at 6 wt %, considering the flowability and bending effects, fibre length of 19 mm seems to be optimum at a level of 2 wt %.

- After firing, when the amount is increased to 4 or 6 wt %, the influence of fibre reinforcing effect is dissipated due to fibre degradation and interfacial characteristics.

- HMOR values are influenced by the fibre addition and are showing a decline trend with temperature.

- The MOE seems not to be affected by fibre length, type and amount in this investigation at room temperature. The decreases in MOE at 1100°C compared to room temperature (RT-after drying at 110°C) values are due to structural changes during firing.

- The calculated values of K_{IC} are decreasing with fibre addition indicating the degradation of the structure with enhanced crack dimensions with increased fibre additions. This is substantiated by SEM observations.

At the end of this, it can be advanced that the prime objective of improving the thermo-mechanical property or the thermal shock resistance of AMC castable can be achieved as the work of fracture is being increased with fibre additions. However, the lesser improvement of work fracture observed at 1100°C, as compared to room temperature is attributed to micro structural changes at the interface of fibre-matrix as well as in the matrix itself.

CONDENSÉ EN FRANÇAIS

Ce travail se situe dans la ligne des travaux qui ont été entrepris au CIREP depuis au delà de six ans.

En effet depuis ce temps plusieurs thèses ont été présentées sur la mise au point de bétons réfractaires basiques, contenant du carbone, dans le but de satisfaire les exigences des sidérurgistes, et de leur permettre de garnir des poches de coulée d'acier avec des revêtements, à cent pour cent, monolithiques. C'est un défi qui est toujours à relever, au moins en Amérique du Nord, depuis plus de quinze ans.

A ce point-ci, il est courant d'utiliser des bétons d'alumine-magnésie et alumine-spinelle-magnésie dans les parois de ces poches de coulée, mais cette solution n'est pas satisfaisante, dans la partie supérieure, à la ligne de laitier. Pour cette zone dite de la ligne de laitier il est convenu d'utiliser des briques de magnésie-carbone.

Le défi se ramène donc à développer des bétons qui soient aussi performants que ces briques, pour résister tant à la corrosion chimique des laitiers qu'à l'écaillement par chocs thermiques.

Au CIREP des développements ont été effectués dans deux lignes distinctes : d'une part en concevant des mélanges avec une prépondérance de magnésie et d'autre part

des mélanges avec une prépondérance d'alumine mais en utilisant des proportions variables de spinelle synthétique et de magnésie fine pour produire du spinelle dit in-situ. Dans tous les cas ces travaux ont été justifies car depuis plus de huit déjà on maîtrise, au CIREP, l'addition de graphite dans les bétons.

Le plan de ce travail a donc été conçu à partir des derniers résultats d'essais industriels qui ont été effectués à l'acierie de Dofasco, Hamilton, Ontario, sur des mélanges d'alumine-magnésie-graphite. En effet les résultats se sont avérés positifs quant à la résistance à la corrosion de ces bétons, mais insuffisants par rapport à la résistance mécanique, à températures intermédiaires. Il est apparu que la résistance à l'écaillage, à la face froide, entre 800 et 1100 °C, était à améliorer. Ce travail consistera donc à évaluer une nouvelle possibilité, celle d'introduire des fibres courtes, dans ces bétons, en vue d'améliorer leur résistance à la propagation des fissures, dans cette gamme de températures.

Le présent mémoire porte uniquement sur les résultats obtenus en utilisant des fibres métalliques. Pour les besoins de la cause deux types de fibres courtes, mais ondulées ont été utilisés, des fibres en acier au carbone 1020 et des fibres en acier inoxydable 406. Le but était de déterminer si la différence de résistance à l'oxydation, entre ces deux acieres, pourrait se solder par un effet notable sur le comportement des bétons, lorsque portés à la température de 1100 °C. Pour détecter un tel effet il a été décidé de mener des mesures de ténacité et de module de rupture à chaud, à 1100 °C. La méthode

expérimentale pour mesurer la ténacité a été celle, mise au point récemment au CIREP, dite de l'essai coin- (wedge-splitting test). Cette méthode permet de déterminer des courbes d'effort-déformation, à partir d'échantillon massif (100 x 100 x 75 mm), pré-entaillé. La géométrie de ces échantillons a été étudiée afin de permettre la propagation stable d'une fissure principale, qui bien sûr bifurquera en se propageant, d'autant plus qu'il y aura insertion d'obstacles (d'où l'idée d'introduire des fibres).

Pour la mesure des modules de rupture à chaud, la méthode standard d'essais de flexion, en trois points, a été mise en œuvre. Si le but central de ce mémoire était d'évaluer la pertinence d'utiliser des fibres courtes pour améliorer les propriétés thermomécaniques des bétons réfractaires alumine-magnésie-graphite, il a été jugé pertinent de bien établir au préalable, l'incidence des fibres sur le comportement rhéologique des bétons, lors de leur élaboration.

Ce mémoire a donc été cédé en deux parties, d'abord l'étude des conditions de mélange des bétons puis l'étude des propriétés thermomécaniques. Pour l'étude du comportement rhéologique, les travaux ont également été menés en tenant compte des acquis récents du CIREP, notamment en se fixant l'objectif de mesurer le diagramme de pompabilité de ces bétons, défini par deux paramètres, leur viscosité dynamique (H) et leur limite d'écoulement (G).

Pour ce genre de travail il a été convenu d'utiliser un rhéomètre permettant de conserver les mêmes proportions d'agrogats et de matrice, que dans les bétons utilisés

pour les essais mécaniques. En effet, il est indéniable que les caractéristiques initiales de coulabilité des bétons jouent un rôle déterminant sur les propriétés mécaniques qui se développent ultérieurement dans les bétons, lorsque mis en températures.

C'est donc dans un tel contexte que ce mémoire a été entrepris à compter du mois de janvier 2004. La composition de base des bétons a été limitée à des mélanges contenant environ 80 % poids d'alumine fondue, avec une distribution gramilométrique fixe, définie par un coefficient d'Andreasen de 0.28. Outre l'alumine, ces bétons contenaient 4 % poids de ciment alumineux (CA 25 d'Alcoa), 6 % poids de fines de magnésie (magnésie de la Mer Morte) 6 % poids de microboulettes extrudées de graphite (recette CIREP) et les adjurants nécessaires pour obtenir une coulabilité convenable pour un béton dit auto-coulant. Cette composition a été choisie dans la lignée des travaux antérieurs menés au CIREP.

Pour les fibres métalliques, il a été décidé de faire varier la longueur des fibres 19, 25 et 50 mm, à des niveaux variables en poids : 0, 2, 4 et 6 % ou 0, 1, 2, 3% en volume. Dans l'ensemble de ce mémoire 24 compositions différentes ont été testées en suivant le plan expérimental, représenté sur la page suivante.

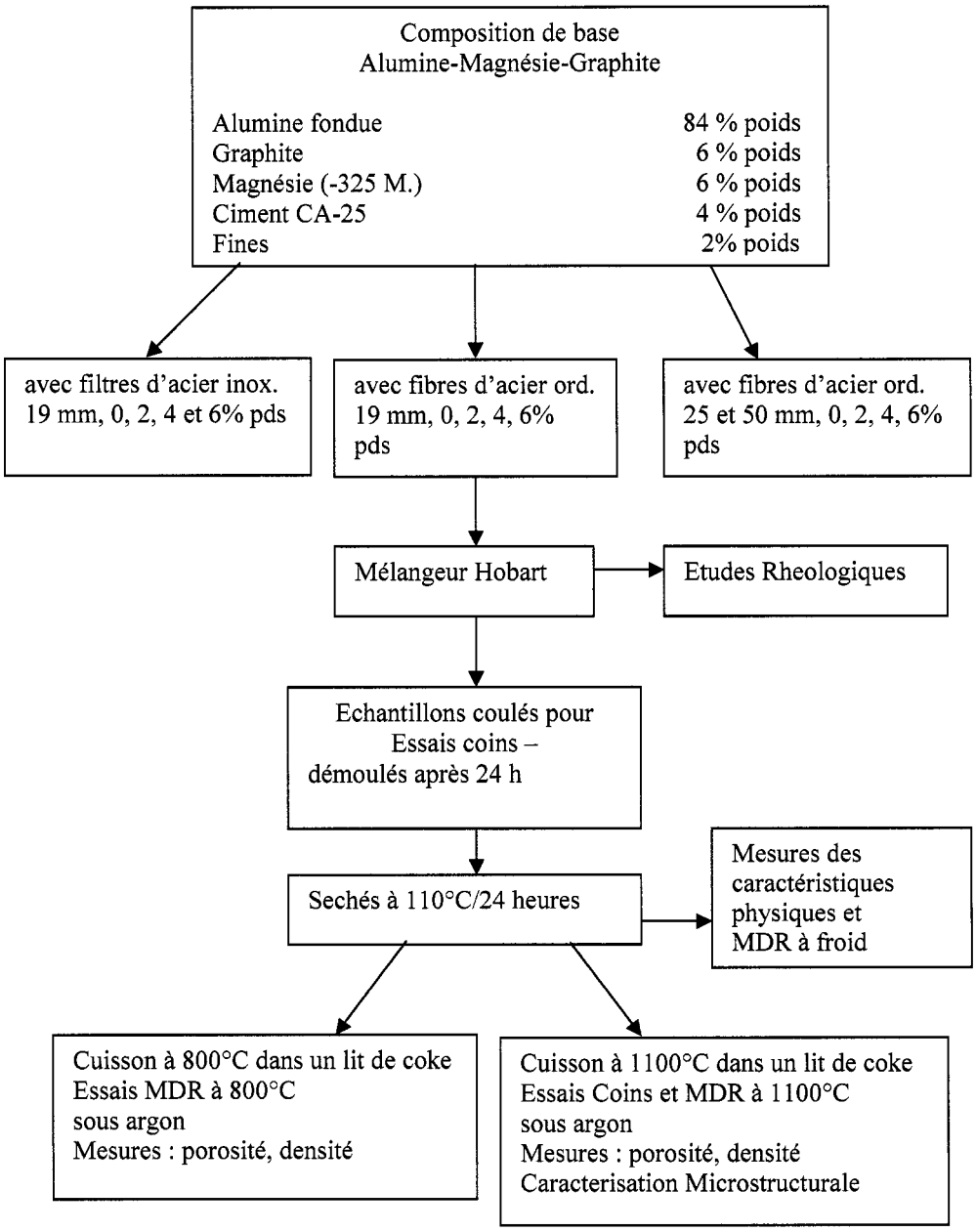
Composition de base
Alumine-Magnésie-Graphite
Alumine fondue 84 % poids
Graphite 6 % poids
Magnésie (-325 M.) 6 % poids
Ciment CA-25 4 % poids
Fines 2% poids
avec filtres d'acier inox. 19 mm, 0, 2, 4 et 6% pds
avec fibres d'acier ord. 19 mm, 0, 2, 4, 6% pds
avec fibres d'acier ord. 25 et 50 mm, 0, 2, 4, 6% pds
Mélangeur Hobart
Etudes Rheologiques
Echantillons coulés pour Essais coins – démoulés après 24 h
Sechés à 110°C/24 heures
Mesures des caractéristiques physiques et MDR à froid
Cuisson à 800°C dans un lit de coke
Essais MDR à 800°C
sous argon
Mesures : porosité, densité
Cuisson à 1100°C dans un lit de coke
Essais Coins et MDR à 1100°C
sous argon
Mesures : porosité, densité
Caracterisation Microstructurale

A la suite de ces travaux, les principaux points à retenir sont :

L'addition des fibres d'acier a pour effet de décroître la coulabilité des bétons. Cette décroissance est directement fonction de la quantité de fibres utilisée et aussi de leur longueur.

L'addition de fibres d'acier (au carbone ou inoxydable) influence drastiquement les propriétés rheologiques des bétons, mais le comportement général demeure le même que celui du béton sans fibre. Au total tous ces bétons se comportent comme des fluides Bingham, sans être dilatant, même pour les bétons contenant jusqu'à 4% poids de fibres, quelque soit la longueur (19, 25 ou 50mm) et jusqu'à 6% poids pour les longueurs de 19 et 25mm.

Il a été possible de déterminer les conditions optimales de pompage pour la plupart des bétons carbonés avec fibres, en termes de seuil d'écoulement et viscosité.

Quant aux considérations portant sur les caractéristiques thermomécaniques, il faudra retenir les points suivants :

- L'énergie de rupture des bétons AMC avec fibre, est plus élevée que l'énergie de rupture du même béton sans fibre. Ceci représente aussi un avantage pour la résistance aux chocs thermiques–

- L'ajout de fibres d'acier inoxydable ne s'est pas avéré avantageux par rapport à l'ajout de fibres d'acier ordinaire.

- La déformation des fibres lors du mélange cause une variabilité dans les résultats qui croit avec la longueur et la quantité de fibres utilisées.

- La quantité optimale de fibres à utiliser se limite à 2% poids, avec préférablement des fibres de 19mm de long. Il est toutefois possible de produire des bétons AMC avec 6% poids de fibres, ayant une longueur de 50 mm.

- Après cuisson, il est clair que l'effet bénéfique des fibres est moindre lorsqu'on utilise 6 et même 4% poids de fibres.

- Les valeurs de modules de rupture à chaud sont grandement influencées par la température et la dégradation des fibres à 800 et à 1100°C.

- Les valeurs calculées des modules d'élasticité sont, pour tous les bétons avec fibres, les mêmes, indépendamment de leur longueur, de leur quantité ou de leur nature (inoxydable ou non), mais sont fonction de l'histoire thermique des échantillons. Ces valeurs décroissent

grandement lorsque les échantillons ont été portés à hautes températures.

- Les valeurs calculées de K_{IC} sont fonction de l'endommagement des bétons, qui croît avec la dégradation des fibres. L'ampleur est fonction de la quantité de fibres utilisée. Ceci est substancié par des observations micrographiques, qui illustrent l'importance des microfissures et des décohésions fibres-matrice.

Au total, suite à ce travail de type expérimental il est possible d'avancer que oui, l'objectif d'augmenter la résistance à la propagation des fissures de bétons carbonés, de type AMC, peut être atteint. Il faut toutefois admettre que de porter les échantillons jusqu'à 1100°C est néfaste, car la stabilité des fibres à cette température est insuffisante, même si elles sont incorporées dans des bétons carbonés, qui a priori devraient maintenir des conditions réductrices, de façon plus marqué, dans l'intérieur des échantillons –

Ce mémoire a donc servi à faire progresser les connaissances accumulées au CIREP. Une partie de ces résultats seront présentés à la Conference des Métallurgistes, à Calgariy, en août 2005. Il serait souhaitable que de tels travaux soient conduits, soit à Polytechnique, soit ailleurs, en utilisant des fibres de nature différente, comme des

fibres courtes d'alumine ou de mullite. Il y a aussi des travaux de nature fondamentale menés sur le phénomène dit de « pull-out » ou d'étirement des fibres, ce qui présente une difficulté accrue compte tenu de la longueur des fibres. Ce mémoire a quand même pu mettre en lumière qu'il semble nécessaire de respecter une longueur optimale de fibre pour éviter l'engorgement du malaxeur et pour conserver les caractéristiques de pompabilité des mélanges.

TABLE CONTENTS

LIST OF TABLES

LIST OF FIGURES

LIST OF NOMENCLATURE

Al	Aluminium
Al_2O_3	Aluminium oxide
AMC	Alumina Magnesia Carbon castable
AMC0	Alumina Magnesia Carbon castable with zero fibre
AMC(X)	Alumina Magnesia Carbon castable with fibre (general)
AMC SS406 192	Alumina Magnesia Carbon castable with 2 wt % of 19 mm length stainless steel fibre
AMC SS406 194	Alumina Magnesia Carbon castable with 4 wt % of 19 mm length stainless steel fibre
AMC SS406 196	Alumina Magnesia Carbon castable with 6 wt % of 19 mm length stainless length fibre
AMC 192	Alumina Magnesia Carbon castable with 2 wt % of 19 mm length carbon steel fibre
AMC 194	Alumina Magnesia Carbon castable with 4 wt % of 19 mm length carbon steel fibre
AMC 196	Alumina Magnesia Carbon castable with 6 wt % of 19 mm length carbon steel fibre
AMC 252	Alumina Magnesia Carbon castable with 2 wt % of 25 mm length carbon steel fibre
AMC 254	Alumina Magnesia Carbon castable with 4 wt % of 25 mm length carbon steel fibre

AMC 256	Alumina Magnesia Carbon castable with 6 wt % of 25 mm length carbon steel fibre
AMC 502	Alumina Magnesia Carbon castable with 2 wt % of 50 mm length carbon steel fibre
AMC 504	Alumina Magnesia Carbon castable with 4 wt % of 50 mm length carbon steel fibre
AMC 506	Alumina Magnesia Carbon castable with 6 wt % of 50 mm length carbon steel fibre
AP	Apparent porosity
ASTM	American Society for Testing of Materials
B_4C	Boron Carbide
BD	Bulk Density
CaO	Calcium oxide
CIREP	Centre for Industrial Refractory of Ecole Polytechnique
CPFT	Cumulative percentage finer than
CS fibre	Carbon steel fibre
EG	Extruded graphite
EAV	Equivalent apparent viscosity
F	Work done
FeO	Iron oxide
FRC	Fibre reinforced cementitious materials/composites
K_{1C}	Fracture toughness in mode 1

LCC	Low cement castable
MF	Melflux
MgO	Magnesium oxide
Na_2O	Sodium oxide
R	Fracture resistance
RT	Tested at room temperature but prior to that dried at 110^0C/24 hr
Si	Silicon
SiC	Silicon carbide
SiO_2	Silicon dioxide
SS fibre	Stainless steel fibre
TiO_2	Titanium oxide
TZ	Transition zone
U	Strain energy
ULCC	Ultra low cement castable
Vol %	Volume percentage
W	Energy required for crack formation
WFA	White fused alumina
wof	Work of fracture
Wt %	Weight percentage
wrt	with respect to

LIST OF SYMBOLS

a	crack or flaw radius
a_c	critical notch or crack or flaw radius or depth
b	width
C_p	specific heat
d	diameter
$d\delta$	change in dimension
D_c	initial diameter
D_f	final diameter
E	elastic modulus
f	fibre
F	force
F_H	horizontal force
F_M	machine force
F_v	vertical force
$g(\alpha)$	geometry factor
G	flow resistance
G_{1C}	critical strain energy release rate
h	height
H	torque viscosity
k	thermal conductivity
l	length

l/d	aspect ratio
L	span length
L_a	dimension measured after firing
L_b	dimension before firing
m	matrix
MOR	modulus of rupture
N	impeller angular speed
P	load
PLC	permanent linear change
P_{max}	maximum pull out load
q	Andreasen coefficient
T	torque
S	surface area
r	radius
R_{st}	resistance to crack propagation
R''''	resistance to crack initiation of crack propagation
α	coefficient of thermal expansion
β	wedge angle
γ	surface energy
ρ	density
ΔT	temperature gradient

μ	poison's ratio
τ	shear stress
τ_i	shear stress at the interface
σ_x	tensile stress in x- direction
σ_y	tensile stress in y- direction
σ_r	radial tensile stress
σ_{fu}	fracture stress of the fibre in tension
τ_{av}	fnterfacial shear strength
σ_T	thermal stress
σ_f	fracture stress
σ_c	critical stress
$\sigma_{\max}$	flexural strength
γ_{wof}	work of fracture
δ_H	horizontal displacement
$\lambda(0)$	compliance factor

LIST OF APPENDICES

CHAPTER 1. INTRODUCTION

1.1 Overall point of view

In modern refractory technology, monolithics are playing a vital role on account of their quick and easy installation process. Refractory castables, bonded by calcium aluminate cement, are the most widely used monolithics. Though they have used in many applications in slag zone area of steel vessels, it is still a nobblematic. Traditionally, magnesia-carbon bricks are used in such slag zones. Due to non-wetting and high thermal conductivity properties of carbon and coupled with magnesia's chemical compatibility with basic slag, these bricks offer excellent spalling and good corrosion resistance at the steel making temperatures.

Conventional alumina–based castables usages are ruled out due to their poor fluxing resistance at high temperatures, high porosity and poor mechanical properties at intermediate temperatures. Though low cement castable (LCC) and ultra low cement castable (ULCC) have superior mechanical properties as compared to conventional castables, they suffer the same drawback of having a poor resistance to corrosion in a basic slag environment. Alumina based castables lack from corrosion resistance and MgO based castable have poor slag penetration and spalling resistance [1]. In order to overcome slag penetration resistance alumina – magnesia castables come into picture. Today alumina-magnesia castables are the only monolithic linings used in barrel and bottom areas in steel ladles due to their good slag penetration resistance. This is due to the absorption of FeO in the slag by MgO and CaO by Al_2O_3 which makes the slag

composition rich in silica [2]. Further to this, spinel castables rich in alumina is better in resistance to slag penetration than stoichiometric or magnesia rich spinel owing to more lattice cation vacancies created in alumina rich spinel [3, 4].

Introducing MgO fines into castables for making in-situ spinel, has led to a serious vulnerability problem when exposed to water vapour at lower temperature through the formation of Mg $(OH)_2$ and also disturbs the workability of a castable. Normally silica fumes are added to reduce the hydration tendency and improve the workability of MgO based castables. Silica fume plays two fold roles, as anti-slaking agent and also mitigating volume expansion due to spinel formation [5, 6, 7].

To tackle all these issues, many attempts have been made to incorporate crystalline carbon in the form of graphite into castables, since other forms of carbon such as pitch, coke, and carbon black are poor in oxidation resistance, though they have shown better dispersibility in water. Nevertheless, incorporation of graphite into castables is not straight forward, owing to its poor wettability which leads to dispersion problem in water and thus high water demand during mixing [8]. Dispersion problem arises due to the fact that graphite is associated with unsaturated bond, as a result has few hydrophilic functional groups on its surface. Ideas of using wetting agents have not yielded expected results; these additives created more porosity.

One innovative idea to solve this dispersion problem, as suggested by Rigaud et al [9], is to introduce graphite not as flakes but as extruded micro pellets and coated with other material which have better compatibility with water.

Zhou and Rigaud have investigated the graphite addition into castables through formation of micro pelletised graphite (micro pellets) and briquettes to reduce the water demand. The same authors also studied the effect of TiO_2 coating on flake graphite through sol-gel coating method and found that the greatest reduction in water intake is obtained when micro pellets are used.

Huiqing He and Rigaud [10] studied the oxidation behaviour of extruded graphite pellets, with various antioxidants such as Si, Al and SiC and B_4C and concluded that addition of 6 wt % of extruded graphite (EG) is optimum for oxidation resistance.

Recent work from CIREP has revealed that extruded graphite coupled with Alumina-Magnesia castable had good corrosion resistance at steel making temperature. However, field trials have revealed that this material suffers from insufficient mechanical properties such as work of fracture and strength at intermediate temperature, say 1100 ^{0}C. An attempt is being made in this work to overcome this problem.

Based on the literature background information, it is inferred that among various existing toughening ways such as fibre reinforcement, transformation toughening, whisker addition, fibre reinforcement alone does toughening effect through fibre bridging, breaking and pullout processes, in ceramic and cementitous materials. In the present work steel fibre has been chosen as reinforcement. The fact that the basic formulation contains graphite as a constituent and since graphite oxidation would create a reducing atmosphere, it may protect the steel fibre from being oxidised at high temperature. Considering the above intuition and practical viability towards conducting trials, an attempt has been made to reinforce the Alumina-Magnesia Carbon (AMC) bonded castables with steel fibres. Since Alumina- Magnesia Carbon castables, are to be used as self-flowing mixture, a study related to rheological properties is warranted and it has been included as a pre-requisite evaluation prior to the study of mechanical properties. A detailed study of steel fibre on workability of self –flowing castable with respect to varying amount, size and type was hence undertaken.

1.2 Rheology of castable

Normally cement containing castables are installed on site through vibration or self-flowing methods. The former requires external force for the placement and the later flows without vibration, the two have then different rheological properties. Rheology is the study of flow of matter under stress or load. It describes the relationship between force, deformation and time.

For practical purposes, three types of flow behaviour have been observed: Newtonian, Non-Newtonian (time independent) and Non-Newtonian (time dependent). The viscosity of Newtonian fluids is dependent only on temperature where as non-Newtonian is dependent on temperature and shear rate. Pseuoplastic, dilatant and bingham plastic are the three important time independent rheological behaviour of fluids. In case of pseudo plastic, the viscosity decreases with increased shear rate and Bingham requires a threshold shear stress before flow occurs which is called yield stress. The viscosity of Non-Newtonian time dependent fluid is dependent on temperature, shear rate and time. Thixotrophy is another important time dependent behaviour in which the viscosity decreases with time [11, 12]. The basic flow patterns are shown in Figure 1.1.

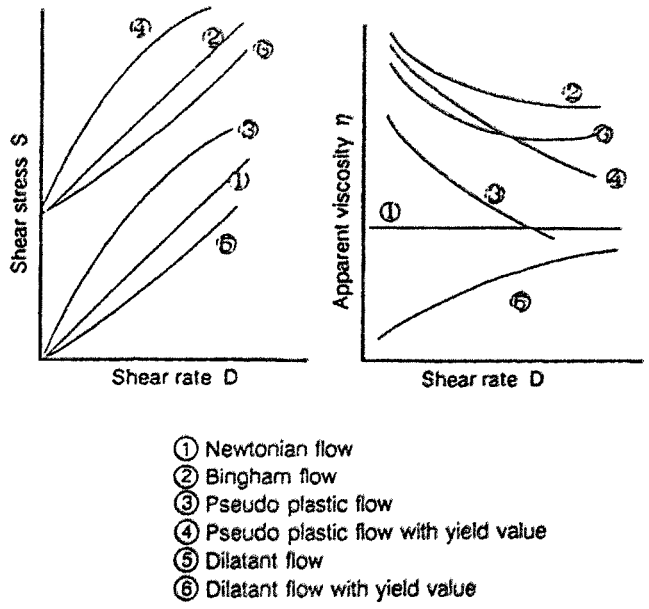

Figure 1.1 Basic flow patterns [12].

The rheological behaviour of a fluid or suspension characterises its viscous behaviour as a function of shear rate. In the field of monolithic refractories, the subject of rheology study includes the solid suspension systems with or without the aggregates. Their rheological characteristics can be expressed by the relationships between shear stress and shear rate.

Practically the differences in flowability are achieved by adjusting particle size distribution and addition of admixtures such as dispersants, plasticizers and setting agents. Particle size distribution is designed in such a way to minimize the interstitial pore volume and to provide adequate surface to react with fines and is characterised by two famous equations, one is proposed by Andreasen and other by Funk and Dinger [13]. These equations 1.1 and 1.2 are given below.

Andreasen equation, $$\frac{CPFT}{100\%} = \left(\frac{D}{D_L}\right)^n \qquad \text{(Equation 1.1)}$$

Where $CPFT$ - cumulative percent finer than

D_L - largest particle size

D - partilce size

n -distribution modulus.

Modified Andearsen (Funk-Dinger) equation,

$$\frac{CPFT}{100\%} = \left(\frac{D^n - D_S^n}{D_L^n - D_S^n} \right) \qquad \text{(Equation 1.2)}$$

Where $CPFT$ - is the cumulative percent finer than

D_S . is the smallest particle size in the distribution.

D - is any particle diameter in the distribution size

D_L . is the largest particle diameter distribution.

n - is the exponent the slope at D_L

Use of fibres into self compacting (flowing) concrete mixes has been studied by many civil engineering researchers [14-17]. Many parameters such as top grain size, fibre content, fibre geometry, aspect ratio are influencing the workability of concrete, but all these workability tests were conducted in terms of slump flow, flow cone J-rings etc. The conclusion is that the workability mainly dependent on the fibre volume and aspect ratio and to a lesser extent on the shape of the fibre. The reason for reduction in flowability of concrete is due to the fact that fibres act as very long and slender aggregates, which justify the decrease of packing density of the aggregates in the mix resulting in a decreased workability.

Tattershall [18] has studied the effect of steel fibres on the workability using rheometer and his finding is that with steel fibre addition concrete conforms to Bingham model. As the fibre content increases both flow resistance (G) and plastic

viscosity (H) increase but when the fibre length increased, only flow resistance alone showed significant increase. Similar results have been observed by L.W. Marston et al, [19] when incorporating steel fibres in refractory material. As the aspect ratio increases, the amount of fibres that can be added to refractory also gets reduced. In order to know the limit of fibre dosage, a formula has been given :

$$PWccrit = 75\pi\left(\frac{SG_f}{SG_c}\right)\frac{d}{L}K \qquad \text{(Equation 1.3)}$$

Where *PWccrit* is the critical fibre percentage by weight of the concrete

SG_f - is the specific gravity or density of fibres,

SG_c- is the specific gravity or density of concrete matrix.

Where $K=W_m/(W_m+W_a)$

Where W_m - is the weight of the mortar fraction, i.e. part of the matrix whose particle size is less than 5 mm.

W_a - is the weight of the aggregate fraction i.e. that part of the matrix whose particle size is greater than 5 mm.

The effect of steel fibre addition to Alumina based Low Cement castable has been studied by Hamadai et al [20] using melt-extracted fibres. Addition of fibre to the tabular alumina based castable reduces the workability of castables. With 4 wt % fibre the flow value is found to decrease to 60-30 % from the initial value of 90-70 %.

1.3 Mechanical properties of concrete

Refractory castables can be considered as high temperature concrete material and their mechanical behaviours at room temperature are in similar line with ordinary Portland cement based concretes. The principle that governs the mechanical behaviour of concrete is also applicable to refractory castables.

A refractory castable (concrete) is a composite material having cement paste (matrix phase) and aggregates as its constituents. As far the stress-strain curve is concerned, individually, both aggregate and cement paste exhibits linear elastic curve but as a composite material, its behaviour deviates from linear into non-linear. The non-linear part of castable under stress is due to the presence of weak interfacial region (TZ) transition zone between aggregate and matrix (cement paste). Actually this interface is a planner (two dimensional) region where physical, mechanical and chemical properties gradually vary from cement phase to aggregate phase [33-34]. The size of TZ is 10-50 μm thick around an aggregate. Because of its high porosity and low strength compared with matrix and aggregate, crack can easily propagate in it. Stress-strain curve of concrete has four stages such as linear, strain localisation region, non-linear and strain softening regions [47-49]. The stress-strain curve clearly indicates that limited amount of toughening is taking place owing to energy dissipation processes through micro cracking, crack branching, crack deflection, crack face friction and crack tip blunting mechanisms [50-51]. Among these, grains bridging plays a dominant role for refractory castable [52]. Some degree of toughening in castable can be brought

out through transformation toughening process, whisker and fibre reinforcement [34-41]. But higher degree of toughening is possible only with fibre reinforcement. Basically toughening improves the strain capacity of the material in comparison with plain concrete. In other words it can be stated that fibre are acting as a load-bearing medium embedded in a matrix.

Normally many types of fibres such a carbon, glass, steel are used in cement based materials. Among them, steel fibre reinforcement is a common one. Fibre reinforcement would be effective only if the ultimate strain capacity of matrix is lesser than that of fibre and elastic modulus of fibres is higher than that of matrix. Another requirement should be the interface region which exists between fibre and matrix must be porous in nature in comparison with matrix and fibre. This implies that interface should posses certain amount of strength. The origin of strength at the interface arises due to three mechanisms such as adhesive bond between the fibre and hydrated cement crystals, frictional bond between fibre and the matrix and finally bonding through chemical interaction between the fibre and matrix [66]. Chemical interaction is possible only at high temperature through diffusion process, or viscous flow or penetration of matrix into the crevices of fibre [69].

When load is applied to fibre reinforced castable, fibres will experience two types of stresses one is normal stress and another one is interfacial shear stress. The interfacial stress is the result of difference in elastic modulus value of fibre and matrix and

increases in proportion with the ratio of E_f / E_m (fibre elastic modulus/matrix elastic modulus).The nature of this stress is that its value is maximum at the entry of fibre to the matrix and is not constant through out. Stress-strain curve of fibre reinforced concrete (FRC) consists of two regions: pre-peak and post-peak curves [56-57]. Matrix takes the load during the pre-peak period where as fibre takes it in post-peak period. When the value of shear stress reaches that of interfacial bond strength, debonding of fibre from matrix will occur, although fibre breaking stress is much higher than that of interfacial shear strength. After that, fibre slippage from the matrix occurs, which is resisted by the frictional stress and lead to progressive pull out of fibre from the matrix instead of catastrophic failure. Analysis of fibre debonding at the tip of a matrix indicates that debonding rather than fibre failure occurs, provided the fracture energy of the interface is sufficiently small compared with that of the fibre [68-70]. The resistance offered by the frictional stress depends on applied normal stress and coefficient of friction. Fibre characteristics that affect the post-peak periods are the aspect ratio, volume fraction, surface roughness, fibre orientation, and interspacing between the fibres [59-61]. For an effective load-transfer, interfacial bond strength should be neither too strong nor too weak and should have a optimum value [69]. Poisson's ratio has very little role to play in fibre reinforced cementations materials due to porous nature of interface where as it plays considerable role in ceramic matrix composite [64]. For a given volume, the number of interfaces will be more as the aspect ratio (decrease in diameter) increases which means more number of debonding and pull out of fibres.

For an effective load-transfer, a minimum length called critical fibre length is required. Fibre volume also drastically changes the shape of stress-strain curve. Below certain volume called critical volume, fibre addition will improve only the toughness not strength [57]. Fibre with corrugated surface induces more anchorage with the matrix which in turn increases the frictional force. This lead to the extension of fibre pulls out region in stress-strain curve [62-63]. The interfacial strength can be measured from pull out test results [71-72]. The same can be used for calculating critical fibre length as well as critical volume.

In case of castables, fibres are added in the form of short fibres which are oriented randomly in three dimensions. Depending on its orientation, it will have an effect on the mechanical behaviour of castable [73]. Normally toughness value increases as the angle of orientation increases from 0 to 45° and anything beyond this limit, will result in declining trend [74].

Refractory castables are subjected to high temperature while in service. Depending on the temperature, many micro structural changes will occur via dehydration of cement [86], reaction of fibre with matrix and formation of liquid phase with in the constituents. The thermal expansion mismatch of fibre and matrix results in radial cracks occurring at the interface between the two phases [79]. All these features have an influence and affect the strength at high temperature as well as the hot modulus of rupture and permeant linear change [54, 77-79].

In ceramics, fracture toughness is estimated using Linear Elastic Fracture Mechanics and the fracture occurs on the assumption that the crack starts propagating catastrophically once initiated [80]. Physically the value of fracture toughness (K_{IC}) indicates the stress intensity at the crack tip which propagated in unstable way. But the same cannot be applied to castable to measure toughness characteristics owing to the presence of limited fracture processing zone due to various toughening mechanism. In castable, the toughness value is calculated through work of fracture rather than fracture toughness. The work of fracture can be calculated through the stress-strain curve by knowing the maximum force and the energy resulted from the area under the curve.

Application of a load to a material with an initial crack size of a introduces a strain energy U, which is stored in machine and material (specimen) as elastic energy. This energy is responsible for the driving force for crack propagation and is defined as strain energy release rate, G. During the crack propagation, a resistance is offered by the material which is termed as fracture resistance(R). In order to overcome this resistance, some work has to be done. So, R can be denoted as the rate of change of work done with respect to crack length [82].

In case of brittle material, failure occurs when $G=R$ is satisfied. Here R is a material constant [49]. However, in quasi-brittle materials the crack steadily propagates until a second condition is also satisfied. In this case R is not constant but keeps changing with crack length.

$$\frac{\partial G}{\partial a} \leq \frac{\partial R}{\partial a}$$

These stable crack growth conditions will govern crack propagation until the crack extension reaches its critical value where both the above conditions are satisfied. Once these two conditions are satisfied, any increase in load will result in unstable crack propagation (failure). To keep stable crack propagation, the applied load P must be decreased. This explains the softening behaviour of cementations materials.

Work of fracture represents the sum of all the energy dissipated during the complete cracking of a material through energy spent in creating surfaces, aggregate bridging, pull out and fibre bridging processes.

The work of fracture is equal to the total surface under the load-displacement curve divided by *2S,* the new created surfaces due to fracture. There is a practical difficulty for the measurement of work of fracture which is associated with the fact that the relation between load-displacement must be known at any time during the propagation of the crack. This requires that the crack is propagated in a stable way and displacement can be followed any time. This was first studied by Harmuth et al [83, 84] using wedge splitting technique (WST). Stable crack propagation is favoured when the machine used is very rigid and has relatively large parting surfaces. The WST integrates those two important aspects. In WST, the load is applied through the horizontal component of the force through the small wedge. The decrease of the

machine force FM reduces the elastic strain energy stored in the testing machine. Due to the effect of the wedge and a relatively low ratio of the specimen volume to fracture surface area, the test method is expected to enhance the stability of crack propagation. Another advantage with this technique is that it allows performing and measuring the mechanical properties even at high temperatures. A detailed literature information on structural materials stress-strain behaviour, fracture of concrete, fracture of cementations materials, role of interface, pull out tests, effect temperature on castable and steel fibre reinforcement in castables are provided in Appendix A.

In a nutshell, the aim of this work is to improve the work of fracture of extruded graphite containing Alumina- Magnesia Carbon castables reinforced with steel fibres.

The present work is divided into two parts.

1. To study the rheological behaviour of Alumina-Magnesia-Carbon self-flowing castable with steel fibre reinforcement.

2. To study the effect of steel fibre on high temperature mechanical properties of Alumina-Magnesia-Carbon (AMC) castable using wedge splitting and three point bending techniques.

1.4 Structure of the thesis

The present work is divided into six chapters and the contents of each chapter are presented below. As we have seen, Chapter 1 provides some back ground information

on Alumina-Magnesia Carbon (AMC) castable system, rheology of castables, mechanical properties of cementitous materials.

Working methodology is dealt with in Chapter 2 where raw materials, experimental design, sieve analysis and particle size distribution of materials, a short description about process details on extruded graphite, mixing and casting procedure, testing of flow and flow decay, rheological measurement, physical and mechanical properties determination and characterisation of materials through scanning electron microscope are all documented. In mechanical properties, more attention has been paid on the description of wedge splitting technique (WST).

Chapter 3 deals with the presentation of results and its analysis of rheology of Alumina-Magnesia-Carbon (AMC) castable systems. Results of flow and flow decay with and without fibres and the effect of fibre length, its amount on flowability, rheological properties in terms of torque Vs. speed, flow resistance with respect to time, equivalent apparent viscosity Vs speed are presented.

Chapter 4 consists of test results on mechanical properties related work. The force-deflection curves for AMC with varying fibre amount and length at room temperature as well at 1100°C, are presented. Work-fracture, MOE, maximum force values obtained from the force-deflection curves is listed. The apparent porosity (AP), bulk

density (BD), hot modulus of rupture (HMOR) and permeanant linear change (PLC) values related test results are provided.

Chapter 5 deals with the analysis part of the thermo-mechanical properties related results. Much emphasis has been given to the work of fracture part with respect to fibre length, type and content. Fracture toughness, and modulus of elasticity results are also dealt with in line with fibre length, amount and chemistry etc. Results have been correlated with micro structural features which are detected through Scanning Electron Microscope.

Finally, the conclusions and recommendations are enunciated in Chapter 6.

CHAPTER 2. METHODOLOGY OF WORK

2.1 Introduction

In this chapter, details about the raw materials, experimental plan, sample preparation, properties evaluation and characterization techniques are discussed. The details of used raw materials are discussed in section 2.2. Section 2.3 outlines the overall view of the experimental plan. The experiments for the measurement of flow and flow decay time are described in section 2.4. The rheological measurement with and without steel fibre reinforced Alumina-Magnesia-Carbon (AMC) castables are elaborated in 2.5. Measurement of physical, and mechanical properties are explained in section 2.6

2.2 Raw materials

Raw materials portion is divided into three parts, consisting of aggregates, fine matrix and additives. Details are given below.

2.2.1 Aggregates

In the present work, white fused alumina (WFA) was chosen as aggregate. It is made from high quality Bayer-processed alumina by fusing in an electric arc furnace at high temperature. Because of its low porosity and large crystal size, it offers better refractory properties. The chemistry and physical properties are shown in Table 2.1. The fractions in mesh size of white fused alumina used were 3/8, 8/14, 14/28, 28/48.

2.2.2 Fine matrix

Fine matrix portion consists of different fractions of white fused alumina fines (-48,-100, -200 mesh), reactive alumina (RAC45B), calcined alumina (C90LSB), micro-silica (MS), calcium aluminate cement (CA14-S), magnesia powder (DSP, -325 mesh) and dispersant (Melfux). The particle size distribution analysis (PSD) of fine matrix components were carried out using a particle size analyzer (COULTER LS200, USA) and are shown in Figure 2.1. The physical and chemical properties along with the supplier details are given in Table 2.2.

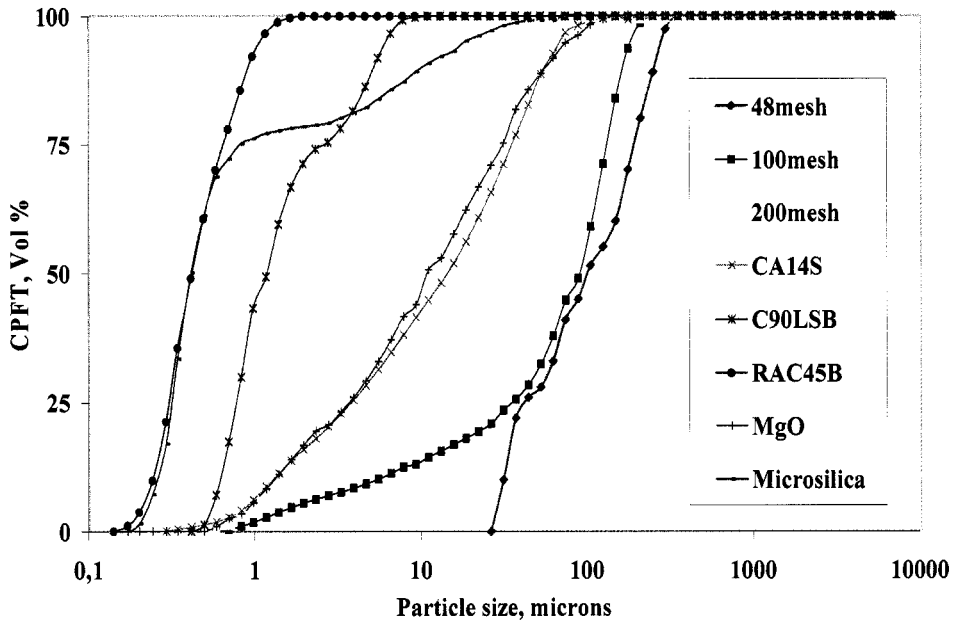

Figure 2.1. Particle size distributions of fine matrix components

2.2.3 Additives

Steel fibres and extruded graphite were added as additive materials. Two types of steel fibres with different chemistry and lengths were used. The properties of steel fibres are given in the Table 2.3 and 2.4 respectively. Extruded graphite with size range similar with 28/48 mesh was used and the respective properties are given in Table 2.5.

Table 2.1 Properties of white fused alumina

Constituents	Wt %
Al_20_3	99.64
SiO_2	0.06
Fe_2O_3	0.03
CaO	0.03
MgO	0.07
Na_2O	0.15
Apparent porosity, %	7.8
Bulk Density, g/cm^3	3.58
Supplier	CE minerals

Table 2.2 Chemical and Physical properties of fine matrix components

Material→ Chemistry ↓	RAC45B	C90LSB	DSP -325	MS	CA-14 S
Al_2O_3	99.8	99.8	0.03	0.28	72
SiO_2	0.01	0.02	0.03	97.97	0.3
CaO	0.01	0.03	0.63	0.12	27
MgO	0.05	-	99.3	0.23	0.4
Na_2O_3	0.04	0.03		-	0.3
Fe_2O_3	0.01	0.01	0.04	0.13	0.2
Density (g/cm^3)	3.94	3.90	3.45	-	
Supplier	ALCAN, Canada	ALCAN, Canada	Dead Sea Periclase	Elkem, Norway	Alcoa, USA

Table 2.3 Properties of the stainless steel fibres

Property	Stainless steel
Density, g/cm^3	7.47
Tensile strength, MPa	350-490
Melting range, °C	1371-1477
Length used , mm	19
Thickness, mm	1.5 mm

Table 2.4 Properties of the low carbon steel carbon fibres

Property	Carbon steel
Density g/cm^3	7.86
Tensile strength,MPa at 20°C	420-840
Modulus of Elasticity,MPa, 20°C	29
Melting temperature , °C	1516
Lengths used, mm	19,25,50
Thickness, mm	1.5

Table 2.5 Properties of extruded graphite

Property	
Apparent porosity %	15
Bulk Density,g/cm^3	2.0
Diameter,mm	0.7
Length,mm	2-4

2.2.4 Processing of extruded graphite

The process chart for making extruded graphite is shown in Figure 2.2

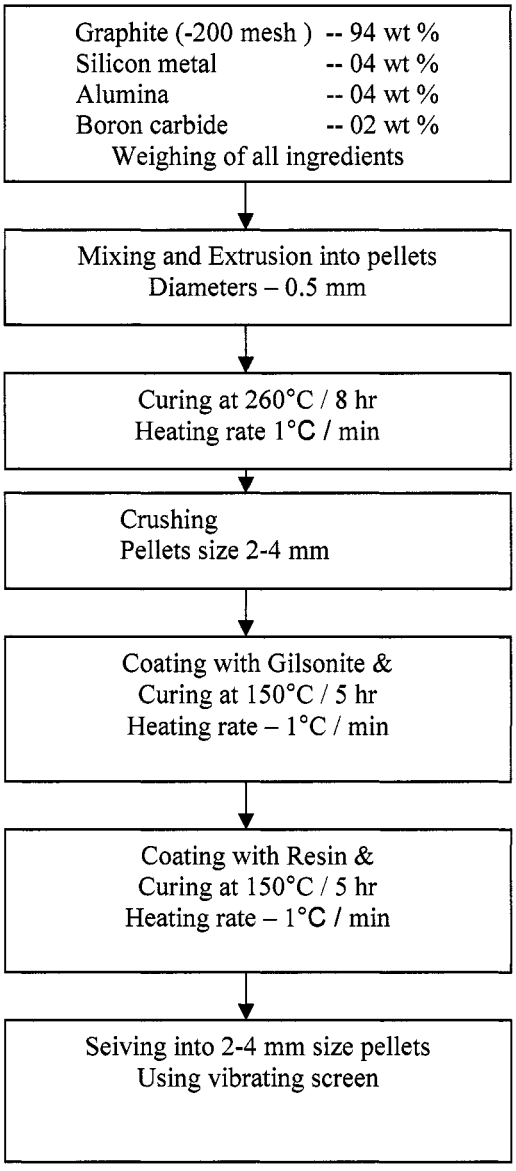

Figure 2.2. Flow chart of extruded graphite processing.

2.3 Work plan

The overall experimental plan is shown in Figures 2.3. The details of different measurements are discussed in the subsequent sections.

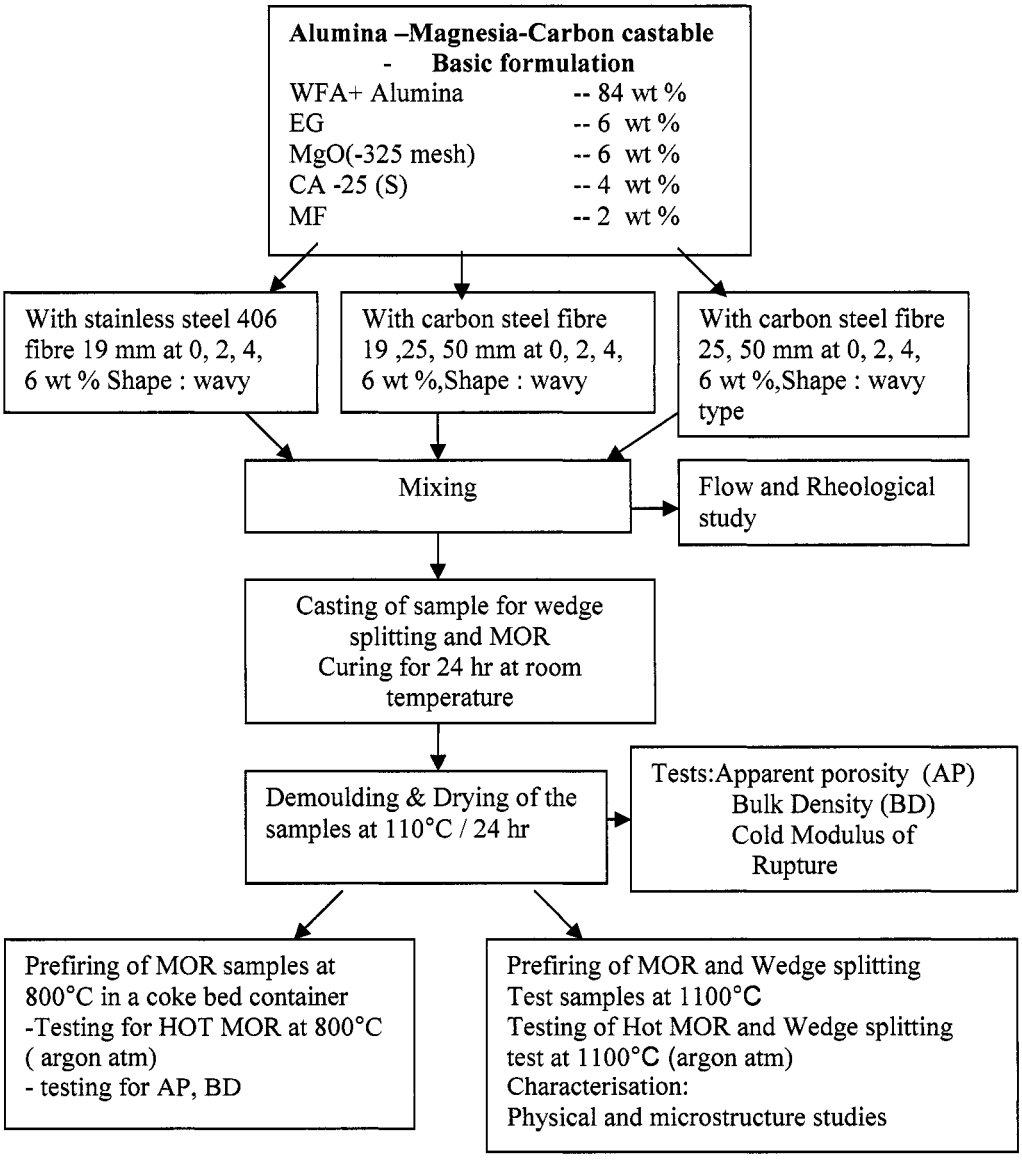

Figure 2.3. Schematic representation of experimental plan.

2.3.1 Basic formulation

The basic formulation used in the present investigation is shown in Table 2.6. It does not contain any steel fibre.

Table 2.6. Basic formulation of castable

Constituents	Wt %
White Fused Alumina, 3/8 mesh	20.0
White Fused Alumina, 8/14 mesh	10.0
White Fused Alumina, 14/28 mesh	12.0
Extruded Graphite, (2-4 mm)	6.0
White Fused Alumina, 28/48 mesh	10.0
White Fused Alumina, -48 mesh	12.5
White Fused Alumina, -100 mesh	2.0
White Fused Alumina, -200 mesh	4.5
Magnesia (DSP),-325 mesh	6.0
Calcined Alumina C90LSB	6.5
Reactive Alumina RAC45B	6.0
Micro Silica	0,5
High Alumina Cement, CA 14-S	4
Dispersant (MelFlux)	0.2
Steel Fiber	0

Particle size distribution curve as shown in Figure 2.4 was plotted, using Table 2.6, for AMC castable without fibre.

2.4 Free-flow and flow-decay measurement

2.4.1 Weighing and mixing

Each formulation of castable raw materials were selected weighed as given in Tables 2.6 and 2.7. Dry mixing of 2 kg of the constituents, was performed using Hobart mixer. It consists of a bowl with a pedal. The pedal is connected to a rotating arm whose rpm can be varied.

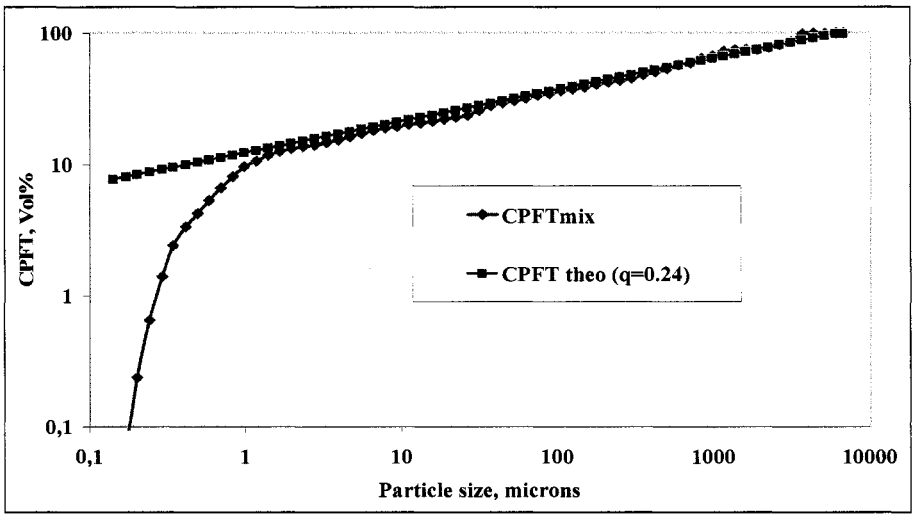

Figure 2.4 Andreasen particle size distribution of AMC castables

Table 2.7 Castable nomenclature

Type	Length	Weight Wt %	Nomenclature
AMC	-	No fibre	AMC 0
AMC + Stainless steel	19 mm	2	AMC SS406 192
		4	AMC SS406 194
		6	AMC SS406 196
AMC +Carbon Steel	19 mm	2	AMC 192
		4	AMC 194
		6	AMC 196
	25 mm	2	AMC 252
		4	AMC 254
		6	AMC 256
	50 mm	2	AMC 502
		4	AMC 504
		6	AMC 506

Initially the mix was allowed for 3 minute dry mixing followed by six minute wet mixing with the addition of required amount (5.75 %, on weight basis) of water.

2.4.2 Free flow measurement

After mixing, the castable free-flow (or self-flow) was measured by cone conforming to ASTM C230. The cone was filled with castable, then removed to spread horizontally under gravitational force for 60 seconds. The spread was measured. The flow measurement was calculated using the following formula.

$$\% \text{ Free flow} = \frac{D_f - D_c}{D_c} \times 100 \qquad \text{(Equation 2.1)}$$

where, D_f - is the final diameter

D_c - is initial diameter (100 mm).

2.4.3 Flow decay measurement

After measuring the free-flow, the castable mix was stored in a plastic container to preserve water from escaping. The sample was taken out from the container after 45 minutes from the time of mixing. Spread was measured and free-flow was calculated using the equation 2.1.

2.5 Rheological measurement

Castable mix (8 kg) was dry mixed for 3 minutes using Hobart mixer and wet mixed for 6 min. with 5.75 % water addition. A rheometer (IBB Rheometer V 1.0, Figure 2.5) was used for the measurement of rheology of castables. During testing, the impeller is driven by a motor at different speeds levels, through the bowl filled with castable and the torque was measured up to 45 minutes, with 15 minutes interval. The relationship between torque (T), the flow resistance (G), the impeller angular speed (N) and the torque viscosity (H) are correlated by straight line equation assuming Bingham nature to castable mix as follows:

$$T = G + (H \times N) \qquad \text{(Equation 2.2)}$$

where, T and G are in **N.m**, H (slope to the equation) and N are in **N.m.s** and **rev/s** respectively. By proper calibration, these constants (G and H) can be converted respectively into the fundamental units of yield stress τ_0 (**Pa**) and dynamic viscosity μ (**Pa.s**)

The method of evaluating G and H values, using the rheometer test results, is shown in Figure 2.6.

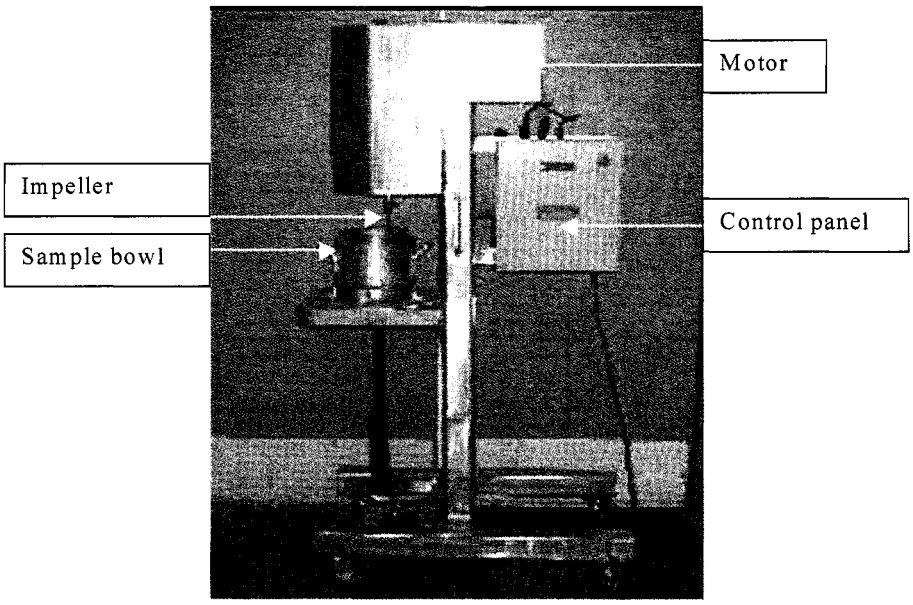

Figure 2.5 IBB Rheometer

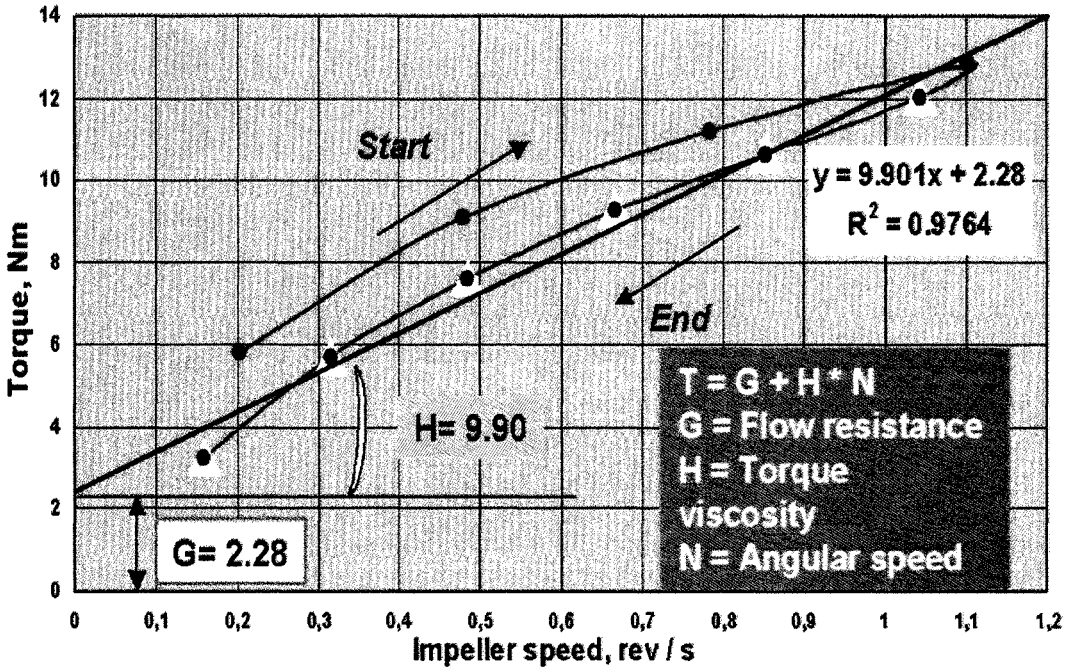

Figure 2.6. Evaluation methods of flow resistance (G) and torque viscosity (H)

2.6 Sample preparation and testing (physical and mechanical)

2.6.1 Sample preparation

The ingredients, 10 kg batch, were weighed as per formulations in the Table 2.7 and were dry mixed in Hobart mixer for 3 minutes followed by 6-mimute wet mixing with addition of water. Sample of dimensions of 160 mm x 40 mm x 40 mm (for MOR) and 100 mm x 100 mm x 75 mm (wedge splitting) were cast and covered with plastic bags in order to avoid moisture loss from the surface and cured for 24 hr at room temperature. After curing the samples were demoulded dried at 110°C for 24 hr.

2.6.2. Firing of samples

Dried samples were pre-fired at 800 and 1100°C for 3 hours in a furnace. Coke powder was used to cover the samples to prevent the oxidation of both EG and steel fibres.

2.6.3 Permanent linear change (PLC)

Permanent linear change of the castable fired at 800 and 1100^0C/3 hr was measured on bars (160 x 40 x 40 mm) by measuring the dimensions before and after firing using the formula given below:

$$\%PLC = \frac{L_a}{L_b} x100 \qquad \text{(Equation 2.3)}$$

where L_a -is the dimension measured after firing

L_b - is the dimension measured before firing

2.6.4 Modulus of rupture (MOR)

For MOR testing, Instron machine (model 5581) was used in 3-point bending mode with a strain rate of 0.2 mm/min. Samples pre fired at 800 and 1100 ^{0} C, were used for MOR testing at 800 and 1100°C in argon atmosphere. The cold modulus of rupture test was carried out on dried sample at 110^{0}C. The following formula was used to calculate MOR of the samples:

$$MOR = \sigma_{Max} = \frac{3FL}{2bh^2} \qquad \text{(Equation 2.4)}$$

F -Maximum load applied, N

L -Span length (126.85 mm),

b - is the width of the sample,

h- is the height of the sample.

2.6.5 Wedge splitting test.

This test is used for calculating work of fracture γ_{wof} , fracture toughness K_{1C} , modulus of elasticity of AMC castables with and without fibres at 110^{0}C as well 1100^{0}C. The schematic diagram of the set-up is given in Figure 2.7 a and b. The Figure 2.7a describes the method of force application. Prefired samples of 100 mm x 100 mm x 75 mm were cut into wedge configuration as shown in Figure 2.7 b.

The vertical force applied to the sample by the piston is transmitted horizontally by a wedge slipping between the two rollers. These rollers are supported with two side

supports installed on both sides of the main notch (the one with 24 mm).The relation between the vertical force (the one applied by the machine) and the horizontal force which results from the vertical one is given by the following equation:

$$F_H = \frac{F_V}{2\tan\left(\frac{\beta}{2}\right)} \qquad \text{(Equation 2.5)}$$

where F_H - is the horizontal force,

F_V - is the vertical force

β - is the angle formed by the two surfaces of the wedge.

The displacement, i.e. deformation and the opening of the sample during cracking are calculated by a similar relation of equation 2.5 and are based on the vertical displacement of the span of the machine and is given by

$$\delta_H = 2\tan\left(\frac{\beta}{2}\right)\delta_V \approx 0.175\delta_V \quad \text{(Equation 2.6)}$$

The modulus of elasticity can also be calculated from slope of the load-displacement in the elastic region of the curve using the following relation:

$$E = \frac{\lambda(0)}{B}\left(\frac{dF_H}{d\delta_H}\right) \qquad \text{(Equation 2.7)}$$

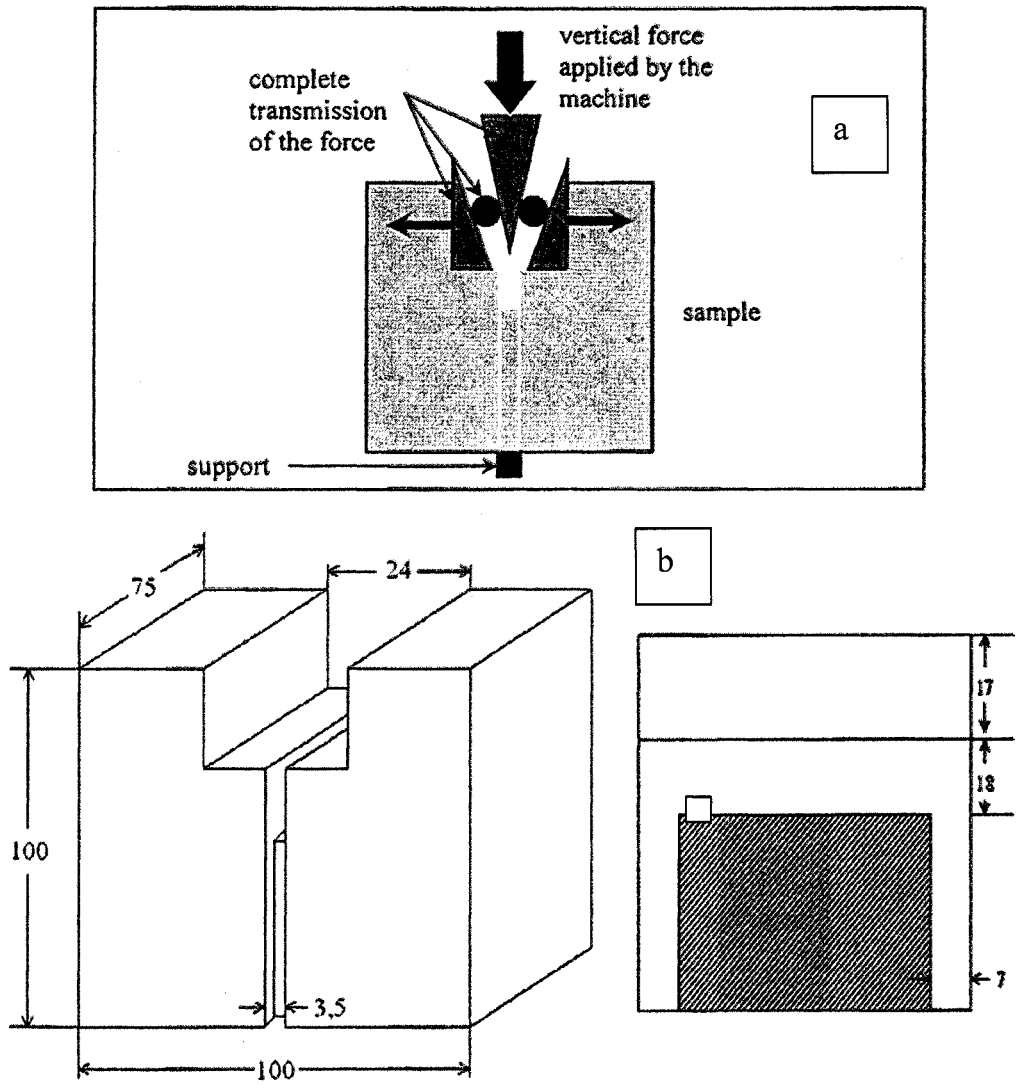

Figure 2.7 a). Testing configuration, b). Sample configuration.

The term $\lambda(0)$ is dimensionless compliance before crack initiation for the given geometry (Figure 2.7b) and is equal to 15.4 (FEM simulation by Harmath).

The critical stress intensity factor was calculated using the following formula;

$$K_{1C}^{S} = kF_{H,Max} \qquad \text{(Equation 2.8)}$$

Constant k is equal to 354.5 $m^{-3/2}$ and was obtained by finite element simulation(Harmuth). Harmuth also provides the values of Y(α) and λ(α) for the geometry presented in Figure 2.7b. In a general way, it can be given by the following equation:

$$K_{1C}^{S} = Y\left(\frac{a}{W}\right)\frac{F_{H,Max}}{BW^{\frac{1}{2}}} \qquad \text{(Equation 2.9)}$$

Here W= 100 mm, B= 61 mm and a= 35 mm.

The work of rupture was obtained by numerical integration of the load-displacement curve. The boundaries used for the integration are $\delta_1 = 0$ $(F_{V1} = 30N)$ and $\delta_2 = \delta$. The test conditions, described below, will determine the reasons of these choices.

$$G_F = \frac{1}{B(W - a_0)}\int_0^{\delta} F d\delta \qquad \text{(Equation 2.10)}$$

The tests were conducted at 1100^0C, using an Instron machine (model 5581).A vertical preload of 30 N was applied to the assembly during initial operation. Two principle reasons explain these choices. Initially the preload makes it possible to maintain the moving parts (wedge, rollers and supports) in place and balance on the sample.

Secondly, it makes possible to limit the negative effect at the beginning of loading, related to the adjustment of the various parts. For this test the loading rate was already optimized by Harmuth and Paransky . The vertical speed used for this project will be the same as that determined by these authors and is equal to 0.5 mm/min. This speed makes it possible moreover to ensure the stable propagation of the crack for the majority of refractory materials, while carrying out the test within reasonable times (30 to 45 minutes) in order to limit the deformation related to creep.

2.6.6 Apparent porosity and Bulk density

The apparent and bulk density of the samples were measured as per ASTM C830.Sample with size 160 x 40 x 40 mm were cut to small pieces removing all skins.

2.6.7 Microstructure Analysis

Optical microscope (OLYMPUS SZ 61) and scanning electron microscope (JMS-840 JEOL) was used for carrying out micro structural studies. Optical microscope was used just to see the features at higher magnifications. The features, especially at interfacial study and fracture surface were studied using SEM. For SEM studies, a coating with gold using sputtering technique was performed order to avoid charging effect.

CHAPTER 3.RHEOLOGICAL BEHAVIOUR OF AMC CASTABLE

3.1 Self-flowability

The self-flow values measured on castables immediately after mixing (10 min) and 45 minutes are presented in Figure 3.1 and Figure 3.2 respectively. In Figure 3.1, the self-flow value of castables decreases with increasing steel fibres content. The influence is more important for 50 mm length. Similar trends are observed for 45 minuets flow values also (Figure 3.2). The steel fibres behave like a needle shaped coarse particle and hinder the flow of castable. The flow values are acceptable (Figure 3.1) even at 4 wt% addition of either 19 or 25 mm steel fibres. The drastic reduction of flow values with 50 mm fibres necessitates vibration to fill the mould.

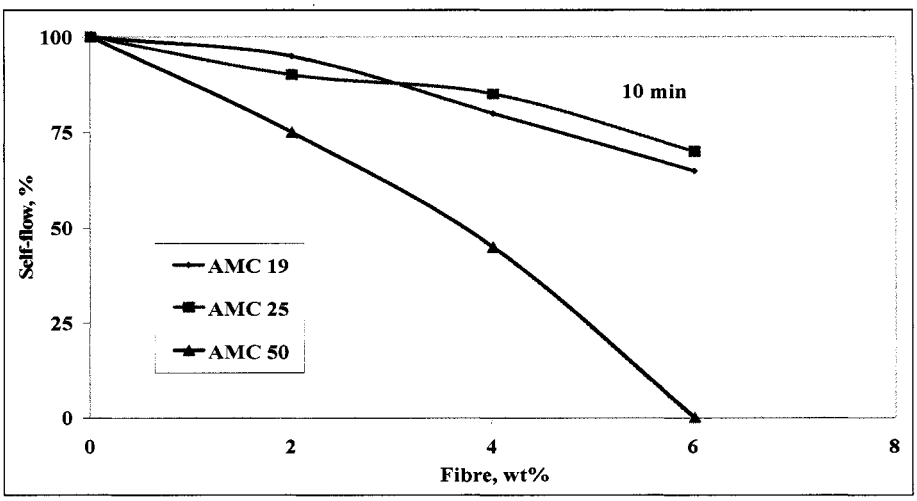

Figure 3.1. Self-flowability of AMC castables containing 19, 25, 50 mm carbon steel fibre as a function of fibre content (0, 2, 4, 6 wt %) after 10 minutes of mixing.

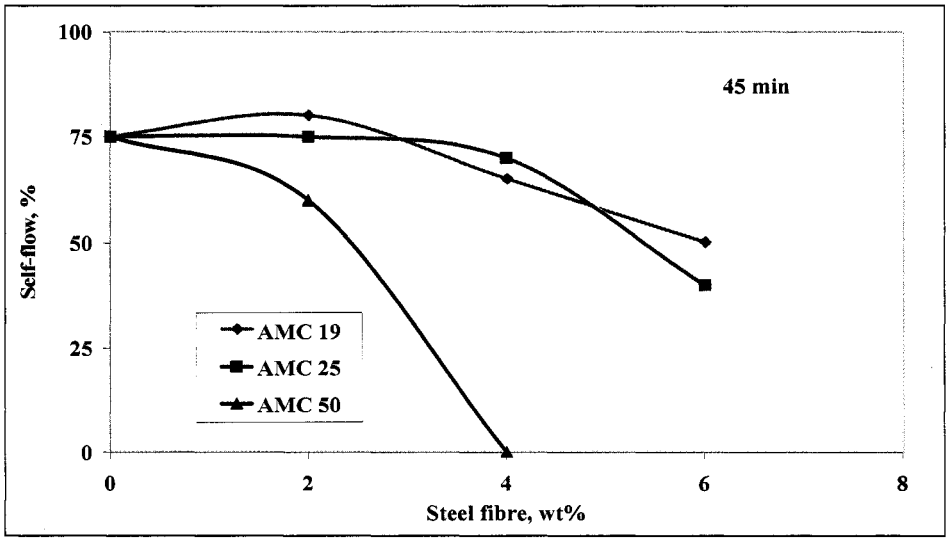

Figure 3.2. Self-flowability of AMC castables containing 19, 25, 50 mm carbon steel fibre as a function of fibre content (0, 2, 4, 6 wt %) after 45 minutes of mixing.

3.2 Rheology

The test results of rheological behaviour of AMC are presented and discussed in this section. The torque versus speed relationship of AMC containing 0 wt% steel fibre is shown in Figure 3.3.

The hysteresis loops in this figure represent the relationship between torque and impeller speed for such a castable after 15, 30 and 45 minutes after mixing. At 15 minutes, the forward cycle reveals pseudo plastic nature of the mix while the reverse cycle displays an almost Bingham behaviour (Newtonian with yield). The hystersis loops of 30 and 45 minute follows almost similar path as that of 15 min one, confirming the stability of mix with time.

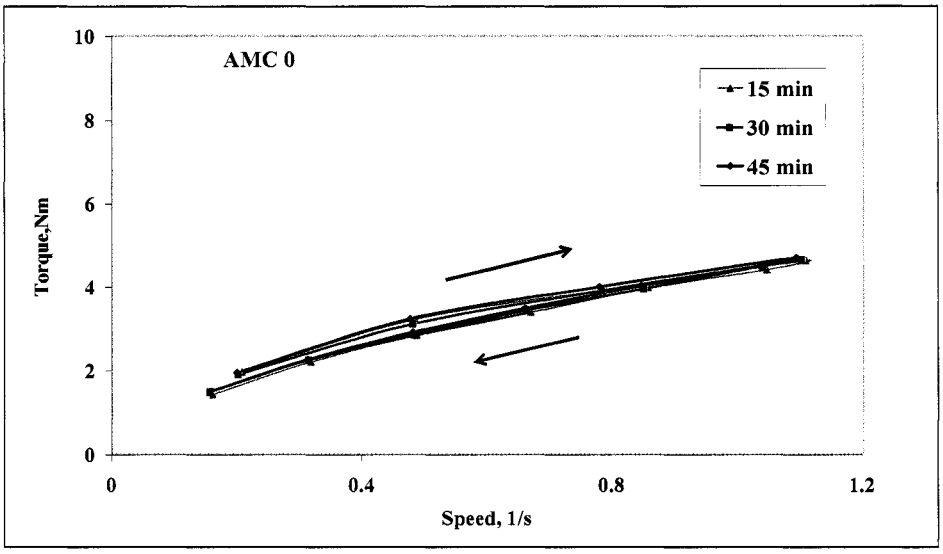

Figure 3.3. Torque vs. Speed curves for AMC with no fibre illustrates the effect of mixing time.

In the forward cycle, the rate of increase of torque is decreasing with testing speed as the mix is getting homogenized. Once it reached the maximum testing speed the homogeneous mix behaves almost linearly in the reverse cycle. The loops area remains almost the same for all testing. In the beginning of the test, the mix cannot be considered as completely mixed and gains in homogeneity with mixing speed. The shearing stress helps to the breaking of agglomerates, fill the voids and improve dispersibility, due to the post mixing action of the impeller. Once the mix reaches the maximum speed, the mix is in a more homogeneous state and then shows Bingham behaviour in the reverse cycle.

The relationship between equivalent apparent viscosity (EAV) and impeller speed shown in Figure 3.4 for AMC 0 depicts typical Bingham behaviour of mix. The values of equivalent apparent viscosity are calculated from the instantaneous torque divided by impeller speed. Even though, the values are not in fundamental unit of apparent viscosity (Pa.s), in real sense it represents the values of apparent viscosity of the chosen system with proper conversion factors.

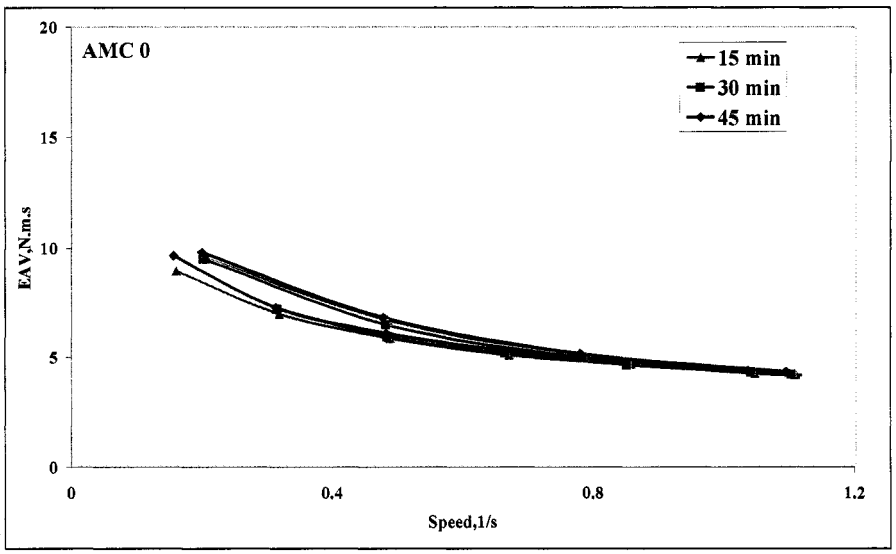

Figure 3.4. EAV Vs. Speed curves w.r.t time for AMC 0 wt % steel fibre.

After considering the mix AMC 0 (mix with 0 wt% fibre), the following discussions are focussing on the influence of fibre length, type and amount on rheological nature of mix and tries to trace whether there is change in rheology from Bingham to dilatancy.

3.2.1 Effect of fibre addition

The rheometer result of AMC192 is shown in Figure 3.5. Addition of 2 wt% does not change the rheological pattern of the mix. The mix follows Bingham behaviour (Figure 3.6). The rheological pattern of all other mixes are also similar in trend and are presented in Appendix B (Figures B1-B6, pages 140-142). The pictures confirm two important points. All the castables are stable with time and they all follow the Bingham behaviour with steel fibre addition to the level of 2 wt%.

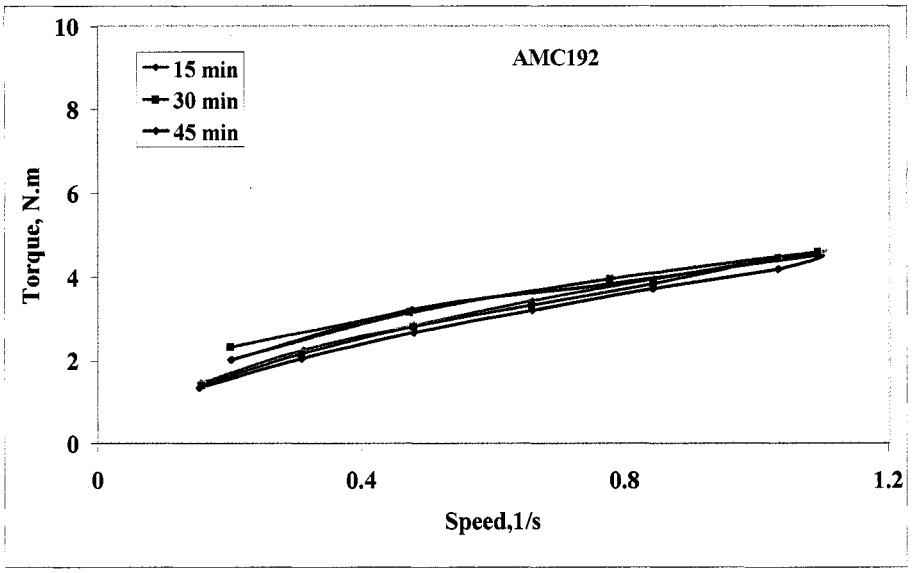

Figure 3.5. Torque vs. Speed curves w.r.t time for AMC castable containing 19 mm carbon fibre at 2 wt % loading.

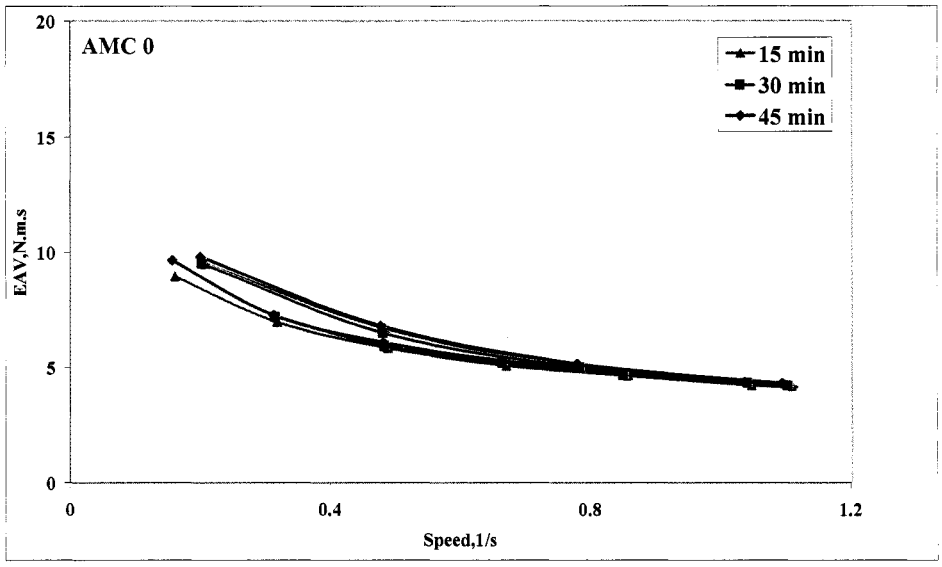

Figure 3.6. EAV vs. Speed curves w.r.t time for AMC castable containing 19 mm carbon steel fibre at 2 wt % loading.

3.2.1.1 Effect of fibre amount

Four different amounts (0, 2, 4, 6 wt %) of fibres have been used in this study. The influence of amount of steel fibre on the rheological behaviour of AMC 19 family is shown in Figure 3.7.

Though the rheological nature remains similar with fibre amount, the curves shifts upward with increasing fibre content. This is due to the increase of resistance to flow as well as viscosity of castable under shear. As the amount of fibre increases in the composite (decreasing matrix), the flow of matrix is hindered by varying shear, which results in an increase in torque value. Same kind of behaviour has been observed for

the other family of castables tested. (AMC 25, AMC 50 and AMC SS406--see Appendix B7 to B9 on pages 143-144).

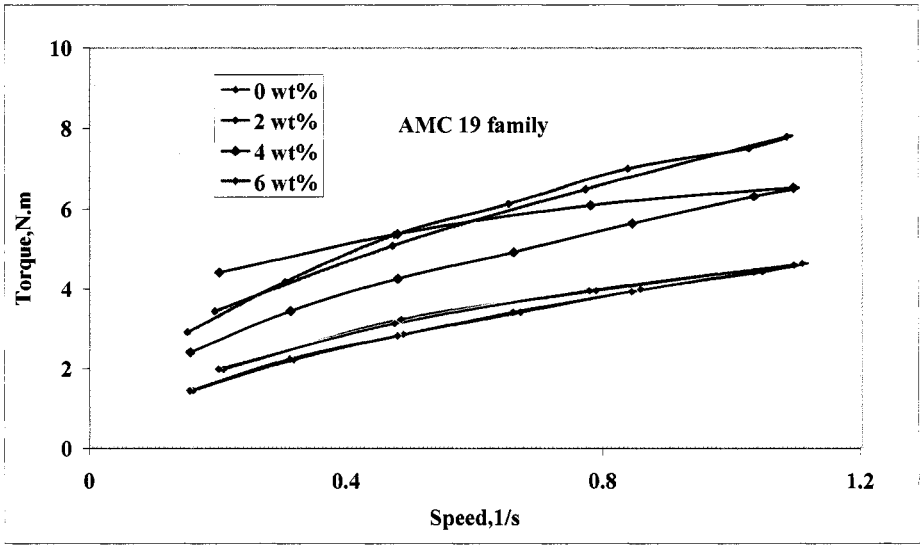

Figure 3.7. Torque vs. Speed curves w.r.t time for AMC castable containing 19 mm carbon steel fibre at 0, 2, 4, 6 wt % loadings.

An important observation in AMC50 family is that castable with 6 wt% fibre could not be tested due to enormous increase in resistance to flow of materials which is discussed in the following sections. Moreover, bending of fibres has been observed during the rheological test and causes problems for testing. This observation is referred as balling effect [16]. Basically when the fibre content exceeds a level, during mixing, fibres tend to bend and improve the coherency with the concrete. Practically it has been observed with 25 mm or 50 mm with 4 wt and 6 wt %, the castable tend to show bending effect.

3.2.1.2 Influence of fibre length

The influence of fibre length on the rheological behaviour is shown in Figure 3.8. Obviously, the increase of fibre length has affected the rheology drastically. Length, upto 25 mm does not show any drastic change in rheology, while the 50mm shows a clear demarcation in behaviour.

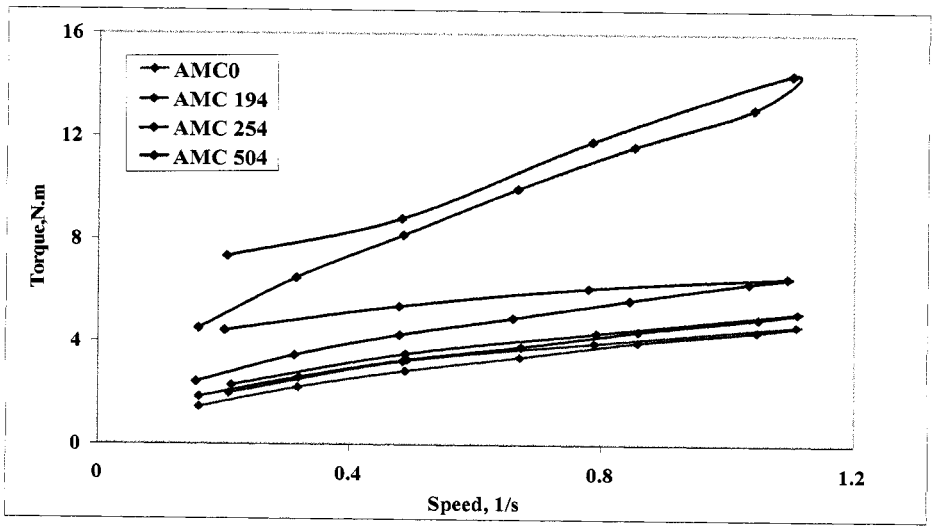

Figure 3.8. Torque vs. Speed curves w.r.t time for AMC castable containing 19, 25 and 50 mm carbon steel fibre at 2 wt % loading.

3.2.1.3 Influence of fibre type

The influence of fibre type on the rheological behaviour is shown in Figure 3.9. From the curve it is confirmed that both stainless and carbon steel fibres impart the same rheological behaviour, thus confirming that density variation in the fibres has little effect on rheology.

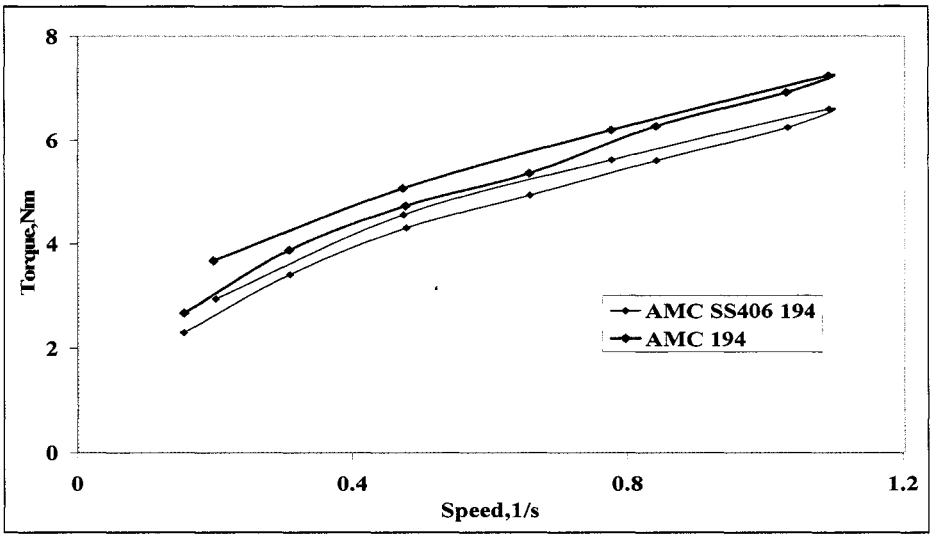

Figure 3.9. Torque vs Speed for AMC castable containing 19 mm stainless steel and carbon steel at 4 wt % loading.

3.2.2 Flow resistance (G) and Torque viscosity(H)

The values of G and H are shown for AMC 19 family of castables in Figures 3.10 and 3.11 respectively. As far as the rheological properties are concerned these two are playing a vital role for the workabibility of castable. From these two properties , it is possible to anaylsis whether a given castable is suitable for a particular application or not. In case of pumpable castable, a lower and upper values can be obtained after conducting trials.

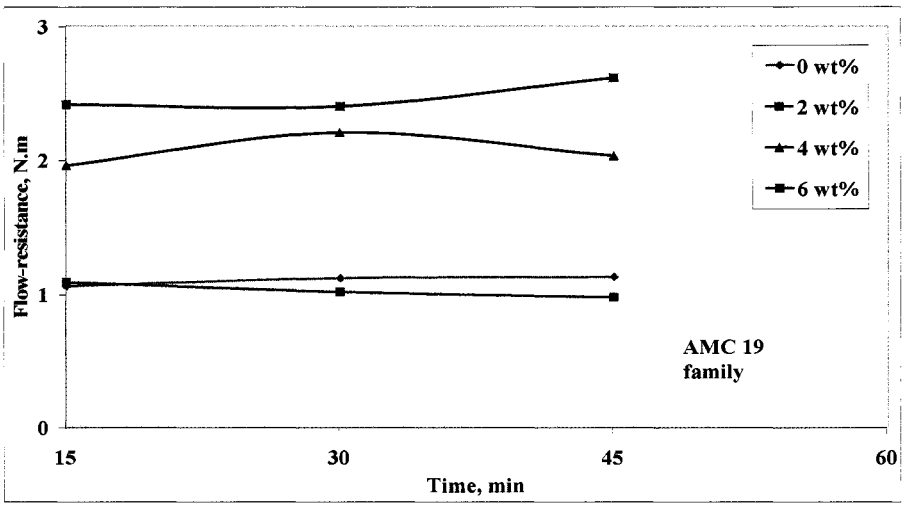

Figure 3.10. Flow- resistance vs Time curves for AMC castable containing 19 mm carbon steel fibre at 0, 2, 4, 6 wt % loadings.

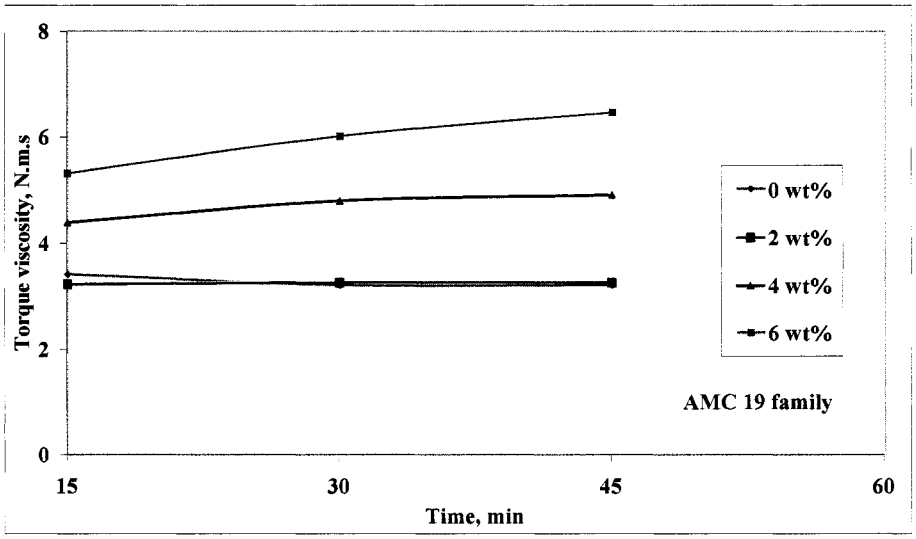

Figure 3.11. Torque viscosity vs Time curves for AMC castable containing 19 mm carbon steel fibre at 0, 2, 4, 6 wt % loadings.

The flow resistance of castable remains stable as a function of time. Similarly, the torque viscosity also remains almost stable with time for all fibre content. Increasing the fibre content to 2 wt% does not make any change in both G and H. Addition of steel fibre above 2 wt% causes at least a 2 fold increase in their values.

Similar kinds of observations have been made on other castable systems and are presented in Appendix B (see Figures B10-B15 on page-144-147). As can be seen from Figure B12, the castables with 6 wt% of 50 mm fibres are very rigid and rheometer test on them could not be conducted. The influence of fibre length is very drastic and is presented in Figure 3.12. Castables, even with 4 wt% of 50 mm steel fibres are very rigid after 30 min. On the other hand the influence of steel fibre type is negligible and the same is presented in Figure 3.13.

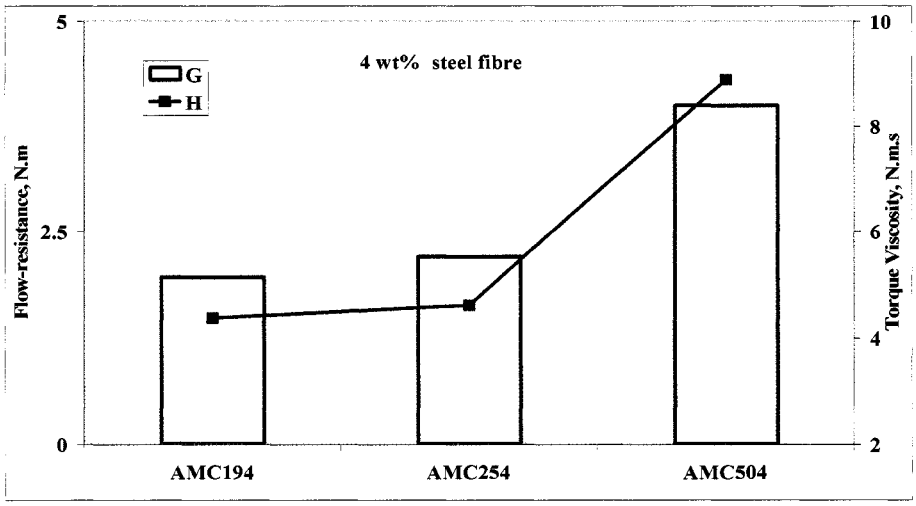

Figure 3.12. Influence of different lengths (19, 25, 50 mm) of carbon steel fibre flow resistance (G) and torque viscosity (H) at 4 wt % loadings.

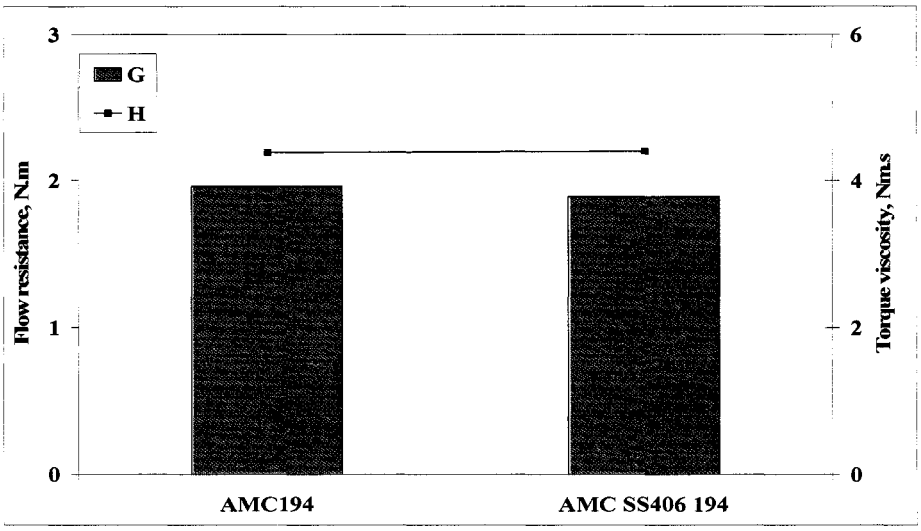

Figure 3.13. Influence of 19 mm fibres with 4 wt % loadings on flow resistance and torque viscosity.

The plot between torque viscosity and flow resistance is shown in Figure 3.14. This gives a clear indication of the influence of length and amount together in a box. The upper and lower limit of the values of G and H can be defined if the castables are pumped and evaluated.

It is observed that the castable AMC 504 and AMC 256 have very high rheological constants and are not suitable for pumping. The reason for such high flow resistance and torque viscosity can be understood from the fact that steel fibres are acting like needle like particles. The extent of the shape factor influence depends on the length of the steel fibre, its amount or combination of two.

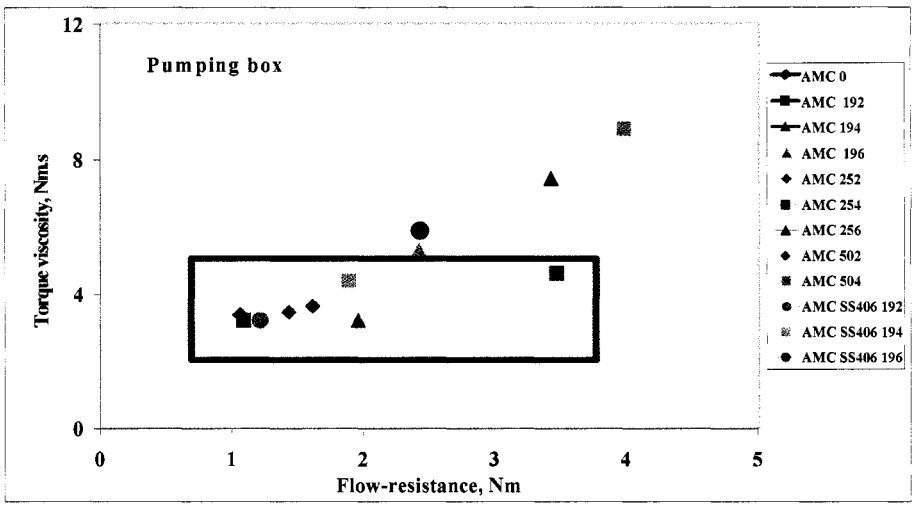

Figure 3.14. Torque viscosity vs. Flow-resistance of 19, 25, 50 mm lengths of carbon steel fibres and 19 mm length of stainless steel fibres at 0, 2, 4, 6 wt % loadings.

The rectangle box represents the formulation range suitable for pumpable castable. To confirm the same, further filed are required.

Based on the above discussion, it can be summarised as follows.

- The self-flowability of AMC decreases with both fibre content and length
- Variation of length effect is more influenced than that of amount. Care must be exercised while designing castable with fibre length of greater than 25 mm.

More specifically, the amount of fibre should not exceed 4 wt% when consider fibre length more than 25 mm.

- The rheological parameters, G and H show similar trends. Here also, the fibre length has shown more influence when the length exceed 25 mm.

- Fibres with similar length but of different type do not show any significant changes either in self-flow or rheology of castables.

CHAPTER 4. MECHANICAL PROPERTIES OF AMC CASTABLE

4.1 Effect of fibre addition

The wedge splitting test (WST) results of AMC 19 with plain castable (AMC 0) obtained at room temperature are shown in Figure 4.1 as force-extension curves. Similarly the test results obtained at 1100°C are shown in Figure 4.2. Here room temperature means that the WST was conducted after subjecting the samples at 110^0C/24 hr.

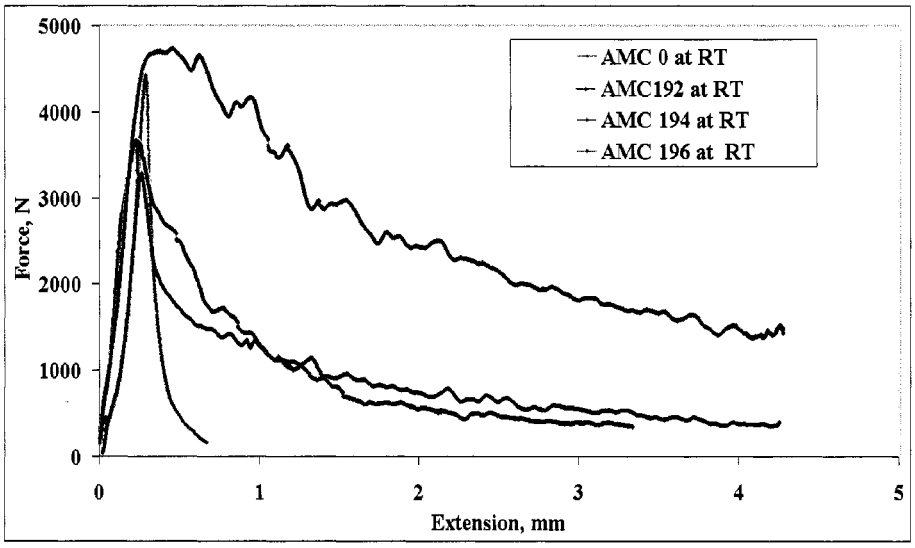

Figure 4.1. Force-extension curves of 19 mm carbon steel fibre reinforced AMC castables with 0, 2, 4, 6 wt % loadings at room temperature (after drying at 110°C/24 hr).

In Figure 4.1, the castable without fibre withstand more load but sample fails with very less extension. In case of AMC 192, the castable takes maximum load until matrix

fracture starts then the reinforcing effect comes into play (fibre bridging and pull-out effects). The post peak reinforcing effect is more pronounced with increasing fibre content from 0 to 6 wt%.

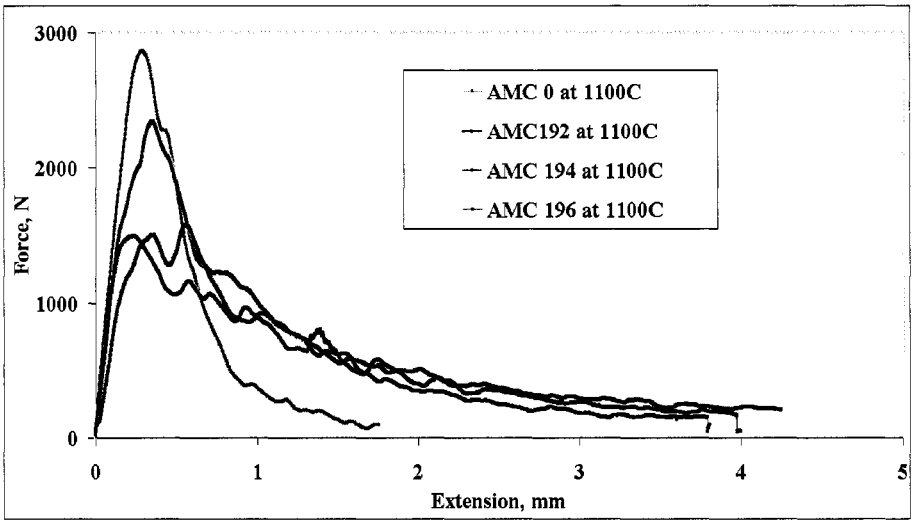

Figure 4.2. Force-extension curves of 19 mm carbon steel fibre containing AMC castables with 0, 2, 4, 6 wt % loadings at 1100°C.

Increase of fibre from 0 wt% to 2 and then to 4 wt% simultaneously decreases maximum force but increases the area under the curve. The possible reason for the strength decrease is the increase in defect with fibre addition in the structure. Again, at 6 wt% the maximum force recover to the original strength with simultaneous increase of area under curve. At 1100 °C, the area under force-extension curves is increasing for the fibre containing castable comparing them with AMC 0. Unfortunately, increasing fibre content does not bring any significant increase in area under curve as expected! This is a complex situation which can be understood only with the help of thorough

characterization of castable for interfacial microstructure, thermal expansion behaviour and oxidation of fibres under firing conditions. The wedge splitting test results of other family of castables AMC 25, AMC 50 and AMC SS 192 are presented in Appendix C (Figures C1-C6 on pages 148-150). In case of AMC 50 family of castables, the maximum force increases with increasing fibre content at room temperature but behaves in a similar way at 1100°C as that of other castables. SS406 family also increases maximum force with fibre content at room temperature but not at high temperature.In order to understand this behaviour clearly, the values of maximum force (F_{Hmax}) are plotted in Figure 4.3 and Figure 4.4

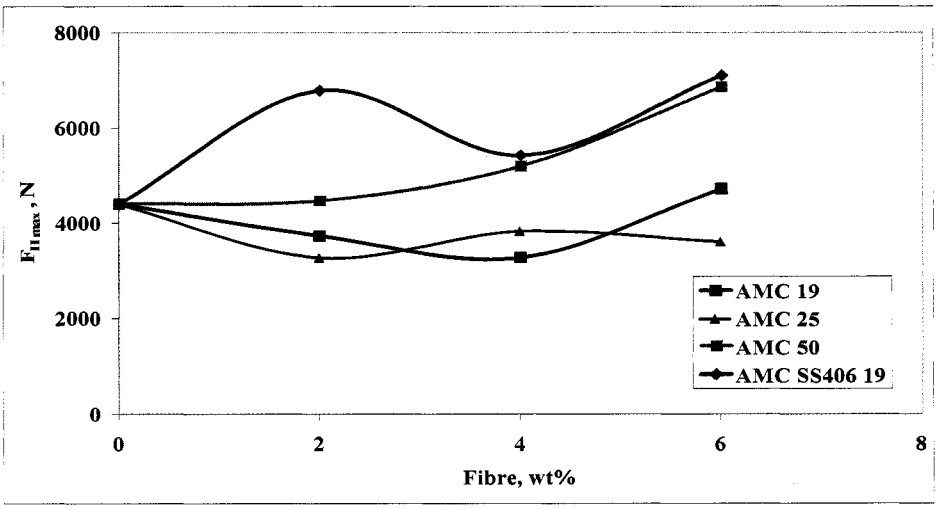

Figure 4.3. Variation of maximum force w.r.t fibre loadings (0, 2, 4, 6 wt %) of 19 mm stainless steel and 19, 25, 50 mm length of carbon steel fibre reinforced AMC castables at room temperature (after drying at 110°C/24 hr).

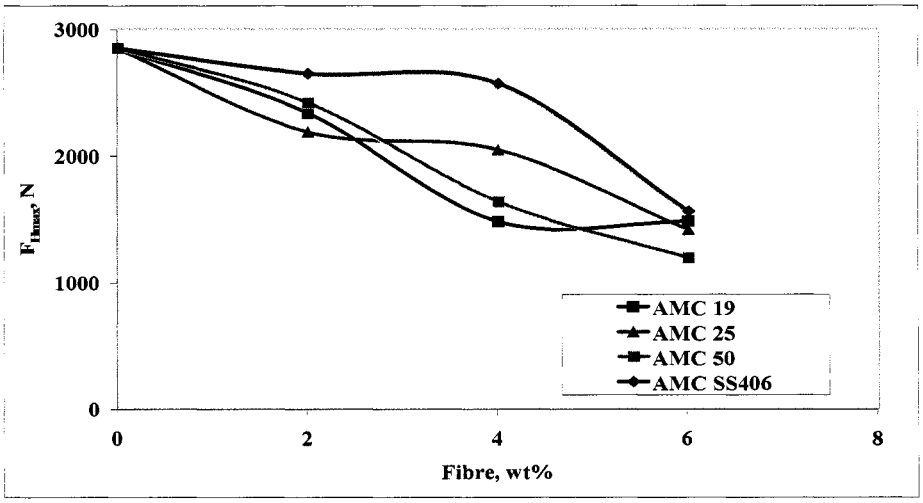

Figure 4.4. Variation of maximum force of 19 mm stainless steel and 19, 25, 50 mm length of carbon steel fibre reinforced AMC castables w.r.t different fibre loadings (0, 2, 4, 6 wt %) at 1100°C.

At room temperature, F_{Hmax} of AMC SS406 family of castables show maximum values than all other castables and also tend to increase with fibre content. This is followed by AMC 50 castables with similar trend. AMC 19 and 25 castables remains stable for all fibre content.

At 1100°C, the F_{Hmax} of all castables tend to decrease with fibre content. Even at high temperature, the F_{Hmax} of AMC SS406 is higher than all castables up to 4 wt%, though the difference is not very significant. At 6 wt% the values become almost similar for all castables.

4.2 Influence of Fibre Length

The effect of fibre length on the force-extension curves (wedge curves) of castables is shown in Figure 4.5 and 4.6

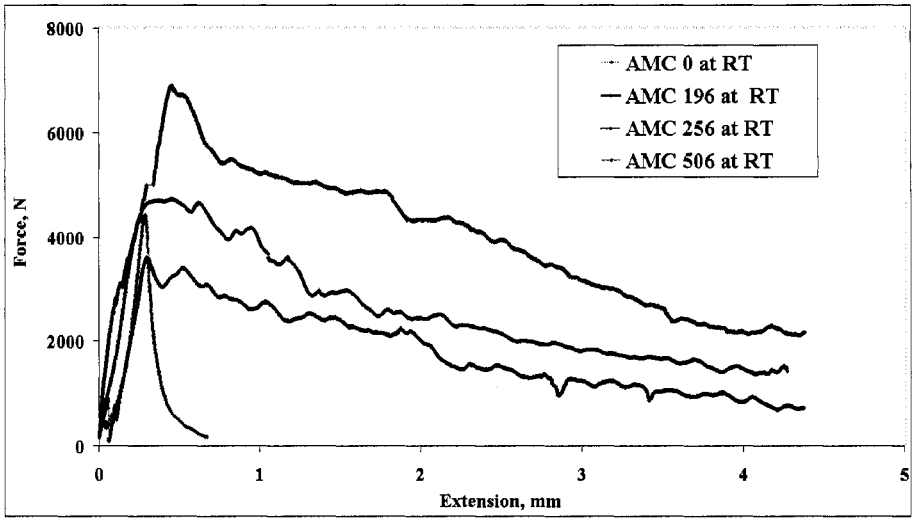

Figure 4.5. Comparison of force-extension curves of 0 and 6 wt % of carbon steel reinforced AMC castables with 19, 25, 50 mm length levels at room temperature.

The wedge curves at 6 wt% fibre content (Figure 4.5), of different lengths are compared at room temperature. Though, AMC 19 and AMC 25 are behaving almost similar way or with insignificant difference, AMC 50 has shown clear demarcation in toughness behaviour. This can be attributed to the better bridging effect of fibre with increased length. Similar results are observed with different amount and are shown in Appendix C (see Figures C7-C10 on pages 151-152).

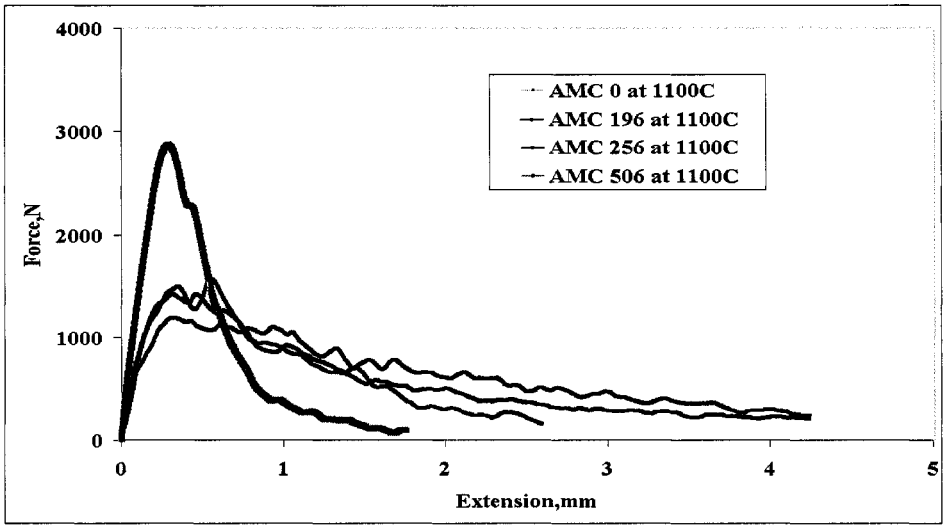

Figure 4.6. Comparison of force-extension curves of 0 and 6 wt % of carbon steel reinforced AMC castables for 19, 25, 50 mm length at 1100°C.

At high temperature (Figure 4.6), the behaviour is similar with all lengths. Again, the effect of length is overcome by temperature and micro structural effects.

4.3 Effect of fibre type

The influence of fibre type on the behaviour of castables is shown in Figures 4.7 and 4.8. Other results are presented in Appendix C (see Figures C11-C14 on pages 153-154). At room temperature, it is observed that the area of SS fibre is more important compared with CS fibre at 19 mm length. At 1100°C, the difference is getting reduced.

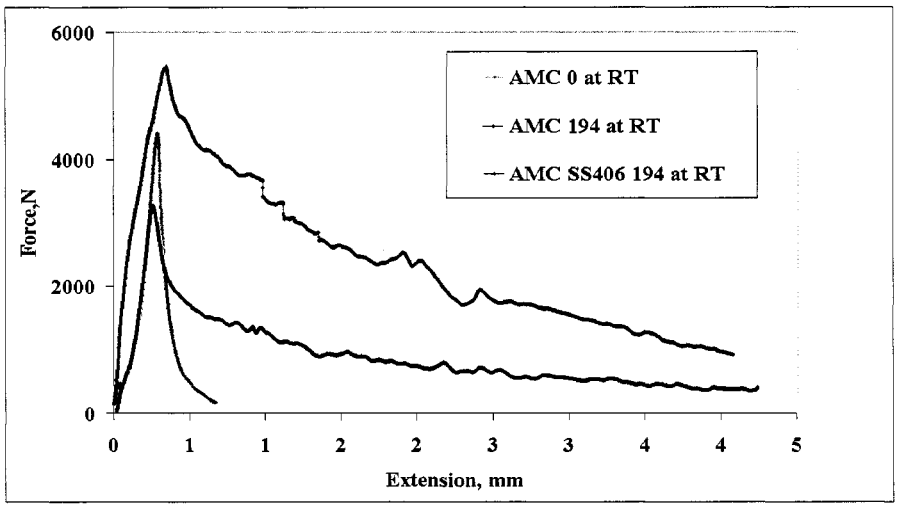

Figure 4.7. Comparison of force-extension curves of 19 mm stainless steel and 19 mm carbon steel fibre reinforced AMC castables with 0 and 4 wt % loadings at room temperature.

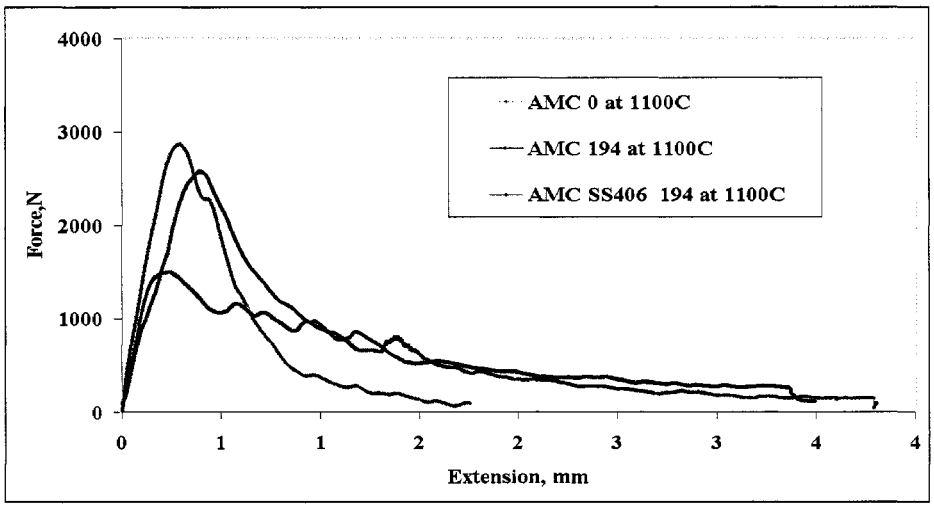

Figure 4.8. Comparison of force-extension curves of 19 mm stainless steel and 19 mm carbon steel fibre reinforced AMC castables with 0 and 4 wt % loadings at 1100°C.

4.4 Work of fracture (γ_{wof})

Work of fracture values of all castables calculated from equation 2.10 are plotted in Figure 4.9 and Figure 4.10 for room temperature and 1100°C respectively.

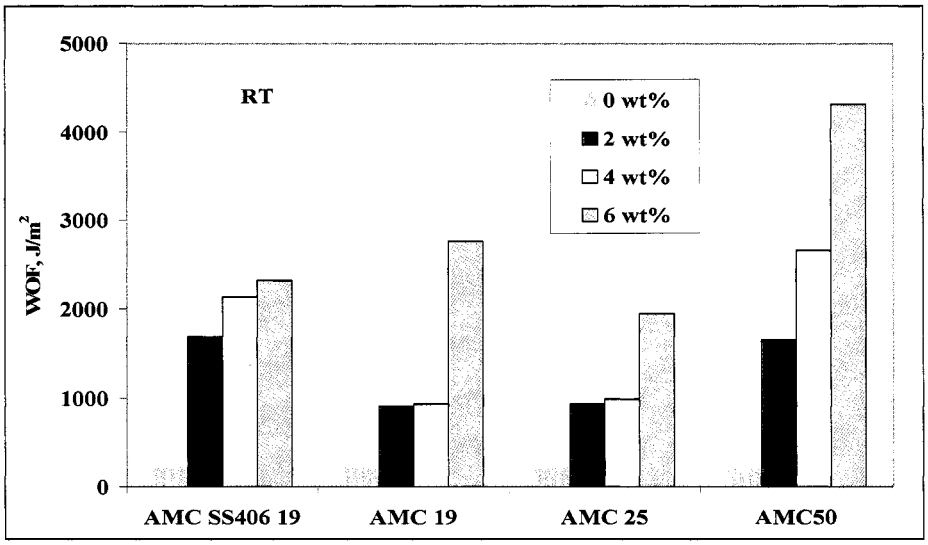

Figure 4.9. Comparison of work of fracture values of 19 mm stainless and 19, 25, 50 mm length of carbon steel reinforced AMC castables with 0, 2, 4, 6 wt % loadings at room temperature.

From Figure 4.9, it is clear that at room temperature, the castables with fibres display more γ_{wof} compared to no fibre castable. The influence of amount and length is highly felt on γ_{wof} for AMC SS046 and AMC 50 family of castables. The fibres are intact and not degraded by any means such as temperature and microstructure changes, etc.

The γ_{wof} of castable at 1100°C is improved with fibre addition but it does not change much with fibre amount and length and the values are almost similar in all cases except

AMC 50. Though, values of AMC 50 increases with fibre amount, the maximum value at 6 wt% is not higher than other castables. An important point to be noted here is that the castables containing stainless steel fibre (SS406) does not show any special improvement when compared to carbon steel fibres.

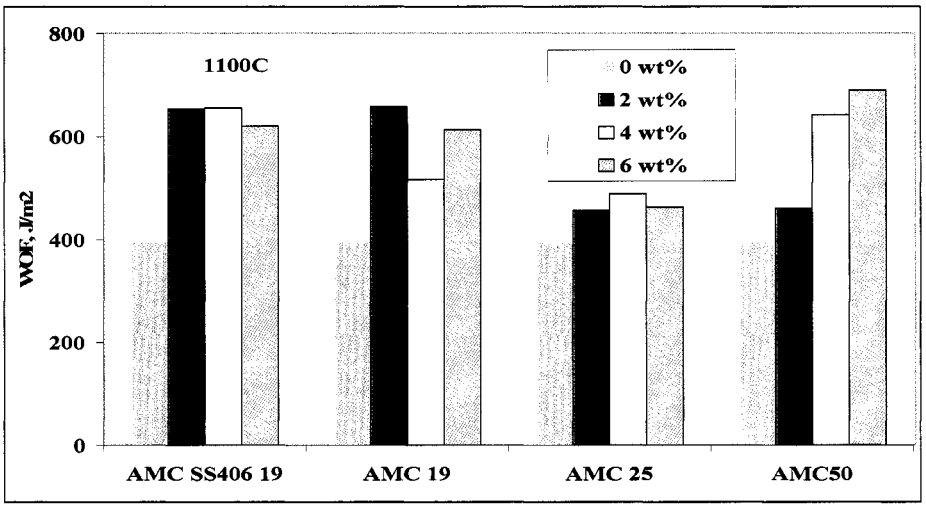

Figure 4.10. Comparison of work of fracture values of 19 mm stainless and 19, 25, 50 mm length of carbon steel reinforced AMC castables with 0, 2, 4, 6 wt % loadings at 1100°C.

When 2 wt% of fibre is added to the castables, the work γ_{wof} is improving due to composite mechanisms. When the amount is increased to 4 or 6 wt% the influence is dissipated.

4.5 Fracture toughness (K_{IC})

The K_{IC} values are calculated from the equation 2.8. The calculated values are presented in Figures 4.11 and 4.12.

In Figure 4.11, at room temperature, the K_{IC} values remains almost similar for AMC 19 and AMC 25 castables. A marked improvement is observed in case of AMC SS406 and AMC 50. At 1100°C (Figure 4.12), the case is totally reverse. The K_{IC} values decreases with fibre addition. Castable with stainless steel fibre tend to maintain the K_{IC} values up to 4 wt% but looses the trend at 6 wt%.

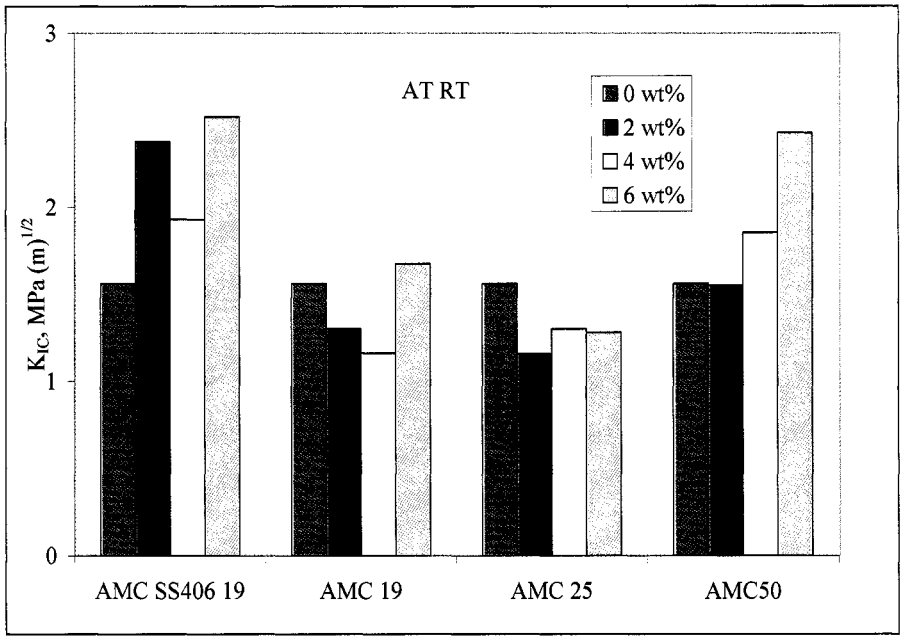

Figure 4.11. Comparison of fracture toughness values of 19 mm stainless and 19, 25, 50 mm lengths of carbon steel reinforced AMC castables with 0, 2, 4, 6 wt % loadings at room temperature.

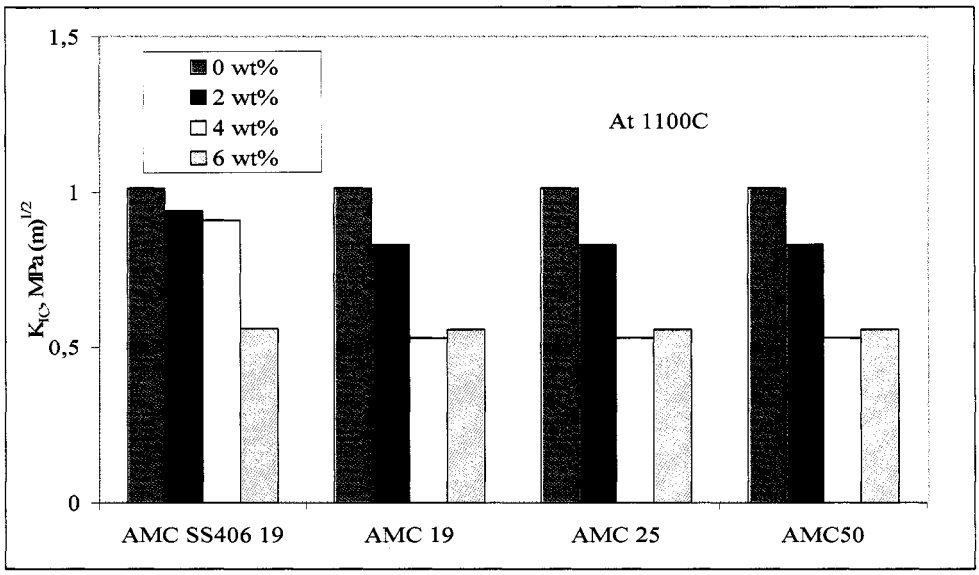

Figure 4.12. Comparison of fracture toughness values of 19 mm stainless and 19, 25, 50 mm length of carbon steel reinforced AMC castables with 0, 2, 4, 6 wt % loadings at 1100°C.

4.6 Hot modulus of rupture (HMOR)

The HMOR data of AMC 19 castables are presented in Figure 4.13. In figure 4.13 it is observed that the HMOR of AMC 0 is reduced slightly at 800°C and then shows an increase at 1100 ^{0}C. The trend is similar to all other castables with an enhanced dip at 800°C. The HMOR values of all the castables with fibre are lesser than AMC 0 at all temperature. The slight dip at 800°C for AMC 0 corresponds to the loss of bond in the structure. The increase in HMOR values at 1100°C is due to contribution from spinel formation. The increment in the dip for fibre containing castables may be attributed to

the formation of structural defects due to the fibre addition. The increase in HMOR values at 1100°C is due to contribution from spinel formation. Similar trends are observed with all castable systems and are presented in Appendix D (see,Figures D1-D4, on pages 155-156). The influences of length and type of fibres on hot strength are seen in Figure 4.14 for AMC reinforced with 6 wt % of fibres. There is no appreciable change in HMOR values with respect to length, but stainless steels maintain higher strength level than AMC with carbon steel fibres.

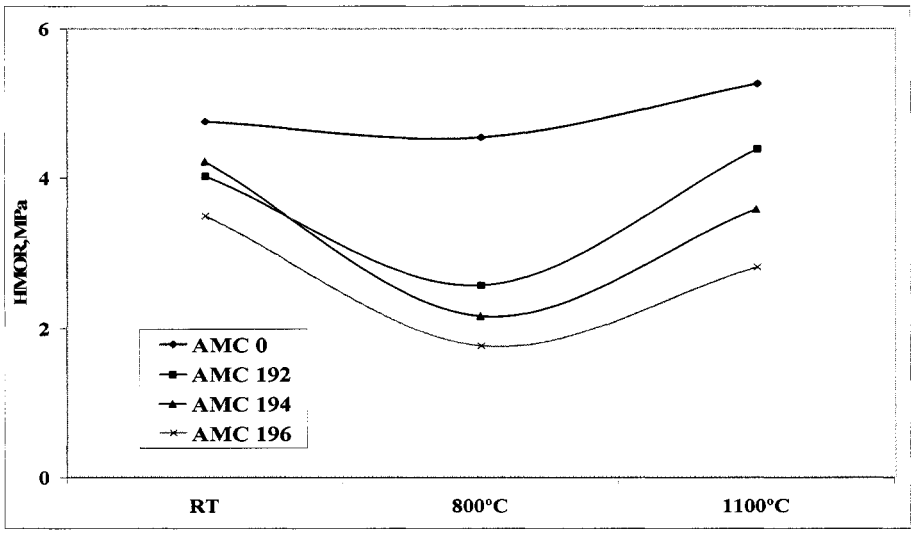

Figure 4.13. Variation of hot modulus of rupture w.r.t. temperature for 19 mm carbon steel fibre reinforced AMC castables with 0, 2, 4, 6 wt % loadings.

At room temperature, as the fibre length increases, value of modulus of rupture drops down. The extent of drops down is more at 800°C compared with room temperature

and at 1100 ^{0}C. Modulus of rupture value drops down is influenced by both fibre amount and temperature.

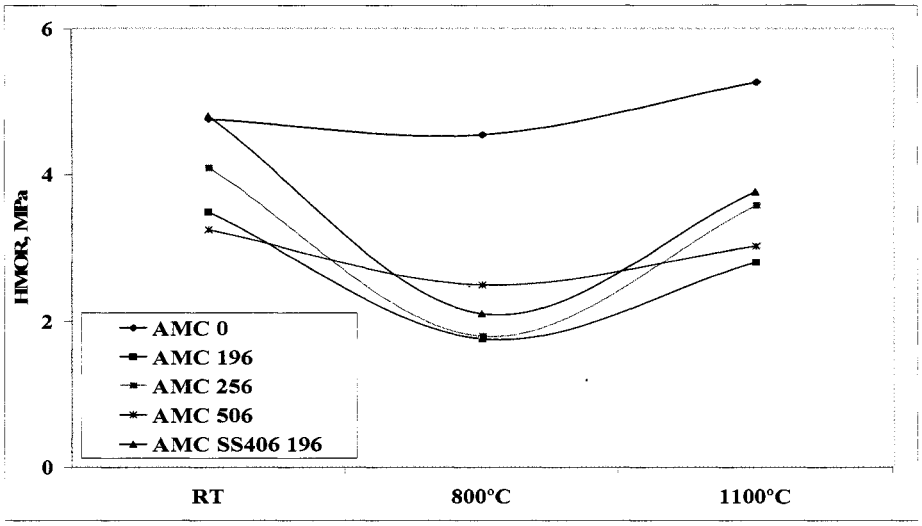

Figure 4.14. Comparison of hot modulus of rupture values of 0 and 6 wt % carbon steel fibre and 0 and 6 wt % stainless steel reinforced AMC castables at different temperatures.

4.7 Physical properties bulk density (BD), apparent porosity (AP) and permanent linear change (PLC)

The BD values of AMC 19 castables are shown in Figure 4.15. The BD remains almost the same at 110°C with an expected slight increase as wt % of fibres increases. At 800 ^{0}C and 1100°C the BD decreases due to increase in porosity of the castables as shown in Figure 4.16. The trend is similar for all castables system as shown in Appendix D (see Figures D5-D10, pages, 157-159). Comparisons of AP values are presented in Figure 4.17.

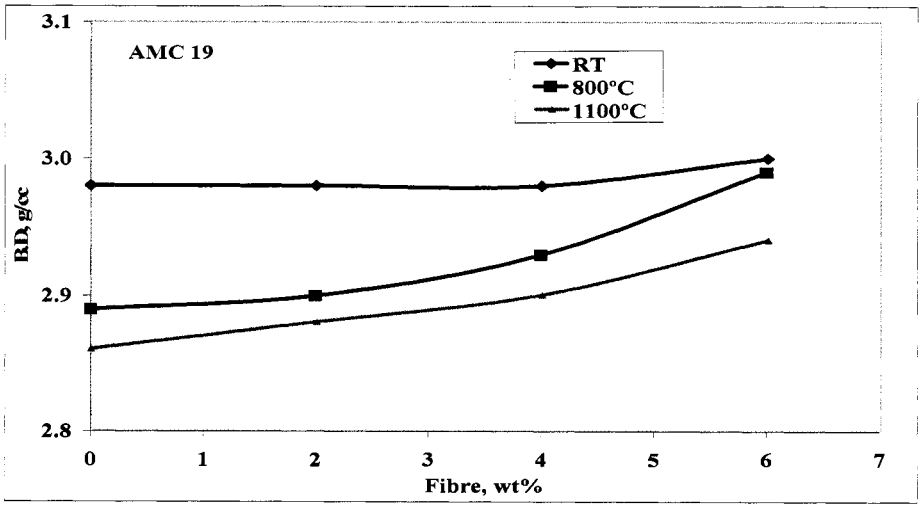

Figure 4.15. Variation of bulk density w.r.t different fibre loading (0, 2, 4, 6 wt %) of 19 mm carbon steel fibre reinforced AMC castables at different temperatures.

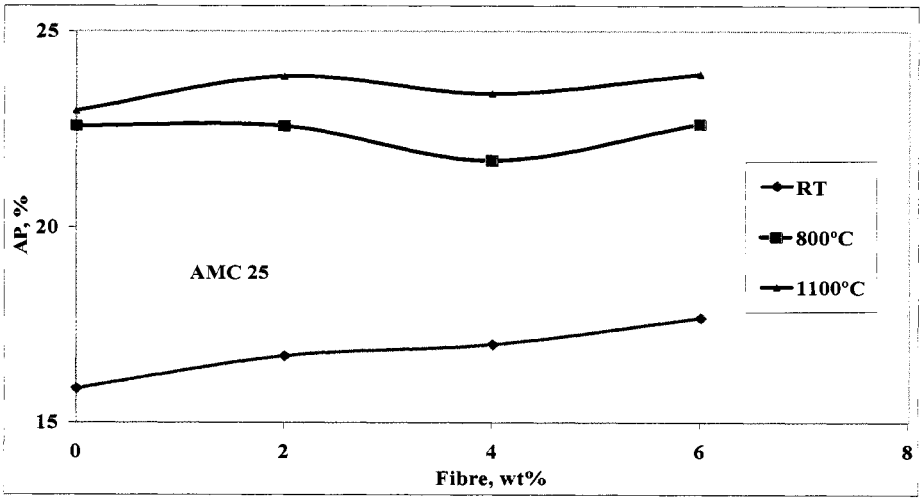

Figure 4.16. Variation of apparent porosity w.r.t fibre loading (0, 2, 4, 6 wt %) for 25 mm length carbon steel fibre reinforced AMC castables at different temperatures.

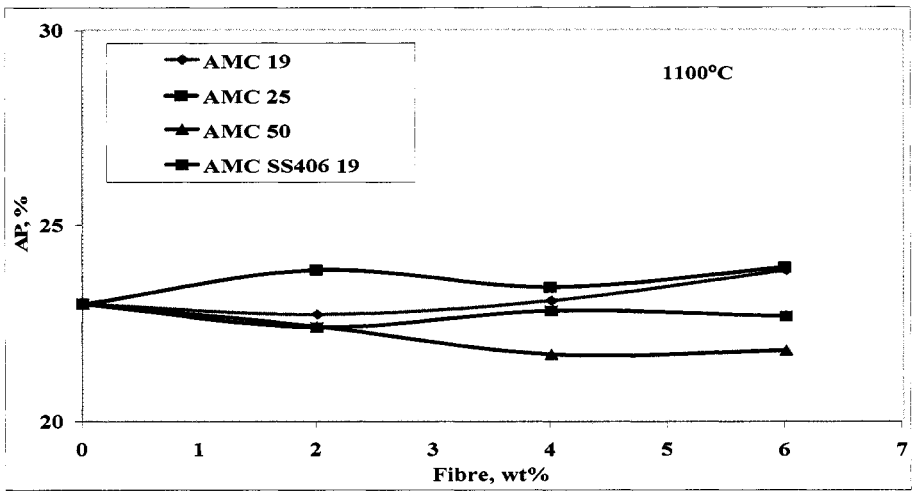

Figure 4.17. Variation of apparent porosity w.r.t fibre loadings (0,2, 4, 6, wt%) for 19 mm length stainless steel and 19,25 ,50 mm lengths carbon steel fibre reinforced AMC castables at 1100^0C.

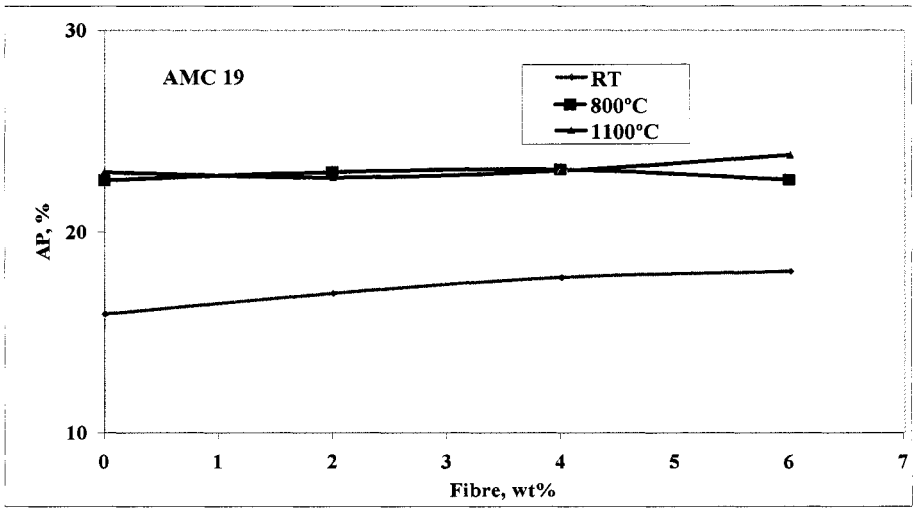

Figure 4.18. Variation of permanent linear change of 19 mm carbon steel fibre reinforced AMC castables w.r.t fibre loadings (0, 2, 4, 6 wt%) at different temperatures.

The PLC of castables is a mere indication of micro structural changes. In Figure 4.18 there is no change in the PLC of AMC 19 with all fibre content at 110 and 800 ^{0}C. At 1100°C, the PLC of castables increases drastically. This is due to the formation of in-situ spinel at 1100^0 C. The PLC results at 4 and 6 wt% of fibre content are not significant. The PLC in case of AMC 25 and AMC 50 (see Appendix D Figures D11-D13 on pages 160-161) remains stable or slightly increases with fibre content up to 4 wt% but shows significant shrinkage at 6 wt%. Increasing length restricts the expansion of castable due to spinel formation. PLC data is compared for length in Figure 4.19. The spectrum is scattered up to 4 wt% but shows clear ordering at 6 wt% showing the importance of fibre length in PLC.

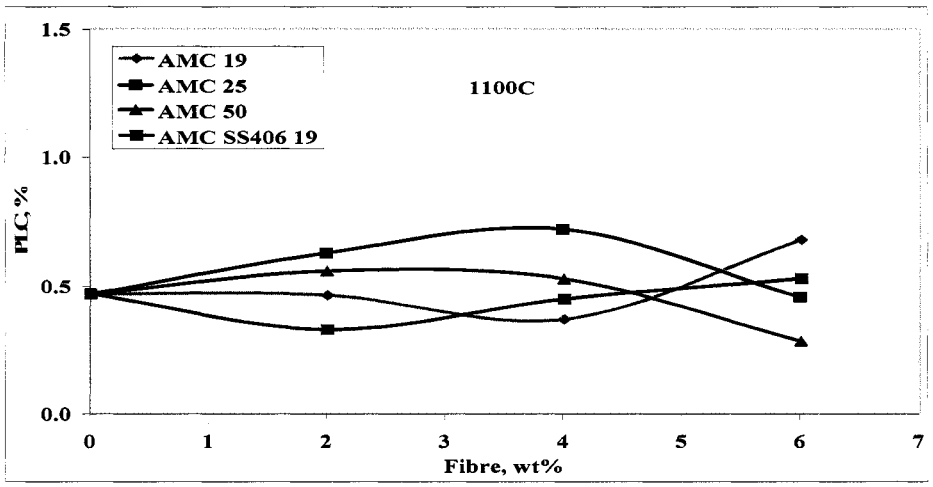

Figure 4.19. Variation of permanent linear change of 19, 25, 50 mm carbon steel fibre and stainless steel fibre reinforced AMC castables w.r.t fibre loadings (0, 2, 4, 6 wt %) at 1100°C.

4.8 Modulus of elasticity (MOE)

The MOE of the all cast samples at room temperature, (Figure 4.20) remains almost similar and the values are not influenced significantly by fibres addition, even though there is a significant difference in MOE values of fibre and castable materials taken separately. For an effective load – transfer, fibre should have higher modulus of elasticity value than that of matrix.

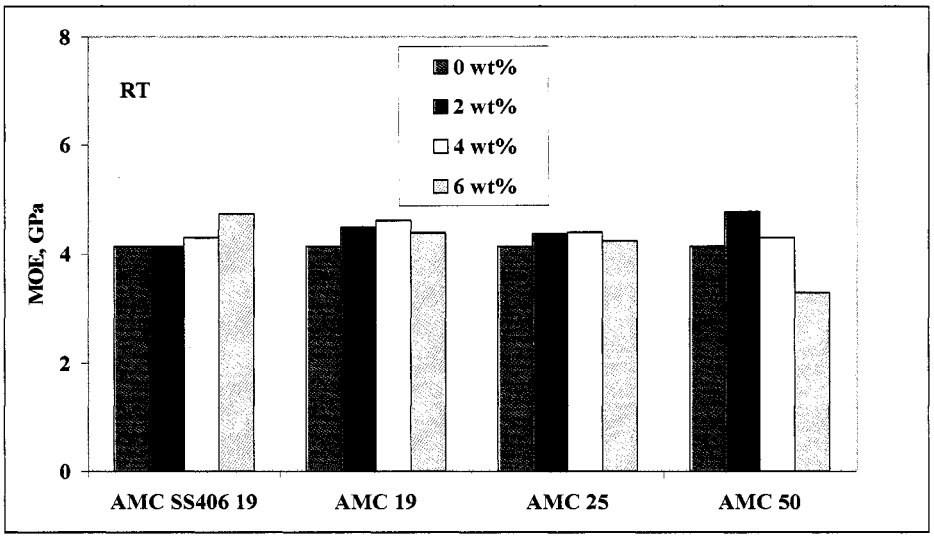

Figure 4.20. Comparison of modulus of elasticity values of 19 mm stainless and 19, 25, 50 mm lengths of carbon steel reinforced AMC castables with 0, 2, 4, 6 wt % fibre loadings at room temperature.

The MOE values (Figure 4.21) at 1100°C is decreasing with fibre content. This is the results of structure with enhanced defects. Modulus of elasticity is calculated from the linear portion of force-extension curve.

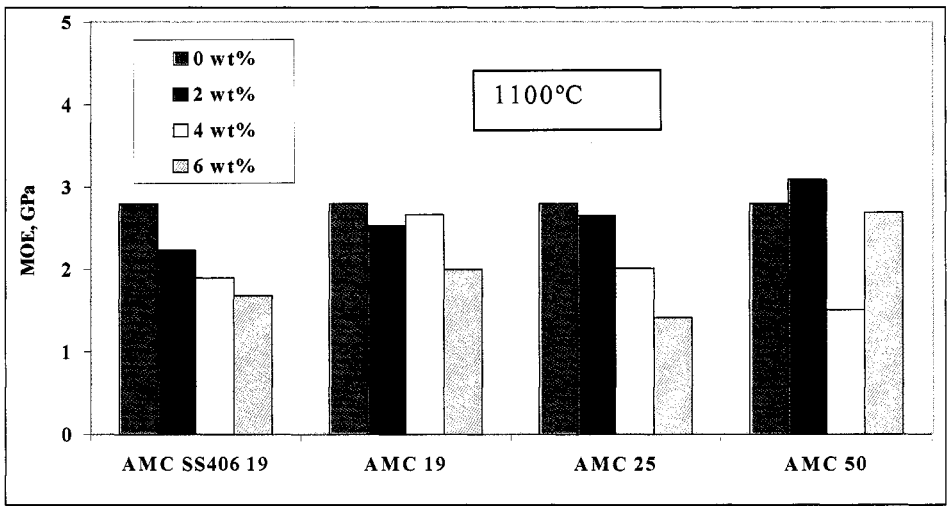

Figure 4.21. Comparison of modulus of elasticity values of 19 mm stainless steel and 19, 25, 50 mm length of carbon steel reinforced AMC castables with 0, 2, 4, 6 wt % fibre loadings at 1100°C temperature.

The relationship between AP and MOR as a function of fibre content for AMC 19 is shown in Figure 4.22. The relationship between AP and WOF as a function of fibre content for AMC 19 at 1100^0C is shown in Figure 4.23. The WOF value increases with the addition of fibre but does not change in accordance with length and amount while the value of AP is almost the same for all the fibre contents.

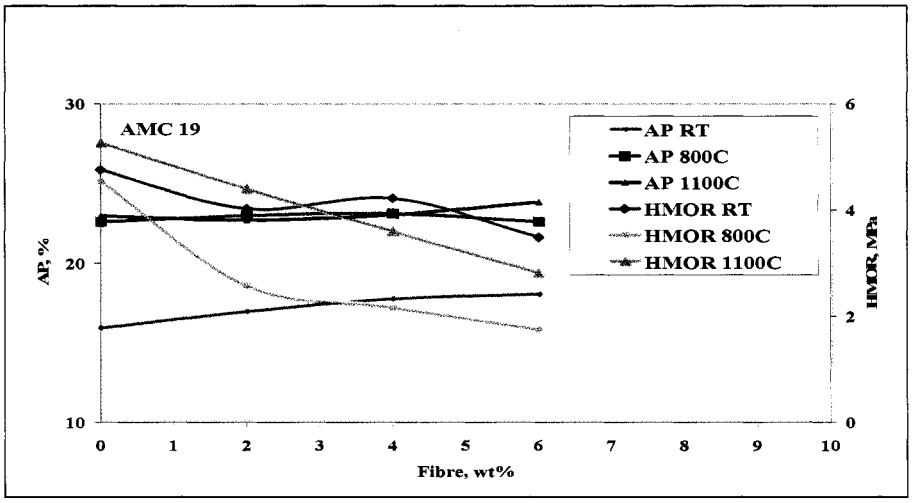

Figure 4.22. Variation of apparent porosity, modulus of rupture value of 19 mm carbon fibre reinforced AMC castable at different fibre loadings (0, 2, 4, 6 wt %) and at temperatures (RT, 800 and 1100°C).

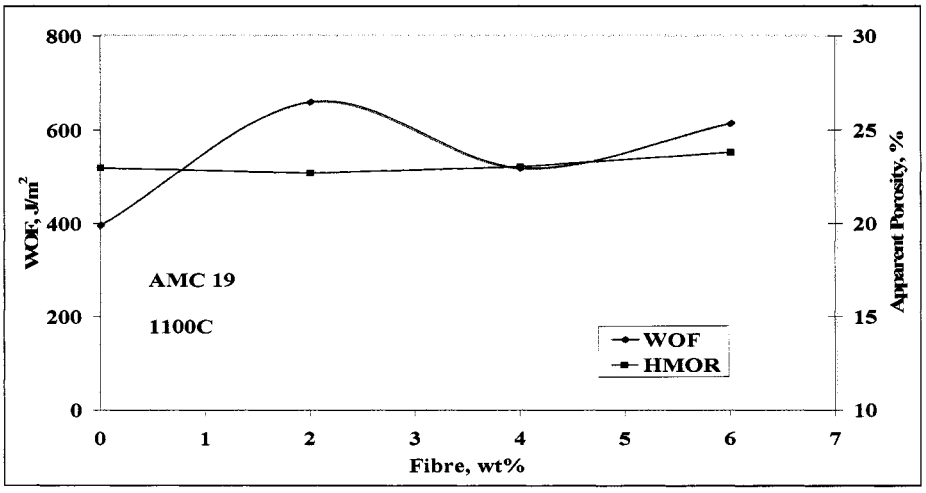

Figure 4.23. Variation of work of fracture and apparent porosity of 19 mm carbon reinforced AMC castables w.r.t fibre loading (0, 2, 4, 6 wt %) at 1100°C.

CHAPTER 5. ANALYSIS OF RESULTS

The results presented in the sections 4.1 to 4.8, have to be discussed together for structure property correlation. The basic objective of this work was to improve and verify if work of fracture (γ_{wof}) of the AMC system is improved by steel fibres reinforcement. As shown previously in Figures 4.1 and 4.9, the force-extension curves can be approximated by two segments. The first segment represents the pre peak region and the second post peak region. The first segment is further divided in to two parts. The first part is associated with linear pre-cracked matrix and the second one is with non-linear cracked matrix. During the first part, all the castables, irrespective of fibre content, show similar trends. The reason is quite obvious since during that segment, deformations are governed by the modulus of elasticity (MOE) of the matrix. In the second part the elongations are dictated by the properties of the fibres. The peak force represents the ultimate strength of composite and is caused by fibre failure [31]. The tail end of the curve corresponds to the pull out of broken fibres and is purely determined by frictional force.

In the second segment region, fibre containing castables show marked difference in their behaviour in comparison with no fibre containing castable (AMC0). This can be explained in terms of difference in toughening mechanisms which exist in the castable systems. For AMC 0, the behaviour is purely due to aggregate bridging effect and that for reinforced AMC is due to both aggregate and fibre bridging effects. This indicates that the extent of bridging is much more pronounced with fibre. As can be seen from

the value of work of fracture (Figure 4.9) and from the force-extension curve (Figure 4.1), the extent of bridging effect varies in accordance with fibre amount and length. Results of AMC SS406 19 and AMC 50 families of castables confirm the same. As the fibre amount increases, the area of interfaces per unit volume increases which in turn impart more fibre debonding and pull out resistance processes. Length factor can be explained in terms of the load carrying capacity. As the length of the fibre decreases the load bearing capacity of the fibre decreases since the ends of the fibre are partially loaded. But length and amount factor is absent in the case of AMC 19 and AMC 25 family of castables. This scatter in results is due to the bending effects of fibres during mixing stage. Fibre shape prior to mixing is shown in Figure 5.1. The fibres with bending position are illustrated in Figures 5.2.

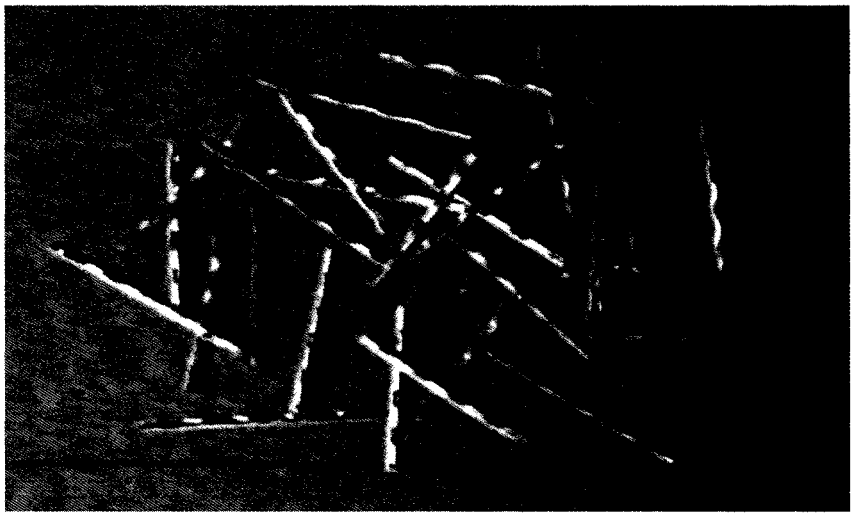

Figure 5.1. Steel fibre used (Wavy type)

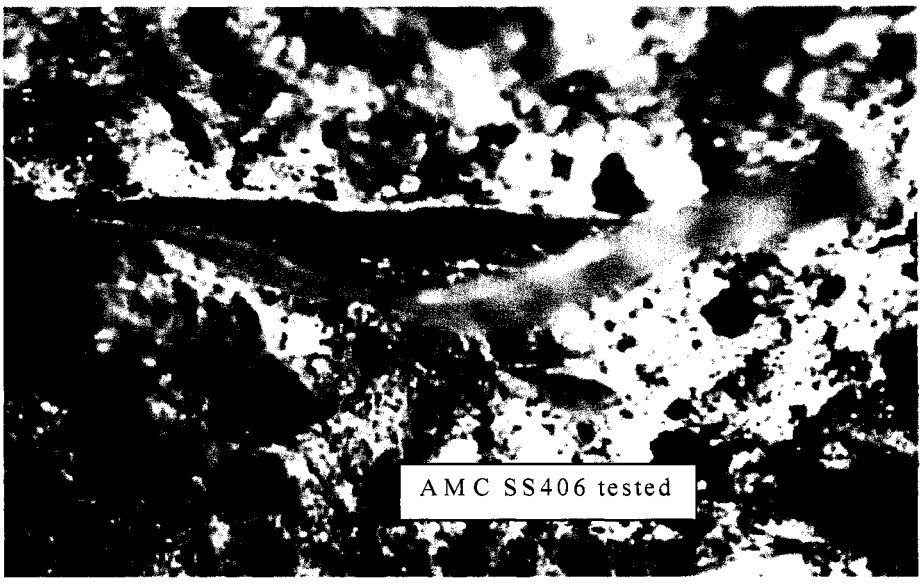

Figure 5.2. Optical microstructure of AMC SS406 254(X10)

During mixing, due to shearing action of paddle mixer and coarse aggregates, the needle like fibres got bend. The distribution of fibres is shown in figure 5.3.

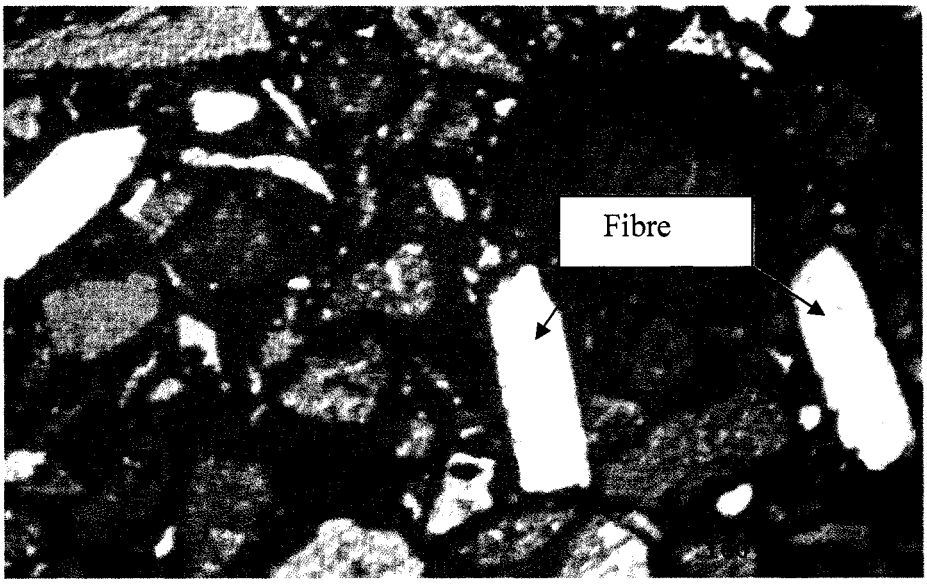

Figure 5.3. Distribution of fibre 254 (X 100)

From Figure 4.7, it is observed that the SS fibres tail end behaviour is some what different from the carbon steel (CS fibre) fibres. SS fibres have influenced the force-extension curve in such a way that after debonding process, pull out curves show an upward shift in comparison with carbon steel fibre i.e. force-extension curve moves upward in case of stainless steel during the second segment region after debonding .The probable reason could be that stainless fibres might have more roughness values than that of carbon steel. Because of these higher values of roughness, the frictional force between the fibre and the matrix also increases. This frictional force changes the interface morphology of the castable and as a result SS fibre regions shifted up. But still experimental validation through roughness measurement, by profilometry or atomic force microscopic methods, is required to confirm the same.

Regarding the maximum force F_H value (Figure 4.3) is concerned, at room temperature its value swings in centre with AMC0 castable. Except for AMC SS406 and AMC 19 families, a scattering of results is observed with respect to fibre content. The peak force value is indicative of composite failure due to fibre fracture and is determined by the rule of mixture law. At room temperature the tensile strength of the steel fibre [61] is much higher than that of castable. By the introduction of fibres, the over all strength of the composite gets enhanced. This explains higher values of peak force obtained for fibre containing castable as compared with no fibre castables. Quite naturally as the volume fraction of fibres increases, the peak force would also increase. At 1100°C (Figure 4.4), all the castables indicate a declining a trend which is due to degradation

of fibre strength at high temperature. The addition of fibres to AMC castable (Figure 4.10) results in the improvement of work of fracture at 1100°C in comparison with no fibre castables. Within the group of fibre containing castables, a scattering of results is observed with respect to increase in length and amount i.e. work of fracture value does not change in accordance with length and amount of fibres. The test results of work of fracture value of fibre containing castables at high temperature have shown a decreasing trend in comparison with room temperature (110°C). But in the case of AMC0 castable, the temperature effect has resulted in the enhancement of the work of fracture. The reason for such a distinct behaviour is due to reinforcing effect of extruded graphite pellets and higher level of porosity at 1100°C, extruded graphite pellets acting like short fibres and causing bridging effect in the matrix. As can be seen from figure 4.22, the value of apparent porosity at high temperature increases to 23 % as compared to room temperature of value of 16 %. The change in porosity levels at 1100°C is due to the dehydration of calcium aluminates hydrated crystals and also from the expansion characteristic of spinel which formed through the reaction between alumina and magnesia. Porosity acts as a discontinuity or defective structure in the matrix and obstructing the propagation of cracks. This is a well known toughening mechanism in ceramics and cementitious materials [32].

Reduction of work of fracture values for reinforced AMC castables at 1100°C, as compared to that at room temperature, can be explained in terms of interfacial bonding and high temperature properties of fibre and matrix. At room temperature, two

mechanisms such as adhesive (hydraulic) and frictional bondings are responsible for the interfacial characteristics of cementitious materials [82]. As the AMC X castable is subjected to high temperature, progressive dehydration of hydrated calcium aluminate (HAC) takes place. At 1100°C, virtually there is no chance for hydrated cement phases to be present in the castables. As a result of this, there is an absence of adhesive (hydraulic) bond between fibre and matrix at high temperature and bond changes into chemical in nature. The spinel formation confirms the onset of solid state reaction through diffusion at 1100°C.

In addition with the interfacial bond mechanisms, the fibre characteristics also changes with temperature. The Figures 5.4 to 5.6 show SEM microstructures of carbon steel fibre (CS) reinforced castables after 1100°C on a wedge splitting test sample. The fibre pull out region is indicated by the arrow mark. At a higher level of magnification, a very thin layer of scale formation has been noticed on the fibre pull out bed. This scale formation is due to the surface oxidation of carbon fibre at high temperature. Normally CS fibres undergo rapid oxidation at 500°C and this oxidation cause embritllement of the fibres. As the sample was tested under Ar atmosphere, the presence for the oxygen is restricted to the amount of air entrapped in the castables.

As per the classical theory, the oxidation of iron consists of three layers in the temperature range of 700-1250°C. The inner most layer is with lowest oxygen content

wustite phase (FeO), the intermediate layer with magnetite (Fe_3O_4) and an outer layer with hematite Fe_2O_3 [79].

It appears from the micrograph that this scale might have adhered with the matrix. As can be seen from the Figures 5.7-5.10, interfacial cracks are formed at interface for both (SS) stainless steel and (CS) carbon steel fibres. The same kind of microstructure was observed by T.Cutard et al [69] and they quoted that while cooling castables at 500°C, thermal expansion mismatch between fibre and matrix leads to compressive radial stress fields at the interface which lead to decohesion region.

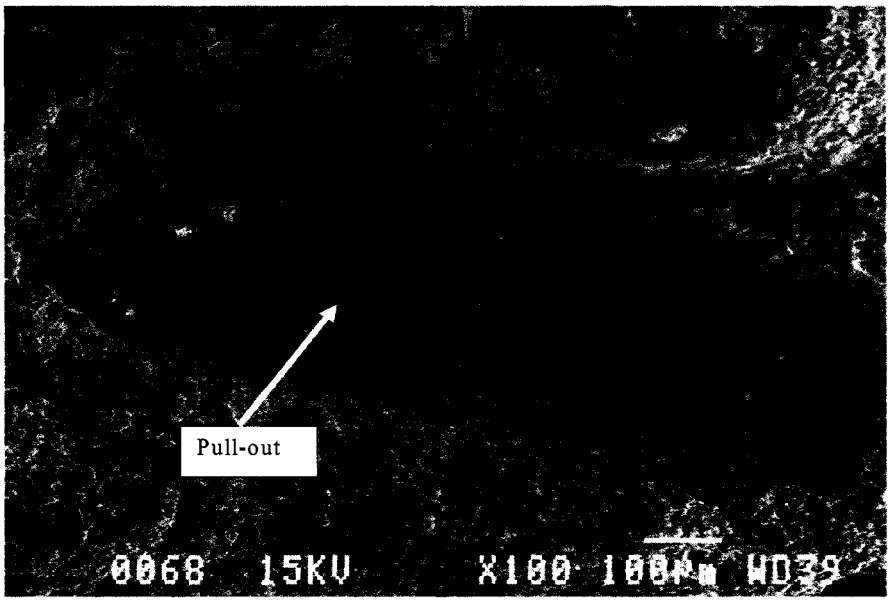

Figure 5.4. Fracture surface of AMC 254

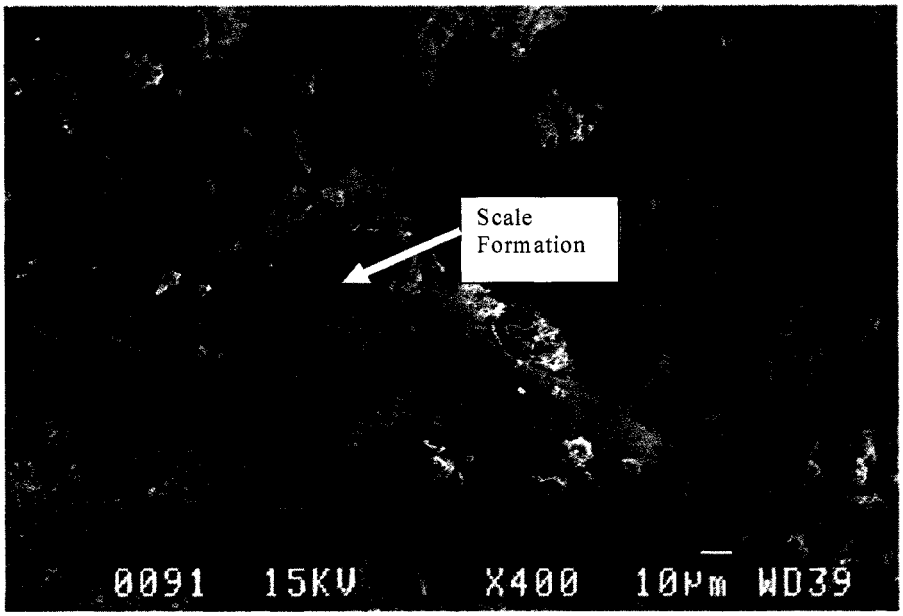

Figure 5.5. Fracture surface of AMC 254 showing scale formation.

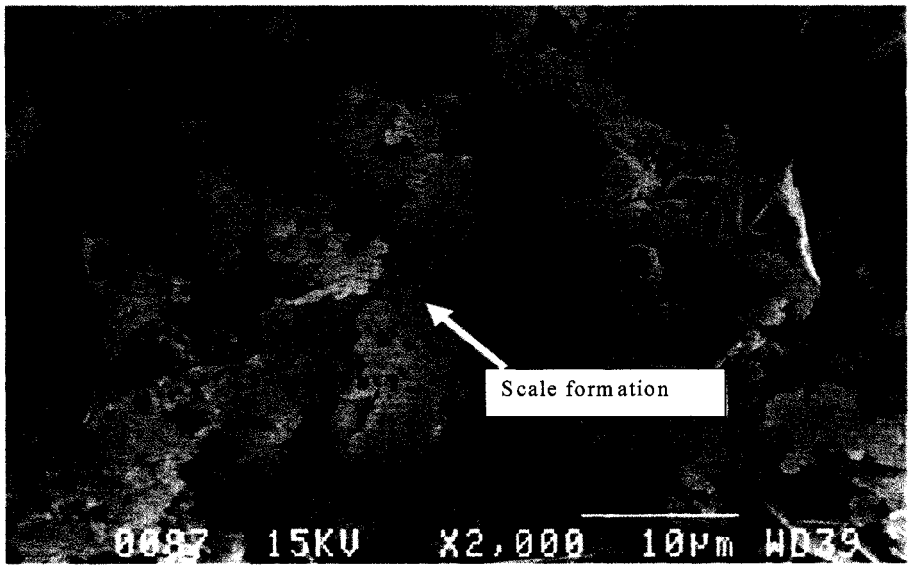

Figure 5.6. Fracture surface of AMC 254 showing scale formation

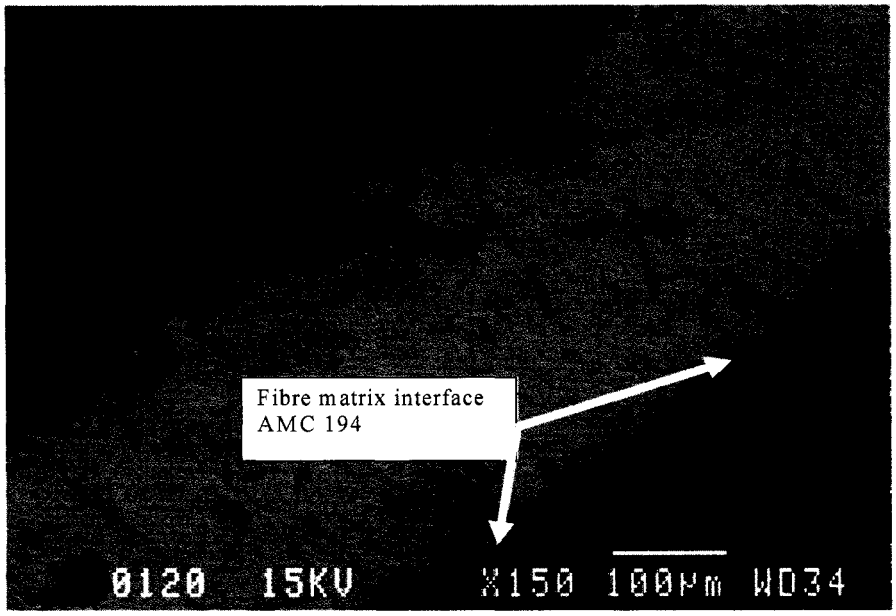

Figure 5.7. SEM photograph of interface in carbon fibre reinforced castable

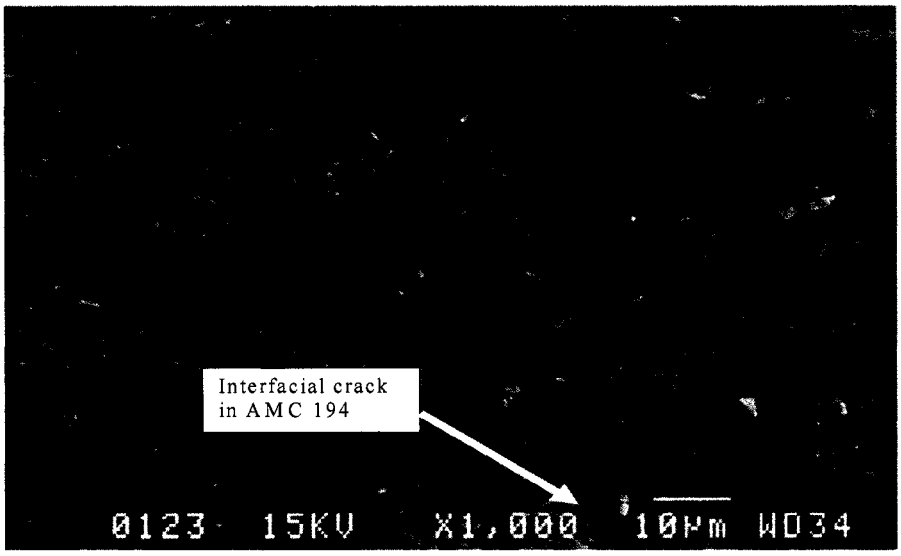

Figure 5.8. SEM photograph of interface in carbon steel fibre reinforced castable.

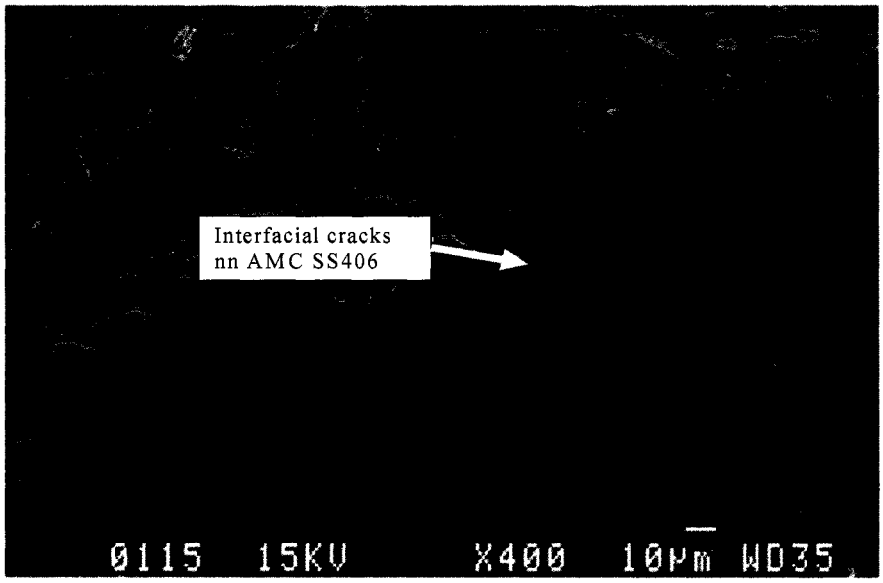

Figure 5.9. SEM photograph of interface stainless steel fibre reinforced AMC castable.

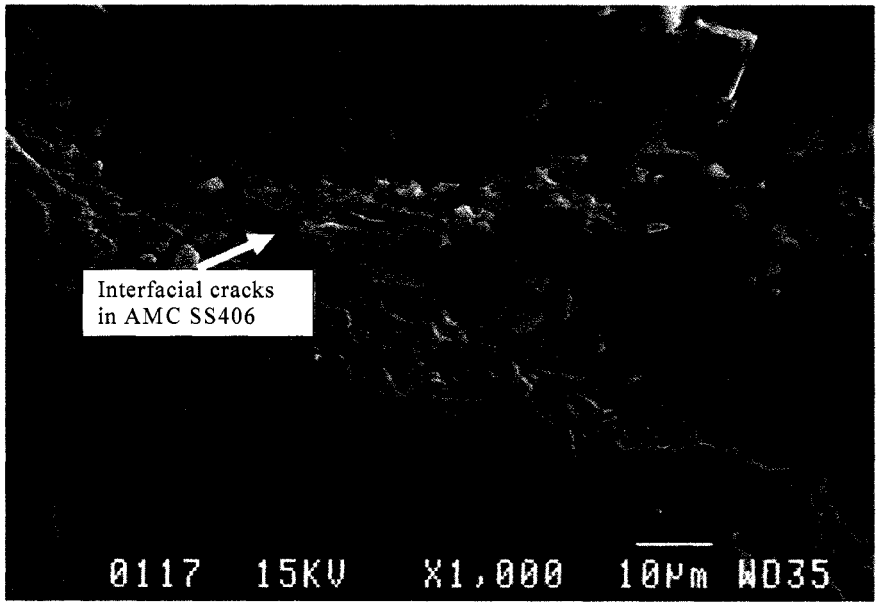

Figure 5.10 SEM photograph of interface stainless steel fibre reinforced AMC castable.

In the present study, before conducting the wedge splitting tests, the samples were pre-fired at 1100°C. While cooling the sample, cracks started appearing at the interface due to the same reason as mentioned by T.Cutard [69]. The extent of micro-cracking is more pronounced in case of SS fibre than that of CS fibres.

As mentioned by Chawla [59], the adherence of fibres into matrix can occur through chemical interaction. Viscous flow or diffusion are said to be the primary factors that can cause the penetration of fibres into the matrix at high temperatures.

The microstructure of SS fibres does not reveal a distinct scale formation in comparison with carbon steel fibre and this can be related to the fact that SS fibre are less prone to oxidation at high temperature as compared to CS fibres. In the pull out bed of SS fibres (Figures 5.11 and 5.12), a porous structure is found. At higher magnification, grain appears to be in a state of viscous flow. This may be due to mild oxidation behaviour coupled with creeping nature of fibres at the interface.

The extent of oxidation seems to be less as compared with CS fibres. That is why a distinct and clear scale formation is not observed. As mentioned by Stephen et al [44] that the plain CS fibres undergo rapid oxidation at temperatures greater than 500^0C where as the SS fibres are not much affected below 1000°C. As the melting point of SS

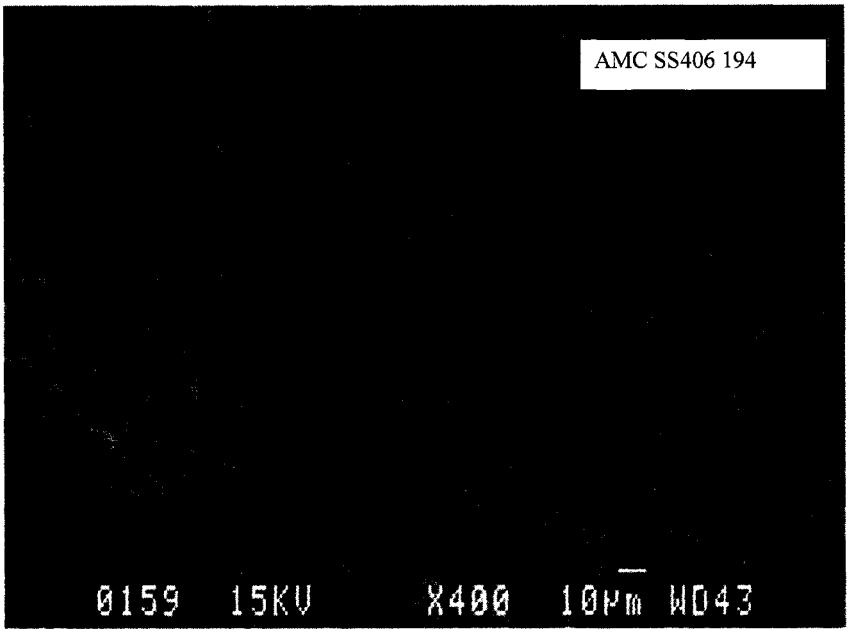

Figure 5.11 SEM microstructure :Pull out bed of stainless steel fibre castables.

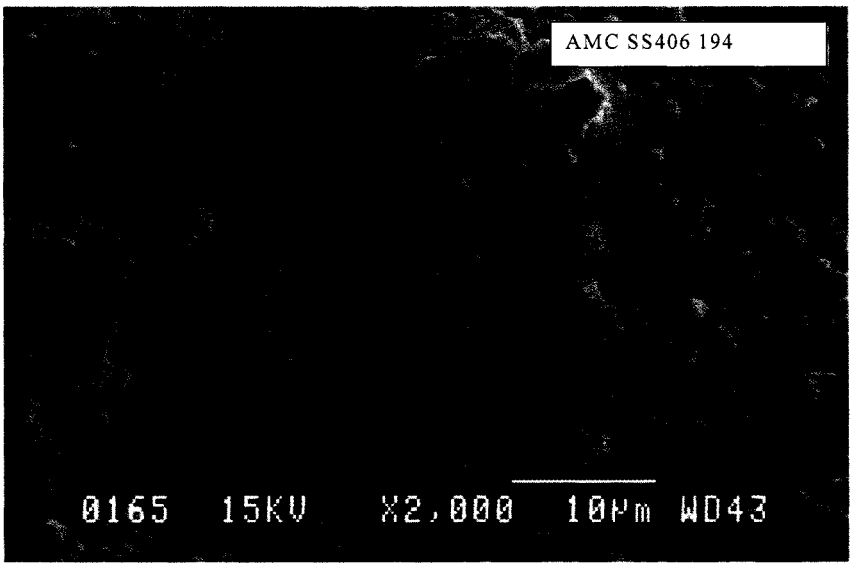

Figure 5.12 SEM microstructure: Pull out bed of stainless steel fibre castables.

fibre is lesser than that of CS fibre and also the testing temperature (1100°C) is nearer to the melting point of SS fibre, there is a chance for creeping SS fibre which might have influenced the interfacial characteristics. Any way, further investigation is required to substantiate the discussion.

Apart from the micro structural aspects, for an effective load transfer, the strength of fibre at high temperature plays a vital role which can be related with the failure mechanisms of composites. If the fibre strength is sufficiently large, the first damage to occur during the loading is a crack which extends completely through the matrix and remains bridged by unbroken fibres over its entire area. Further loading causes periodic matrix cracking at a stress equal to the fibre fracture stress. On the other hand, if the fibre strength is lower than a critical level, fibre failure occurs behind the tip of a growing crack. In that case matrix cracking causes complete failure of the composite. However the zone of unbroken fibres behind the crack tip can lead to substantial toughening. This has been observed by D.B Marshell et al, [81] in the case of ceramic matrix composites.

Referring to the work of David et al [67], the SS steel fibres exhibit only 5 % (SS 310 grade) of its tensile strength at 950°C. Though this value may fluctuate with respect to different grades, but cannot deviate much from the same. Findings of D. B. Marshell [81] and David et al, [67] strongly substantiate the reduction in work of fracture value of fibre containing AMC castables at high temperature as compared to that at room

temperature. But fibre addition improved the work of fracture value as to that of no fibre at 1100°C. David et al, [67] found that addition of 2 vol% of SS fibre to castable at 950°C resulted in no improvement in the load deflection curve compared with plain castable. Of course, they conducted test in air atmosphere.

From the above discussions, it can be stated that at high temperature the interfacial bond changes to chemical in nature. Micro structural changes that occurred at the interface coupled with tensile strength reduction of fibres, at 1100°C, are found to be the main factors for the reduction of work fracture of reinforced AMC castable at 1100°C, in comparison with AMC0 at room temperature. Nevertheless, fibre addition results in improvement of work of fracture compared to no fibre containing castables at 1100°C. There is a scatter in results of work fracture value is observed with respect to length and amount. The discrepancy is attributed to the bending effects of fibres during mixing.

An important point to be noted here is that the castables containing SS fibre (SS406) does not show remarkable improvement when compared to CS steel fibres. Referring to the figure 4.10, AMC SS409 castable and AMC 19 with 19 mm length, show similar results at all levels.

In Figure 4.13, it is observed that the hot modulus of rupture (HMOR) of AMC 0 is reduced slightly at 800°C and then shows an increase at 1100°C. This trend is similar to

all other castables with an enhanced dip at 800°C. The HMOR values of all the castables with fibres are less than AMC 0 at all temperatures. The slight dip at 800°C for AMC 0 corresponds to the loss of bonding in the structure. It has been practically observed that the fibre containing castables after drying at 110°C tend show peeling of grains in terms of bond loosening between aggregates and fine matrix portions. For a given volume, due to the needle like fibres, the surface area per unit volume increases. This increase in turn demands more amounts of cement particles to coat or bind the fibre and coarse aggregate. As a result of this, the continuous network of cement particles is getting affected, leading to bond loosening. Other reasons could be due to segregation of fines during curing at room temperature due to settling effect. Apart from these, a reduction in the packing density of aggregates can also cause this. These effects have a direct relation with fibre amount. The increment in the dip for fibre containing castables may be attributed to the formation of structural defect as explained above. Fibre degradation mechanism and decohesion regions are found to be the reason for HMOR reduction at 800^0C. Changes in HMOR value are observed with respect to length, amount and type of fibres (Figure 4.14). This is quite obvious and needs no explanation.

As shown in the Figure 5.13, the formation of in-situ spinel through the reaction of alumina and magnesia, is found to be the reason for increase in HMOR value at 1100^0C from a lower value at 800°C. The PLC value of 0.5 % at 1100°C confirms the formation of spinel which has an expansive character [80]. This spinel formation

imparts strengthening effect in the matrix, and compensates the damage caused by the decohesion region during pre-firing stages.

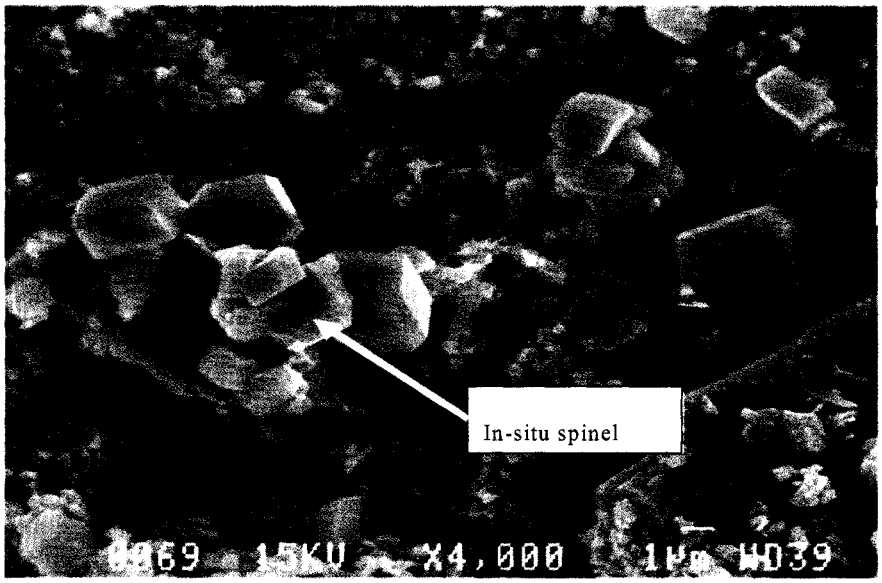

Figure 5.13 SEM microstructure: Formation of in-situ spinel.

In this context, a comparison of peak force values (figures 4.3-4.4) with HMOR (Figure 4.13) is required. At room temperature fibre addition improves the peak force value as compared to AMC0, where MOR shows a reverse trend. Both are showing a decline trend at 1100°C in comparison with AMC0. The reason for such a discrepancy can be explained in terms of mode of crack propagation. In case of HMOR - three point tests, unstable crack propagation is favoured rather than stable crack propagation, as it is the case with wedge splitting test.

The values of BD and AP (Figures 4.15, 4.16, and 4.17), remain almost the same for a particular temperature irrespective of fibre amount and length. But the same varies

with temperature which is of course associated with the micro structural changes of plain castable. The addition of fibres has least effect on PLC (Figure 4.18) value at 1100°C. The increase in the PLC value is due to expansive character of spinel which formed in the matrix. Comparing the results of AP with HMOR, (Figure 4.22) clearly indicates that at room temperature, the AP values increases very slightly with the fibre content and the MOR values decreases very insignificantly, hence the packing is not affected by the fibre addition, but this is debateable. At 800 and 1100°C, though the porosity remains at same level, the MOR values show decreasing trend with different magnitude. This confirms the fact that the micro structural changes in the matrix induced by the fibre addition influences the HMOR values.

The MOE of the samples, at room temperature (after drying at 110°C-Figure 4.20), remains almost similar and the values are not influenced significantly by the fibre addition though individually, there is a significant difference in MOE values of fibre and castable materials. This can be understood from the fact that the MOE was calculated from the linear portion of the force-extension curves using the formula given in equation (2.7). Whatever the value obtained from the linear portion of force-deflection curve simply represents the MOE value of matrix phase irrespective of fibre amount and length.

At room temperature, as there is no change in AP values with respect to the fibre addition, MOE also follows the same trend as that of AP with fibre addition. But this is

not case at 1100°C. The MOE value (Figure 4.21) decreases with increasing fibre amount due to micro structural changes that occurred at 1100°C. Decohesion region that occurred at the interface during pre-firing stage and spinel formation at the matrix are responsible for the reduction in modulus of elasticity value. The damage caused by the micro structural features increases as the amount of fibres increases and reflects in the bond strength of the castable system. In other words, the damage caused by the fibre addition is negligible at room temperature (110°C) compared to that at 1100°C is considerable and reflected in MOE values.

The K_{IC} values (Figures 4.11 - 4.12) show a scattering trend at room temperature with respect to fibre amount and type where as its value at 1100°C, decreases in line with fibre addition due to reduction in the peak force value. The general trend at room temperature shows K_{IC} increases with fibre addition. Overall, 30 % improvement in work of fracture value is obtained with steel fibre addition to AMC0 castables at 1100°C. No appreciable improvement in the work of fracture value is obtained for SS fibre (19 mm) as it displays the same value (640 J/m^2) as that of CS (19 mm). Bending effect coupled with fibre strength reduction at 1100°C, are found to cause scatter in results with respect to length and amount of fibres.

It has been observed from the work of fracture results, among the possible combinations, AMC with 19 mm carbon steel fibre with 2 wt% and AMC 50 mm carbon steel fibre length with 6 wt % results in maximum values at 1100°C.

Considering the difficulties from a rheological point of view, to use fibres of 50 mm length, it is then clear that for such a practical reason, it is much better to limit the use of fibres with 19 mm in length.

CHAPTER 6. CONCLUSIONS AND RECOMMENDATIONS

The present work focuses on the improvement of thermo-mechanical properties of AMC castable at intermediate temperature keeping the long term goal of replacing the existing MgO-C bricks in the slag zone area steel vessels. In order to achieve the primary aim, steel fibre has been chosen as reinforcement to an alumina –magnesia-carbon self-flow system. The formulation contains white fused alumina grains as main raw material with extruded graphite, magnesia, calcined alumina, reactive alumina, and steel fibres as secondary additions.

On account of the fact that the AMC castables are to be self-flow in nature, the work related with rheological properties had to be determined. Two types of steel fibres (stainless and carbon steel fibres) were used in the study with three different lengths 19, 25 and 50 mm at levels of 2, 4 and 6 wt %.

Rheological properties of AMC castables with and without steel fibre were studied using an IBB rheometer. The influence of steel fibres on the workability was assessed in terms of flow resistance and torque viscosity under varying shear rates. Traditional flow cone test was also used to measure the flowability and flow decay time.

Wedge splitting techniques and three point bending tests were used to measure the work of fracture and hot modulus of rupture for studying the thermo-mechanical

properties at 1100°C. For the sake of comparison, the same tests were also conducted for room temperature after drying at 110°C/24 hr.

Required samples with proper standard dimensions were cast as per the experimental plan varying fibre content, type and length. The respective samples were pre-fired in a coke container to prevent oxididation of steel fibres at high temperature and graphite. As per the plan the sample were evaluated for the force –extension behaviour in Ar atmosphere using wedge splitting at room temperature as well as at 1100°C. Physcial property measurements were conducted for dried and fired samples. Samples were subjected to three point tests in order to measure hot modulus of rupture after drying (110°C) and prefiring at 800,1100°C. Micro structural features were also studied using optical and SEM techniques.

Following paragraphs illustrate the outcome of the results of rheology followed by wedge splitting test.

Incorporation of steel fibre reduces the self-flowability and its decay time. The extent of reduction increases in proportion with fibre amount and length. Fibre acts as a needle like particle and resisting the flow in terms of shape factor. The resistance to flow increases as the fibre amount and length shoots up.

Fibre addition also affects the rheological parameters such as torque viscosity, flow resistance,etc. An increase in these parameters is observed in line with the increment in fibre amount and length. Though fibre incorporation hiked the above mentioned parameters, AMC castable still maintain the basic Bingham flow behaviour which is an essential requirement for pump ability. Even at a dosage level of 6 wt % with 19 mm,25 mm and at a length of 50 mm with 4 wt % , the same Bingham flow model as that of no fibre castable can be retained. It is to say that the existing castable is pumbable with 2 wt % at a length level of 19 or 25 mm. The pumping box plot has been constructed for assessing the formulation region suitable for pump ability.

Wedge splitting test results at room temperature and high temperature are discussed in the subsequent paragraphs.

1. Addition of fibres resulted in the improvement of work of fracture at room temperature.
2. Fibre and aggregate bridging effects are the primary mechanisms responsible for improvement. Fibre imparts more bridging on the crack than that of aggregate and resulted in higher value of work of fracture as compared with no steel fibre AMC castable. Among all, 50 mm length with 6 wt% combination results with higher level of work of fracture. Adhesive and frictional bonds are considered to exist at the interface.

3. The extent of improvement in work of fracture value is observed in tune with fibre amount and length for the case of AMC 50 and AMC SS 409 where as scattered results are obtained for AMC 19 and AMC 25 families. Bending effect during mixing is found to be the cause for such a discrepancy.

4. At 1100°C, with the addition of fibres, improvement in work of fracture is also observed but quantitatively it is much less than that at room temperature. The influence of fibre amount and length is not obtained in proportionate manner. Rather, a scatter, in results is observed. No marked difference in work of fracture value is observed between SS and CS fibres. Localised micro cracks are noticed at the interface of both SS and CS fibres due to the thermal expansion mismatch. Maximum value of work fracture is obtained with 50 mm CS fibre at a level of 6 wt % .

5. The possible reasons for the reduction of work of fracture at 1100^0C compared to room temperature are mild scale formation at the interface, strength reduction of fibres and micro structural changes at the interface. At 1100°C, the adhesive bond at the interface changes into a chemical with same kind of inter-diffusion of fibre and matrix. Interesting feature is the hike in the work of fracture of reinforced castable at 1100°C as compared to its room temperature. Extruded graphite, coupled with micro-crack toughening is considered to impart toughening effect at high temperature.

6. The MOE values remain unaffected by the fibre additions at room temperature, but a reduction of the same is observed at 1100°C. Structural changes occurring at high temperatures are responsible of this reduction.
7. The K_{IC} values are showing a decreasing trend with fibre addition at 110°C. The hot modulus of rupture value also depicts a declining trend proportional to the amount of fibre addition and temperature.

The primary aim of this work was to improve the work of fracture of alumina-magnesia-carbon castable at 1100°C and it has been achieved through the reinforcement of steel fibre. With 19 mm fibre at 2 wt % level, it is possible to improve the work of fracture of AMC castable at 1100°C to the tune of 30 %.

As a summary, considering the flowability and rheological tests and also the γ_{wof} results obtained at 1100°C, it can be stated that the 19 mm length with 2 wt % level would be the best choice. On account of flowability factor, the AMC with 50 mm length and 6 wt % is not recommended for usage, though it leads to the AMC system with the highest work of fracture.

In this work, certain grey areas have been left which would need to be addressed to better understanding the micromechanics and the following works are recommended:

1. Interfacial bond strength is an essential parameter that governs the behaviour of composites at room as well at high temperature (1100°C). To measure the interfacial bond strength, pull out tests have to be conducted at the respective temperatures.
2. In order to correlate the structure –property relation, interfacial study at 1100°C using environmental assisted scanning electron microscopic technique is warranted.
3. Further to, thermal expansion characteristics data is required to better understanding of interfacial - micromechanics at high temperature.
4. In order to use more fibre dosage level and also increase in length, proper mixing procedure coupled with special mixture machine design, is necessary.
5. A study under oxidizing condition is a mandatory one, as it would reveal more information on the real fibre behaviour at high temperature.

REFERENCES

1. HAKAGAWA, H., NAKAMURA, Y., SAWANO, K., TAMURA, S., TSTSUI and NAKAMURA, H. (1997). Development of MgO-CaO-Al_2O_3 castable for steel ladle slag line, Proceedings of UNITECR' 97, 203-212.

2. SUMIMURA, H., YAMAMURA, T., KUBOTA, Y. and KANESHIGE, T. (1991). Study on Slag Penetration of Alumina - Spinel Castable, Proceedings of UNITECR' 91, 148-151.

3. YAMAMURA, T., KUBOTA, Y., KANESHIGE, T. and NANBAM, M. (1993). Effect of spinel clinker composition on properties of alumina-spinel castable, Taikabustu Overseas, Vol. 13 (2), 39-45.

4. FUJII, K., ISAO, F. and TAKITAI, I. (1992). Composition of spinel clinker for teeming ladle casting materials, Taikabutsu Overseas, Vol.12 (1), 4-9.

5. THOMAS, A. B., PARR, C., REVAIS, C. and FRYDA, H. (2001). Chemical interactions in calcium aluminate cement based castables containing magnesia, Proceedings of UNITECR' 01, Vol. 1, 15-21.

6. KRIECHBAUM, G. W. and GNAUCK, G. W. (1994). The influence of SiO_2 and spinel on the hot properties of high alumina low cement castable, Proceedings of UNITECR' 94, 150-159.

7. NANDI, P., GRAG, A., CHATTORAJ, B. D. and MUHOPADHAYAY, M. S. (2000). Effect of silica and temperature on spinel-based high alumina castables, Journal of American Ceramic Society Bulletin, Vol. 79, 65-69.

8. TERANISH, K., KAWAMURA, T., YASUI, K. and IMAI, I. (1998). Application of MgO-C castable to ladle furnace slag line, Taikabutsu Overseas, Vol. 18 (1), 38-42.

9. ZHOU, N. and RIGAUD, M. (1998). Different approaches to incorporating natural flake graphite into Al2O3-SiC-C castables, Refracories (China), Vol. 7 (4), 3-10.

10. HUIQING, H. (2002). Optimisation of antioxidant additives in Carbon containing castables, Ph.D. Thesis, Ecole Polytechique de Montreal, Canada.

11. ISHIKAWA, M. (1999). Refractory concrete, Taikabustu Overseas, Vol. 9 (3), 7-12.

12. WATANABE, K., ISHIWAKA, N. and WAKAMATSU, M. (1998). Rheology of castable refractories, Taikabustu Overseas, Vol. 9 (1), 41-53.

13. FUNK, J. E., DINGER, D. R. and FUNK, J. E. (2004). Particle size distribution control for refractories forming rheology, Refractories Applications and News, Vol. 9 (4), 21-29.

14. SWAMY, R. N. (1975). Fibre reinforcement of cement and concrete, Materials and Structures, Vol. 8 (45), 235-254.

15. BAYASI, M. Z. and SOROUSHIAN, P. (1992). Effect of steel fibre reinforcement on fresh mix properties of concrete, ACI Materials Journal, Vol. 89 (4), 369-374.

16. NARAYANAN, R., KAREEM and PALAJIAN, A. (1982). Factors influencing the workability of steel fibre reinforced concrete, Concrete, Vol. 16 (10), 45-48.

17. GROTH, P. (2002). Fibre reinforced concrete, PhD Thesis, Lulea University, Swedan.

18. TATTERSALL, G. R. (1991). Workability and quality control of concrete , Chapman & Hall, London.

19. MARSON, L. W. and ROONEY, R. (2005). The effect of fibre dosage levels on the performance of castable refractory materials, The Refractory Enginners, Vol. 5, 11-16.

20. SAMADI, H. and FARD, F. G. (2003). The effect of fibre addition on low cement castables, Proceedings of UNITECR' 03, 268-271.

21. VAN VLACK, L. H. (1964). Physical ceramics for engineers, Addition-Wesly Publ. Co. Inc, London.

22. COTTERELL, B. and MAI, Y. W. (1996). Fracture mechanics of cementitious materials, Blackie Academic & Professional, New Zealand.

23. EVANS, A. G and HEUER, A. H. (1980). Transformation Toughening in Ceramic: Martensitic Transformations in Crack – Tip Stress Fields, J. Am. Ceram. Soc., Vol. 63, 241-248.

24. LANGE, F. F. (1982). Transformation Toughening, J. Mater Sci , Vol. 17 (1), 225-263.

25. KELLY, M. and ROSE, L. R. F. (2002). The martensic transformation in ceramics- its role in transformation toughening, Progress in Materials science, Vol. 47, 463-557.

26. BUDIANSKY, (1998). Small – Scale Crack Bridging and the Fracture Toughness of Particulate – Reinforced Ceramics, J. Mech. Phys. Solids, Vol. 36, 167-187.

27. DUTTA, S. (2001). Fracture toughness and reliability in high temperature structural ceramics and composites: Prospects and challenges for the 21-st century, Bull.Mater.Sci., Vol. 24 (2), 117–120.

28. FABER, K. T. and EVANS, A. G. (1983). Crack Deflection Processes – II. Experiment, Acta Metel, Vol. 31, 577-584.

29. BUDIANSKY, B. (1995). Toughening of ceramics by short aligned fibres, Mechanics of Materials, Vol.21, 139-146.

30. DONALD, I. W and MCMILLAN, P. W. (1976). Review of ceramic matrix composite, J. Mat. Sci., Vol. 11, 949-972.

31. MARSHALL, D. B and EVANS, A. G. (1985). Failure Mechanisms in Ceramic-Matrix Composites, J. Am. Ceram. Soc., Vol. 68, 225-231.

32. NAGARAJA, G. M. (2001). Dual role of microcracks: toughening and degradation, Can. Geotech. J, Vol. 38, 427-440.

33. TIJISSENS, M. G. A., SLUYS, L. J. and VANDER, A. E. G. (2001). Simulation of fracture of cementitious composites with explicit modeling of micro structural features, Engineering fracture mechanics, Vol. 68, 1245-1263.

34. ANDREEV, K. and HARMUTH, H. (2003). FEM simulation of the thermo-mechnical behaviour and failure of refractories- a case study, Journal of Materials Processing Technology, Vol. 6, 72-77.

35. SIMONIN, F., OLAGNON, C., MAXIMILEN, S. and FANTOZZI, G. (2002). Room temperature quasi-brittle behaviour of an aluminous refractory concrete after firing, Journal of European Ceramic Society, Vol. 22, 165-172.

36. FERRETTI, E. (2004). A discussion of strain softening in concrete, International Journal of Fracture, Vol. 126, L3-L10.

37. GIACCIO, G. and ZERBINO, R. (1998). Failure Mechanism of concrete, Advn.Cem. Based Materials, Vol. 7, 41-48.

38. SHAH, S. P., SWARTZ, S. E and QUYANG, E. (1995). Fracture Mechanics of Concrete: Applications of Fracture mechanics to Concrete, Rock and other Quasi- brittle materials, John wiley & sons Inc.

39. VICTOR, C. and MOHAMED, M. (1996). Toughening in cement based composites. Part1: cement, Mortar and concrete, Cement & Concrete Composites, Vol. 18, 223-237.

40. SURENDRA, P. S. (1997). An overview of the fracture mechanics of concrete, Concrete and Aggregate, Vol. 19, 79-86.

41. SCHMITT, N., BURR, A., BERTHAUD, Y. and POIRIER, J. (2002). Micromechanics applied to the thermal shock behaviour of refractory ceramics, Mechanics of Mateials, 725-747.

42. TAYLOR, LYDON, F. D. and BARR, B. I. G. (1997). Toughness measurement on steel fibre reinforced high strength concrete, Cement and concrete composites, Vol. 19, 329- 340.

43. STEPHEN, D. S. and ROBERT, H. H. (1980), Stainless-Steel Fibre reinforced castables, Journal of American Ceramic Society Bulletin, Vol. 59, 742-745.

44. FILHO, R. D. T., JOSEPH, K., GHAVAMI, K and ENGLAND, G. L. (1999). The use of sisal fibre as reinforcement in cement based composites, Revista Brasileria de Engenharia agricola e Ambiental, Vol .3.2, 245-256.

45. VICTOR, L. C. and MOHAMED, M. (1996). Toughening in Cement Based Composits. Part.11: Fibre reinforced Cementitious Composites, Cement & Concrete Composites, 239-249.

46. PERUMALSAMY, H. B. and SHAH, S. P. (1992). Fibre-Reinforced Cement Composites, McGraw-Hill, Inc.

47. CHENG, F. P., KODUR, V. K. R. and WANG, T. C. (2004). Stress-strain curves for high strength concrete at elevated temperatures, Journal of Materials in Civil Engineering, Vol. 2, 84-90.

48. YAO, W. and WU, J. L. K. (2003). Mechanical properties of hybrid fibre-reinforced concrete at low fibre volume, Cement and Concrete Research, Vol. 33, 27-30.

49. HSUEH, C. H. and BECHER, P. F. (1996). Residual thermal stresses in ceramic composites Part I: with ellipsoidal inclusions, Mater. Sci. Eng., Vol. A 212, 22-28.

50. HSUEH, C. H. and BECHER, P. H. (1996). Residual thermal stresses in ceramic composites, Part II: with ellipsoidal inclusions, Mater. Sci. Eng., Vol. A212, 29-35.

51. KAWAMATA, A., MIHASHI, H. and FUKUYAMA, H. (2003). Properties of hybrid fibre reinforced cement-based composites, Journal of Advanced Concrete Technology, Vol. 1 (3), 283-290.

52. NAAMAN, A. E. (2003). Engineered Steel fibres with optimal properties for reinforcement of cement composites, Journal of Advanced Concrete Technology, Vol. 1 (3), 241-252.

53. SHAH, S. P. and QUYANG, C. (1991). Mechanical behaviour of fibre-reinforced cement based composites, J. Am. Ceram. Soc, Vol. 74 (11), 2727-2753.

54. CHARALAMDIDES, P. G. and EVANS, A. G. (1989). Debonding properties of residually stressed brittle matrix composites, J. Am. Ceram. Soc., Vol. 72 (5), 746-753.

55. BENTUR, A. (1989). Materials Science of Concrete 1, The American Ceramic Society Inc.

56. COOK, J and GORDON, J. E. (1964). A Mechanism for the control of crack propagation in All Brittle Systems, Proc. R. Soc., sect. A , 282, 508-20.

57. LUNDGREN, K. (1999). Three-dimensional Modellinfg of Bond in Reinforced Concrete, PhD. Thesis. Chalmers University of Technology, Swedan.

58. CHAWLA, K. K. (2003). Ceramic matrix composites, Kluwer Academic publication.

59. LAWRENCE, P. (1972). Some theoretical considerations of fibre pull out from an elastic matrix, J. Mater. Sci., Vol. 7, 1-6.

60. CHANDRA, N and GHONEM, H. (2001). Interfacial mechanics of push-put tests; theory and experiment, Composites: Part A, Vol. 32, 575-584.

61. SHANNAG, M. J., BRINCKER, R. and HANSEN, W. (1997). Pull out behaviour of steel fibres from cement based concrete, Cement and concrete Research, Vol. 27 (6), 925-936.

62. NAAMAN, A. E. AND SHAH, S. P. (1978). Pull–out Mechanism in steel fibre reinforced concrete, J. Struct. Div, Vol. 102, 1537-1548.

63. Quyang, C. P and Shah, P. S. (1994). Pull out of inclined fibres from the cementitious matrix, J. Eng. Mech, Vol. 120, 2641-2659.

64. KINGERY, W. D. (1955). Factors affecting thermal shock resistance of ceramic materials, J. Am. Ceram. Soc., Vol. 38 (1), 3-15.

65. HASSELMAN, D. P. H. (1969). Unified Theory of Thermal shock fracture initiation and crack propagation in Brittle ceramics, J. Am. Ceram. Soc.,Vol. 52 (11), 600-604.

66. DAVID, R., LANARD, R. and D. HERBERT, (1971). Use of steel wire fibres in refractory castables, Journal of American Ceramic Society Bulletin , Vol. 50 (5), 497- 500.

67. ANAN, K. (1995). Application of Fibres to Monolithic refractories, Taikabustu Overseas, Vol. 14 (3), 3-9.

68. CUTARD, T., CAILEUX and BERNHART, G. (2002). Pull out of metallic fibres from a ceramic refractory matrix, Composites: Part A Applied science and manufacturing, Vol. 33 (10), 1461-1466.

69. BRADT, R. C and HASSELMAN, D. P. H. (1991). Fracture Mechanics of ceramics, Plenum press.

70. MUKHOPADHYAY, A. K., DATTA, S. K. and CHAKRABORTHY, D. (1999). Fracture toughness of structural ceramics , Ceramics International, Vol. 25, 447-454.

71. NAKAYAMA, J., ABE, H. and BRADT, R. C. (1961). Crack stability in the work-of –fracture test: Refractory applications, J. Am. Ceram. Soc., Vol. 64 (11), 671-675.

72. HARMUTH, K., RIEDER., KROBATH, M. and TSCHEGG, E. (1996). Investigation of the non-linear fracture behaviour of ordinary ceramic refractory materials, Materials science & Engineering A , Vol. 214, 53-61.

73. HARMUTH, H. and TSCHEGG, E. K. (1997). A fracture mechanics approach for the development of refractory materials with educed brittleness, Fatigue Fract. engng Mater. Struct., Vol. 20 (11), 1585-1603.

74. MOBASHER, B. and PELED, A. (2004). Use of R-curves for characterisation of toughening in fibre reinforced concrete, International conference on fracture mechanics of concrete and concrete structures, Colorado.

75. KOPANDA, J. E. and MACZURA, G. (1990). Production processes, properties and applications for calcium aluminate cements, Alumina Chemicals: Science and Technology hand book, The American Ceramic Society, Inc., 171-83.

76. MACZURA, G., GNACK, V. and ROTHENBUHLER, P. (1983). Fine Aluminas For High Performances refractories, International conference on refractories, The technical association of Japan, Vol. 1, 560-575.

77. SCHMUCKER, M., KANKA, B. and SCHNEIDER, H. (2000). Temperature – induced fibre/matrix interactions in porous alumino-silicate ceramic matrix composites, Journal of the European ceramics society, Vol. 20, 2491-2497.

78. SUN, W., TIEU, A. K., JIANG, Z., ZHU, H., and LU, C. (2004). Oxide scales growth of low-carbon steel at high temperature, Journal of Materials Processing Technology, Vol. 155- 156, 1300-1306.

79. KO, Y. C. (2000). Influence of the characteristics of spinels on the slag resistance of Al2O3-MgO and Al2O3 –spinel castables, J. Am. Ceram. Soc., Vol. 83 (9), 2333-35.

80. MARSHALL, D. B. and COX, B. N. (1987). Tensile fracture of brittle matrix composites influence of fibre strength, Acta Metal., Vol. 35 (11), 2607-2619.

81. MINDESS, S. (1989). Interfaces in concrete, Materials Science of Concrete 1, The American Ceramic Society Inc.

APPENDIX A

Mechanical Properties Of Cementitious Materials

1.1 Introduction

Structural materials can be classified into three types in terms of their stress-strain behaviour namely brittle elastic, ductile elastic-plastic and quasi-brittle. The different behaviour is due to the presence of fracture zone ahead of crack tip. At room temperature, brittle material, for example ceramics, no fracture process zone is present whereas in ductile material, it is present. The main factor which distinguishes these two materials from each other is bonding. In metals ductility is promoted by the movement of dislocations for an applied stress where as in ceramics, immobile nature of dislocation, leads to no plastic work. The reason for such immobile nature of dislocations can be understood through bonding [21]. Directional bonding nature and electrostatic force of repulsion are the two factors which prevent mobilisation of dislocation in both Ionic and covalent crystals. On the other hand this can be also explained that the stress required to move a dislocation in ceramics is higher than that of fracture stress.

For quasi-brittle materials there is a limited Fracture Process Zone but its size is less compared with ductile materials. Concrete and refractory castable are examples of quasi-brittle materials [22].

2.1 Toughening mechanism in ceramic

Most of the ceramics are hard and having very high lattice resistance because of covalent and ionic bonding. The fracture toughness value falls into 1-5 MPa $m^{(1/2)}$ range.

Various toughening mechanisms exist in ceramic matrix composites are crack deflection, micro cracking, transformation toughening, crack branching, and crack bridging. All of these mechanisms essentially redistribute stress at the crack tip and increase the energy needed to propagate a crack through the composite material, thereby resulting in improved toughening.

2.1.1 Transformation toughening of zirconia

The basic mechanism behind is that when partially stabilised zirconia tetragonal particles are embedded in a matrix, and up on subjected to applied stress, transformation of tetragonal to monoclinic is taking place. Due to expansive nature of this transformation, compressive stress filed is created which tend to close the crack. Evans et al, have studied an in depth analysis of this martensic transformation which occur near the crack tip [23-25].

2.1.2 Ductile phase toughening

This is when metal particles are deliberately incorporated into the ceramic matrix. As the crack propagates and meets the ductile particle, it deforms plastically and consume more energy for its propagation. This is so called crack bridging mechanism [26].

2.1.3 Whisker reinforced toughening

Whiskers, which are nothing but defect free single crystals, are added to ceramic matrix, in order to toughen them. Actually whiskers acts like short fibres reinforcing the matrix. When crack propagates, the whiskers are debonded and pulled out from the matrix followed by frictional sliding. For the whiskers to be pulled out from the matrix, more energy has to be spent and thus toughening takes place [27].

2.1.4 Crack deflection mechanism

Elongated particles for example, Si_3N_4, ZrO_2 are reinforced with glass phase. Toughening takes place as the fracture occurs through the glassy phase followed by grain pull out [28].

2.1.5 Fibre reinforced ceramic

When the crack moves through a brittle matrix containing unidirectional fibres, the following mechanisms may be expected to operate via matrix fracture, debonding at the crack tip by crack deflection, debonding in the crack wake, followed by deflection,

frictional sliding between the fibre and matrix, fibre failure and fibre pull out. This is considered to be the most effective way to enhance the toughness of ceramic [29-30]. The stress –strain curve of the fibre reinforced ceramics is shown in Figure A1. The fracture toughness values which can be obtained through various toughening mechanisms are given in Table A1.

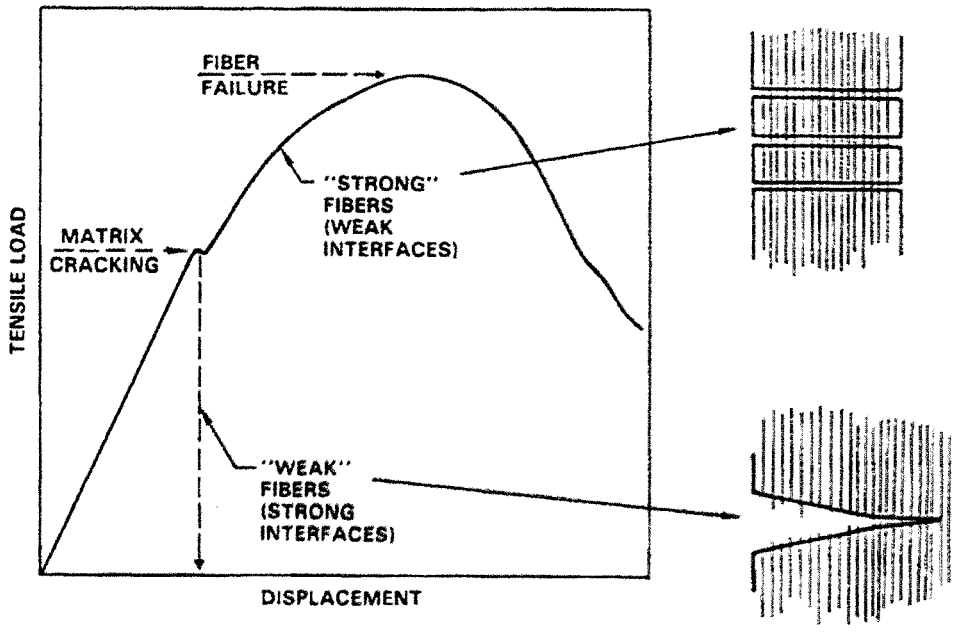

Figure A1. Stress-strain curve of Fibre reinforced ceramics. [31]

Table A1. Fracture toughness values for toughening various mechanisms in ceramics.

Toughening mechanism	K_{IC} value, MPa $m^{1/2}$
Fibre reinforced ceramics	18
Cermets,Transformation toughening,whisker reinforced ceramics	5-10
Glass,Alumina	1-5

In addition with several other mechanisms such as viscoelastic, ferroelectric domain motion due to applied electric field, micro cracks toughening are also possible but in terms of quantitative improvement towards toughness is concerned, that mechanisms are insignificant [32].

3.1 Fracture of concrete material

3.1.1 Microscopic view

On macroscopic view, concrete is a composite material having cement paste and aggregate as its constituents. The matrix phase consists of small aggregates bonded by cement .The cement paste consists of fully and partially hydrated cement grains and possibly with voids. Up on further examination, one may detect small cracks which originate from the shrinkage due to drying .Further zooming into the material, reveals that the hydrated cement it self is a cauliflower-like particle separated by voids and reinforced with hydrated cement crystals. Besides the above, in between matrix phase

and aggregate, a thin section, called interfacial zone also exist Actually the interface is a transition zone with planar (two dimensional) nature where the physical, mechanical and chemical properties gradually varies from cement phase to aggregate phase. More illustration can be given with an example of grain boundary in polycrystalline [33]. This transition zone is 10 -50 micron thick around an aggregate. The main and important characteristic of this interfacial (TZ) zone is that strength wise it is weak compared to matrix and aggregates due to more porous in nature.

The presence of matrix, aggregate and interfacial zone, introduces heterogeneity in the concrete. One important observation is that cracks are pre-existing in the interfacial zone prior to the application of external stresses as a result of shrinkage during drying and thermal stresses during firing and high temperature treatment. The number and width of these micro cracks in the interfacial zone depend mainly on curing history of concrete and thermal shrinkage extent [34].

Al though concrete materials can be considered as a composite material, its mechanical performances are quite different and cannot be explained by simply applying composite theory [35]. As shown in Figure A2 individually both matrix and aggregates phases show linear stress-strain behaviour up on subjected to external stress. But as a composite material, it deviates from linear elastic to non-linear to some extent.

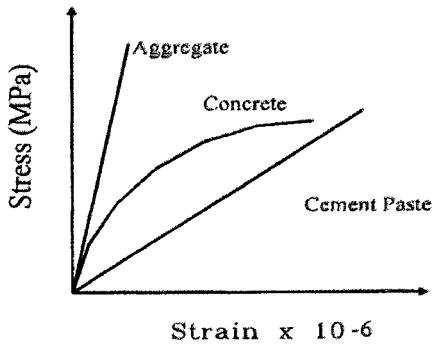

Figure A2. Stress-strain curve of cement paste, aggregates and concrete.

3.1.2 Fracture of concrete

The deformation of concrete can be divided into several stages based on initiation and propagation of internal flaws as shown in Figure A3.

The first stage is before point A which is about 30 % of the peak load .Propagation of internal flaws, which primarily consists of interfacial voids between cementations matrix and aggregate, is negligible during the first stage. The second stage is from point A to B which is about 80 % of the peak load. The internal cracks initiate and propagate during this stage. In this stage these cracks are isolated and randomly distributed over the specimen volume and the distribution of strain in the loading direction is approximately uniform over the entire length. The third stage is between point B and C. During this stage the internal cracks start to localise into a major crack. The major crack propagates with increasing load. When the strain localisation, distribution of strain is no longer uniform over the specimen length. Propagation of the

major crack is stable up to peak load(C). Stable crack growth means that the major crack propagates only when the load increases. The fourth stage is after the peak load. The major crack continuously propagates even though the load decreases.

We may consider two parts; one is associated with pre-peak and another is post-peak stage. During the pre-peak stage, the strain remains almost uniform along the entire length of the specimen. But after the peak –load the strain stops to develop uniformly due to the macro-crack and matrix crack propagation [36-38]. The deformation becomes localised.

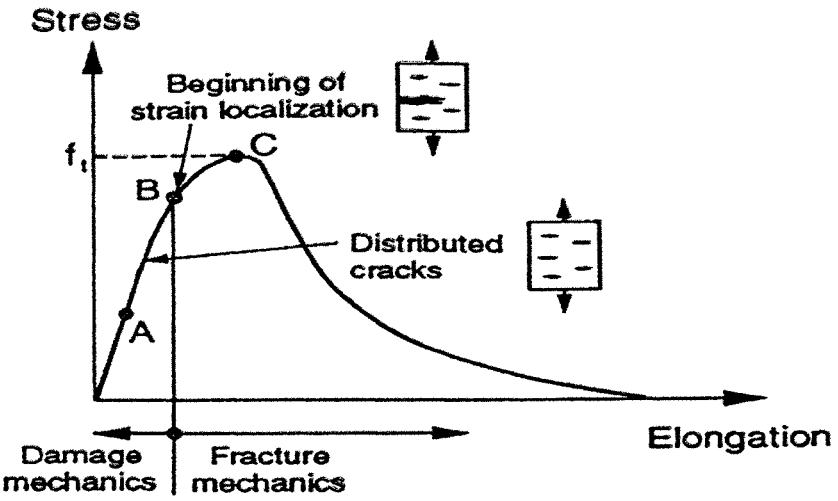

Figure A3. Schematic representation of behaviour of concrete under uniaxial loading (Shah et al, 1995) [38].

4.1 Toughening mechanisms in cement materials

The stress-strain curve clearly indicates that limited amount of toughening is taking place owing to energy dissipation processes through micro cracking, crack branching, crack deflection, crack face friction and crack tip blunting mechanisms. These mechanisms as shown in Figure A4 are direct results of interlocking nature of aggregate and aggregate roughness [50, 51].

4.1.1 Micro-crack shielding.

The micro cracks that develop in the materials reduce the elastic modulus of the undamaged material; therefore the material appears to be tougher than the original undamaged materials. The origin of micro-cracks results from the water –filled pores, air voids and shrinkage due to the curing process. Another interpretation could be that formation and propagation of micro cracks at aggregate-matrix interface requires additional energy and thus toughening the material. The micro-cracks have random orientation with respect to main crack plane.

4.1.2 Crack deflection.

When a matrix crack intercepts an aggregate, an alternative path is presented for the direction of continued crack propagation. Since matrix-aggregate interface is having low strength and high porosity and offers least path of resistance to crack propagation. Due to this least resist path, crack is deflected along the matrix –aggregate with non-planner manner.

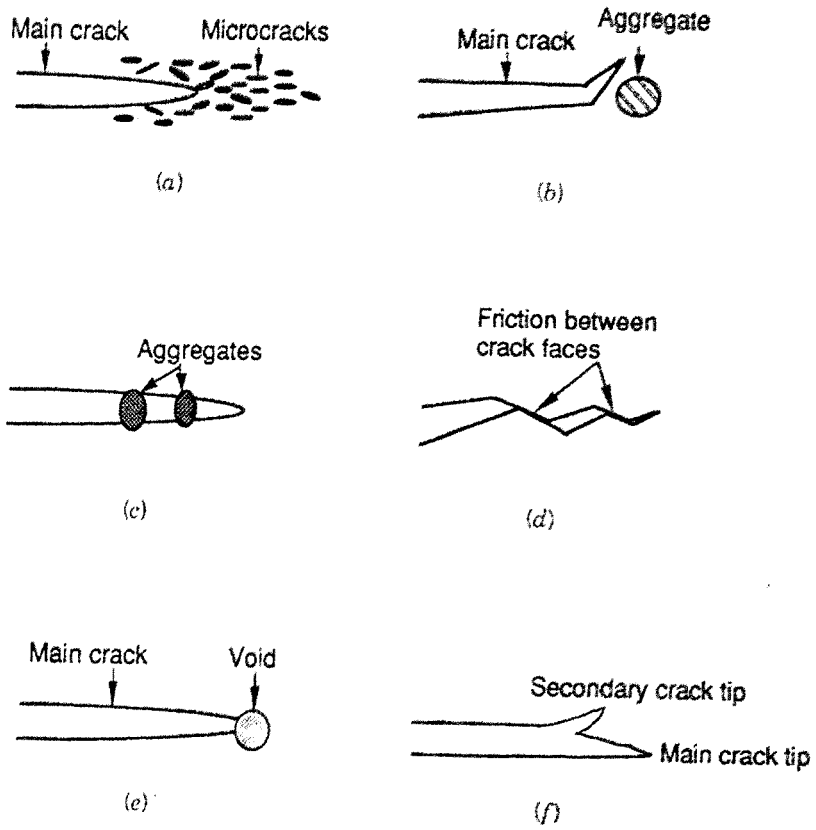

Figure A4. Toughening mechanism in concrete (Shah et al, 1995) [40]

4.1.3 Crack trapping

When the matrix crack approaches an aggregate, neither it will be deflected nor go through the aggregate but instead trapped in a site near by the aggregate. This will happen only when the aggregate is well bonded with the matrix and also its toughness is greater than that of matrix.

4.1.4 Aggregate bridging

Due to differential value of modulus of elasticity between matrix and aggregate, an interfacial stress is developed. Here crack front is being bridged by the row of aggregates. At one point of time, the aggregates debonded from the matrix, followed by pull out. This is the most significant load transfer mechanism that lead to major contribution towards the toughening of cement, although other mechanism are also operative but their contributing is insignificant. And this toughening has a direct relation with aggregate size [41].

In addition surface roughness of aggregates plays an important role in controlling interfacial property. Rough surface makes the interfacial bonding relatively stronger than smooth one. Usually all these mechanisms contributing towards toughening of cementations materials are lumped together and taken into account by a conceptual fracture process zone which is conceptionally similar to plastic zone in metals. Important thing is that this fracture process zone changes its size during propagation of a crack.

5.1 Fibre reinforced toughening in cement based composite

Fibres are introduced into the cement materials to control crack propagation through interfacial bond which exist between matrix and fibres [42].

5.1.1 Fibre types

There are several types of fibres which can be incorporated into cementitious materials and can be classified into three different classes via organic, inorganic and metallic. Organic fibres are used only for limited temperature applications i.e. below 200°C. For high temperature applications; inorganic materials like Alumina, Carbon, Zirconia, and Silicon carbide are preferred. Metallic fibres like stainless steel, carbon steel are also used for construction purposes widely. But their only disadvantage is that they are prone to oxidation at high temperature [44, 45].

5.1.2 Fracture of FRC

When the composite is subjected to load, due to the difference in the elastic modulus value of fibre and matrix, shear stress are created in the interfacial zone. This stress is responsible for load –bearing or load transferring capacity of the composite and is not constant through out and has its maximum at the fibre entry.

Fundamentally the ultimate strain capacity of matrix is low compared with fibre. When the load is applied to the material, initially it will be taken up by the matrix and the resulting stress –strain curve would be linear and unaffected by the fibre parameters such as aspect ratio, volume fraction etc. After this, the matrix no longer able to bear the load, cracks start growing and the load is transferred to the fibre via the interfaces. In this stage stress-strain curve deviates from linear into non-linear due to the bridging action of fibres on micro-cracks and is called strain hardening. The density of cracks

increases with increasing load until it reaches the saturation level. The extent of strain hardening is determined by the microstructure of the matrix and the volume and interfacial strength. When the hardening capacity has been exhausted, some of the fibres begin to debond from the matrix, resulting in the localisation of deformation. This localisation manifests itself in the opening of cracks in a particular plane. As more and more debonding of fibres occurs, deformation also increases under decreased applied load. At one stage all the fibre debonded from the matrix resulting in a drop in the load bearing capacity and all the cracks merge and forms a macro crack or through crack. Thereafter the residual load capacity is entirely determined by the frictional contact between the fibres and matrix until the fibres are completely pulls out from the matrix and ultimately failure occurs. Frictional force, exist between the fibre and matrix, offers resistance to pull out of fibres from the matrix. As a result of this, progressive pull out of fibre is taking place along the entire length. At this progressive stage both elastic and frictional shear stress are acting simultaneously. Since crack path is diverted during fibre debonding and pull out processes, significant toughening is observed in the material [46, 47]. Figure A5a, b, c indicates the stress-strain relationship curve for cementitious material with and with out fibres. Figure A5a, b, c shows the stress-strain curves of plain concrete and reinforced concrete. Fibre volume effect is illustrated in figures A5b and A5c respectively. More detailed discussion is given in the subsequent section.

In case of steel fibres, an additional toughness is observed due to its bending effect. Fu-Ping Cheng et al, [48] have investigated the stress-strain curves for high strength

steel reinforced concrete (portland cement) at high temperatures starting from 100 to 800°C in steps of 200°C and found that variables such a s concrete strength, type of aggregate, and amount of steel fibres are affecting the high temperature property. Concrete with steel fibre exhibits enhanced toughness above 400°C to plain concrete. The presence of steel fibre has little effect on Modulus of elasticity with temperature. The aggregate type has an effect on the ultimate strain attained in concrete exposed to elevated temperatures.

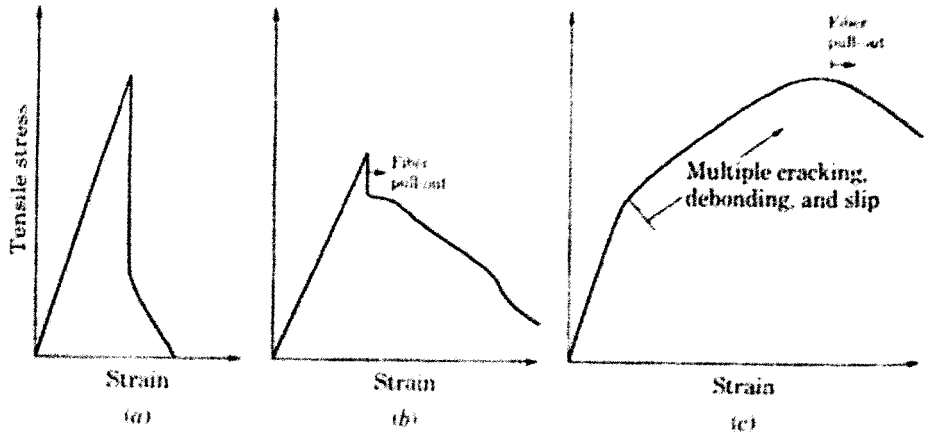

Figure A5. The stress-strain curve of concrete under uniaxial loading. a) No fibre b). Fibre reinforced concrete, Below critical volume, c). Fibre reinforced concrete with above critical volume [47].

5.1.3 Factors that affects toughening in FR cementitious materials

The main controlling parameter which decided the load bearing capacity is interfacial bond strength between the fibre and matrix. Several factors which influence the bond strength are fibre aspect ratio of the fibre, volume fraction, surface roughness, residual stress, fibre orientation, inter spacing between the fibre etc [49].

There are two kinds of stresses possible at the interface. One is mechanical and another is thermal in nature. Mechanical can be either elastic or frictional type. In addition with mechanical stresses, thermal stress also plays a vital role at interface for load transfer. The main origin of this kind of stress is due to the mismatch in thermal expansion coefficient of matrix and fibre. Depending on its nature whether compressive or tensile, it will plays decisive role [50, 51].If the matrix thermal expansion coefficient is higher than that of the fibre, then on cooling from high temperature radial compression will result. i.e. the matrix will grip the fibre. Such a radial gripping of the fibre by the matrix will increase the strength of the matrix thus decreasing the possibility of crack deflection at the interface. On the other hand if matrix thermal expansion coefficient is less than that of fibres, tensile stresses will be produced at the interface.

For a given volume fibres, the number of interfaces depends on the aspect ratio of fibre. Higher the aspect ratio results in more interfaces which in turn increases more number of debonding and pull out of fibres. For brittle fibre fibres with high aspect

ratio is preferred due to the fact that probability of finding a flaw is less in a small volume material.

Below certain volume [47], called critical volume fibre addition will not promote strength but only improves toughness. This is a direct consequence of less number of fibres which are involved in load-bearing purpose. Above the critical volume both strength and toughness would be enhanced. For a given fibre content, below critical volume crack initiation takes place in the matrix locally, but in the case of high volume level, multiple cracking will occur uniformly through out the matrix.

Geometry of fibre also plays important role through frictional stress. Fibres with congregated surface induce more anchorage with matrix which in turn increases the frictional force. This lead to an extension of fibre pulls out region in stress-strain curve. Several fibre types like straight, congregated, circular, bone-shape are available for the purpose of reinforcing. Among them bone-shaped gives more toughening effect [52, 53]. The effects of different Poisson contractions of fibre and matrix will lead to a radial tensile stress at the interface. This stress in fact will aid to the debonding process.

6.1 Role of interface

Fibre –matrix interface affects the behaviour of composites. A strong interfacial bond will allow an on coming crack to go unimpeded through the interface and the

composite will fail in a brittle manner. In other words presence of a strong fibre-matrix interface does not allow any extra expenditure of energy in the fracture process [54]. The interaction of a crack in the matrix with a weak interfacial bond, on the other hand, is likely to lead to debonding at the interface, followed by crack deflection, crack bridging, fibre fracture and finally fibre pullout [55]. All, these additional energy absorbing phenomena lead to enhanced fracture toughness and a non-catastrophic failure mode. These situations are depicted in Figure A6 and Figure A7.

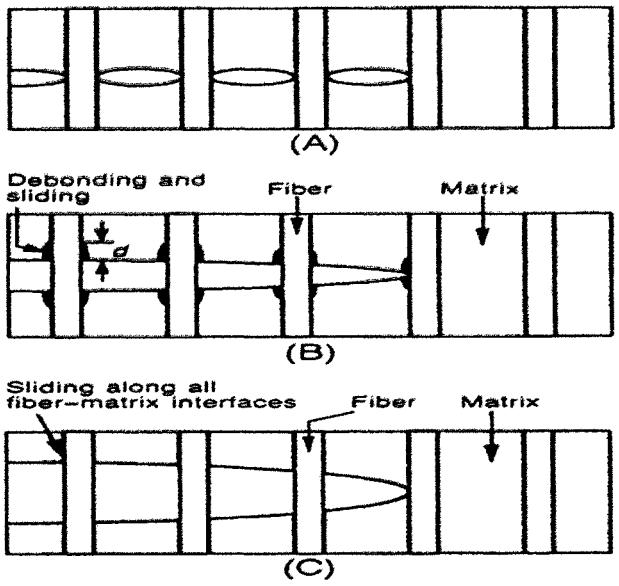

Figure A6. Three types of interfaces: [54]

A). Strongly bonded interface B). Debonded sliding fibres C). Unbonded fibre.

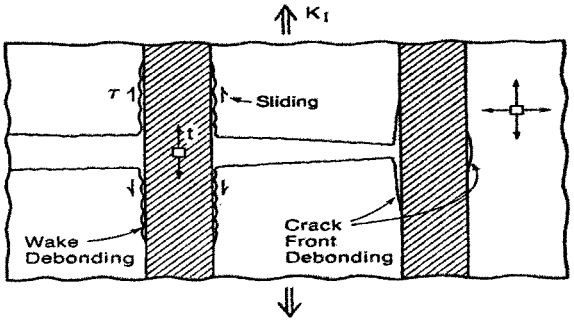

Figure A7. Interface with optimum strength --- crack wake debonding and front debonding [55].

A model for crack deflection at the interface was proposed by Cook and Gorden [57] for ceramic matrix composites. This model is based on stress approach. Consider a crack is meeting the interface between the matrix and crack. At the crack tip the stress distribution will be as shown in Figure A8a. The crack diverting sequences is explained in Figure A8 b.

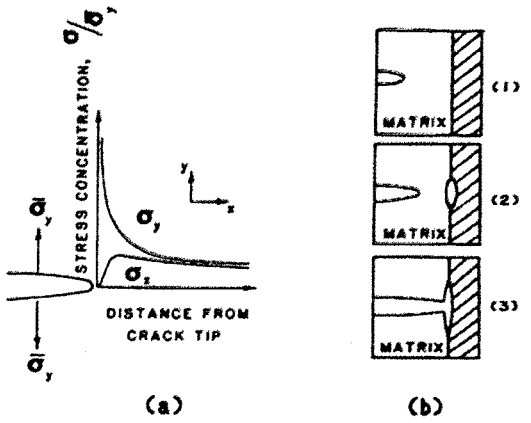

Figure A8. a) Stress distribution at the crack tip b). Schematic description of the crack arrest: 1) crack approaches a weal interface 2) interface fails ahead of the main crack 3) T-shape crack stopper- main crack is diverted [56].

The main applied stress component σ_y has a very high value at the crack tip and decreases sharply with the distance from the crack tip. The component acting normal to the interface σ_x is zero at the crack tip and then falls off in a manner similar to σ_y. Now, if the interface tensile strength is less than the maximum value of σ_x, then the interface will fail in front of the crack tip. Cook and Gordon estimated that the interfacial strength of 1/5 or less than that of the main stress component σ_y, will cause the opening of the interface in front of the crack tip. On the other hand, it is also possible to analyse in terms of fracture energy parameter [58]. This formulation is based on the assumption that the propagation of the debonding zone requires a certain energy and the debonding will occur only when the energy flowing in to the interface exceeds the value of the specific resistance energy.

6.1.1 Interfacial bond

Normally three types of bonding such as frictional, chemical and mechanical bonding exist between the fibre and matrix [58-59]. Figure A9a shows an ideal, smooth interface while Figure A9b shows a real interface which is rough and will allow interlocking.

The bond can be a adhesive bond between the steel and fibre or frictional bond between steel and the surrounding matrix. Mechanical bonding is nothing but simply keying of two surfaces. Interlocking would be better if the fibre has rough surface or

having specific geometry. This type of bonding can also be promoted through a situation where the matrix in a composite radially shrinks more than the fibre on cooling from a high

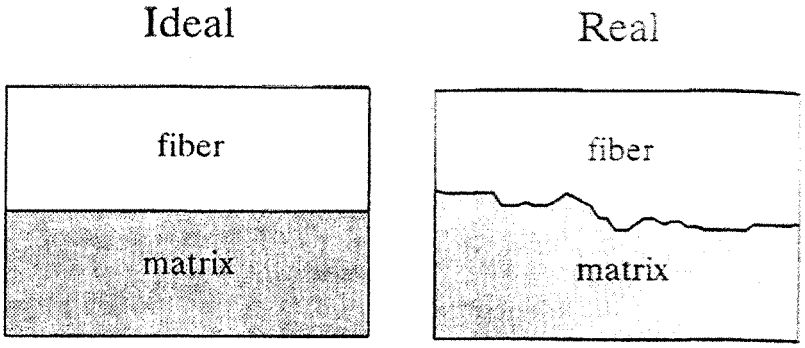

Figure A9. Nature of interface. a) Smooth ideal interface [59].

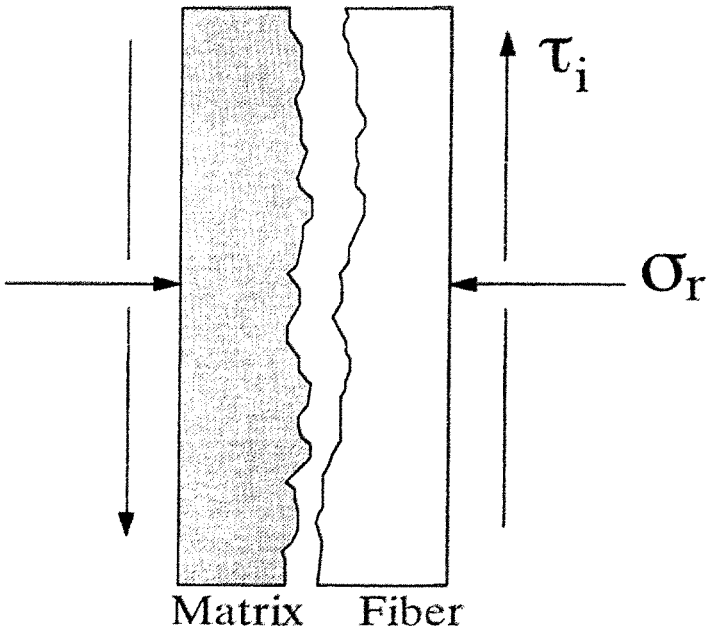

Figure A9. Nature of interface. b). Rough real interface [59].

temperature. This would lead to a gripping of the fibre by the matrix even in the absence of any chemical reaction. The matrix penetrating the crevices on the fibre surface, or by liquid or viscous flow or high temperature diffusion can also lead to mechanical bonding.

In chemical bonding atomic or molecular transport, by diffusion processes is involved. Solid solution or chemical compound may occur at the interface resulting in reinforcement –matrix interfacial reaction zone with a certain thickness [90].

6.1.2 Load transfer from matrix to fibre-shear lag model

Let us load the concrete axially. Assume no direct loading of fibres occurs. Then, the fibre and the matrix will experience locally different axial displacements because of the different elastic moduli of matrix and fibres. The larger the difference between the elastic modulus of the fibre and matrix, the larger will be the difference in their axial displacements. Different axial displacements in the fibre and the matrix results in shear strains which are produced in the matrix in planes parallel to the fibre axis [59]. The transfer of the applied load to the fibre occurs by means of these shear strains in the matrix. Figures A10a and A10b shows the unstressed and stressed state of interface. The main draw back of this theory is that it assumes perfect bonding between fibre and matrix, Poisson's ratio are equal, frictional stress are assumed to be constant, no stress concentrations at the free end of fibres. Up on application of load there are two things can happen either fibre will break or it will get pulled out from the matrix.

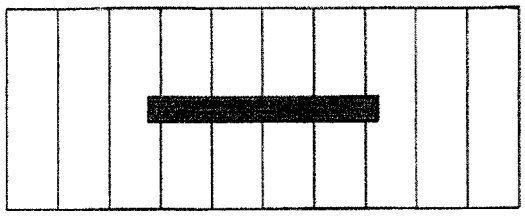

Figure A10 a). Fibre embedded in a matrix : unstressed state[59].

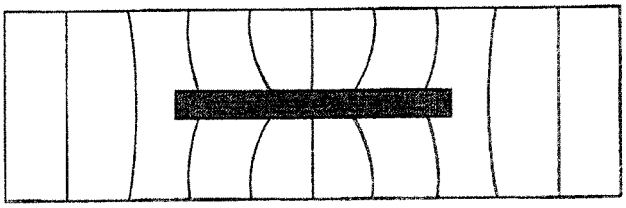

Figure A10 b). Fibre fibre embedded in a matrix: stressed state [59].

Imaginary vertical lines become distorted on application of load.

According to Lawrence [60], fibre debonding occurs, when the shear stress reaches the interfacial bonding strength assuming constant frictional exist between fibre and matrix.

The fibres pull out to takes place,

$$\frac{l}{d} \geq \frac{\sigma_{fu}}{4\tau i}$$

where d –is the diameter of the fibre

σ_{fu} – is the fracture stress of the fibre in tension

τ_i - is the shear force corresponding to the interface failure.

Here the l/d – is the aspect ratio called critical aspect ratio. Practically it can be measured through pull out curve.

For the fibre to break,

$$\pi r^2 \sigma_{fu} \leq 2\pi r l \tau_i$$

In practice, the FRC composites consist of short fibres which are either randomly dispersed in three dimensions. The load-bearing capacity is smaller than that of composites with aligned and continuous fibre. The effects of both length and orientation effects of fibres have to be taken into account load-transfer mechanism in terms of fibre efficiency.

6.1.3 Interfacial bond strength

The interfacial shear strength can be measured through fibre pull out, push in, micro bond techniques, etc. Among them fibre pull out is widely used for Fibre reinforced cementitious materials. In case of Ceramic matrix composite push-in test is predominantly adopted using Nano-Indentation technique. From the pull out test, the work done during the fibre pull out can be calculated.

6.1.4 Pull out test

In pull out test, a fibre is cast into a cement based matrix, after getting dried, loaded into in tension until the fibre debonds and is withdrawn. Pull out of a fibre from a cement is used to characterise the interface bond between the matrix and the fibre.

High temperature test is also possible by holding the sample at high temperature and apply the load in tension. In order to find out the critical fibre length required for effective load transfer, fibres are embedded with different embedment length and the corresponding the pull out load is measured [61,62]. The peak pull out load measures the interfacial bond strength between fibre and matrix. A schematic loading set-up is shown in Figure A11 Figure A12 illustrates the pull out curve for different embedded lengths. From the data of embedment length versus peak pull out stress, the critical fibre length can be obtained. The interfacial shear strength can be calculated using the equation 2.5 given below.

$$\tau_{av} = \frac{P_{\max}}{2\pi r L} \qquad \text{(Equation 2.5)}$$

where Pmax –is the maximum pull out load

r –is the fibre radius

L- is the fibre length

Naamen [63] and shah investigated the pull out of steel fibres at different angles. They reported the peak load and the work required to completely pull out inclined fibres at different inclination angles. The peak pull out loads for fibres inclined relative to the loading direction is almost as high as those for fibres parallel to the loading direction where as the work required to completely pull out an inclined fibre is higher than that

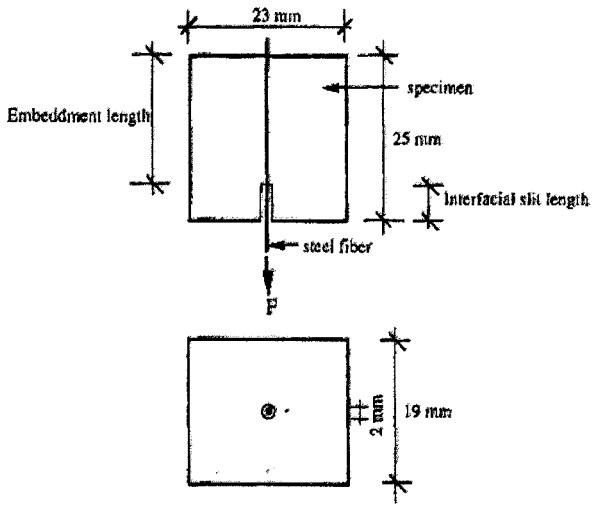

Figure A11. Line diagram of Pull out test [62].

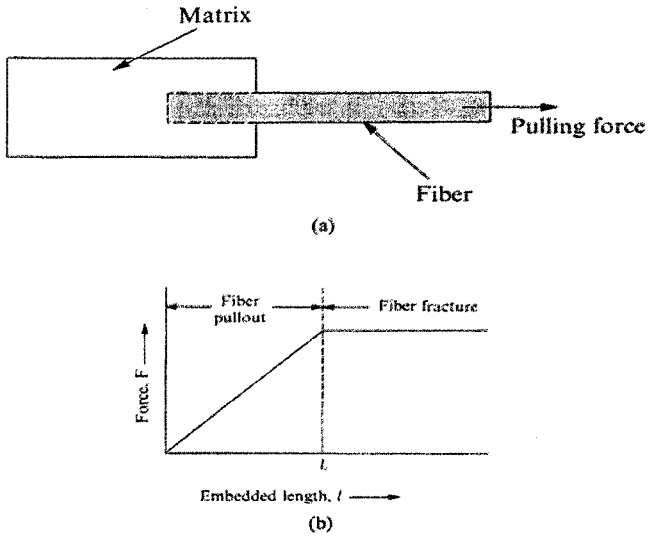

Figure A12. Embedment length versus the force [59].

of parallel fibres. The maximum work required occurs when the inclined angle is 45^0. The increase of load and pull out work can be explained as follows. When the fibre is pulled out from a matrix at an inclined angle, the matrix wedge at the fibre exit point

exerts a normal force, N, as shown in Figure A13 on the fibre to allow the axial force in the fibre to change its direction A frictional force F, which results from both N and the relative movement between the fibre and the matrix occurs at the same time, causes bending of fibre where as F provides an additional frictional stress on the embedded part of the fibre. Both bending and frictional stress are responsible for pull out behaviour of inclined fibre [64]. However, when the angle is greater than 45^0, the bending of the inclined fibre may result in spalling of the concrete wedge, which decreases the pull out and work of the inclined fibre.

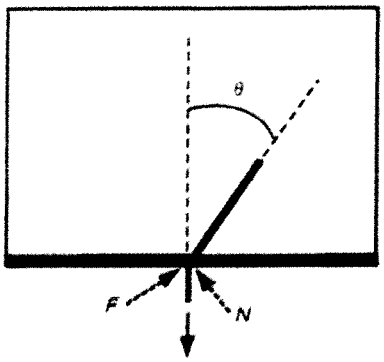

Figure A13. Component of force acting in a inclined fibre during pull out test [63].

7.1 Strength parameters related with thermal shock

Refractory materials are subjected to high temperatures, so naturally exposed to thermal stress. Thermal stress are internal stresses that arise when there is a constraint

on change in dimension. The constraint may be due to temperature gradient, crystal structure anisotrophy, phase transformations, materials having different thermal expansion co-efficinects, etc. Since refractory materials are having low-thermal conductivity compared to metals, thermal gradients are introduced and can be calculated as shown below (65).

$$\Delta T = \left(\frac{C_p \rho}{k} \right) \qquad \text{(Equation 2.6)}$$

ρ - is the density of the material

k -is the thermal conductivity

C_p - is the specific heat

When a ceramic material is cooled from both the surfaces, then thermal stress are induced, which can be related with thermal gradient. Hassleman [76] developed a theory to explain the crack's resistance of ceramic materials to thermal shock. Due to the thermal shock, material is under forced deformation. Initially it was first studied by Kingery who derived the criteria for elastic materials (ceramics) to fracture under thermal stress and it is based on strength criteria of the material. Cracks will be initiated in materials when the thermal stress σ_T of the material exceeds the fracture stress σ_R of the material.

$$\sigma_T = \left(\frac{\alpha E \Delta T}{(1-\mu)}\right) \qquad \text{(Equation 2.7)}$$

μ - is the poison's ratio

α – is the coefficent of thermal expansion

E –is the Elastic modulus

ΔT- Max temperature difference

The above equation represents only the thermo-elastic fracture initiation process. But Hasselman has derived expressions for thermal shock damage resistance parameter for the cracks which are already exist in a material. The expressions are given below.

$$R_{st} = \sqrt{\frac{\gamma}{\alpha^2 E}} \qquad \text{(Equation 2.8)}$$

$$R''' = \frac{E\gamma}{\sigma^2{}_f (1-\mu)} \qquad \text{(Equation 2.9)}$$

Where γ - is the work of fracture

μ - is the posson's ratio

σ_f–is the fracture stress of the material.

E – is the elastic modulus

8.1 Temperature effect on castable

Castables are basically a high temperature concrete materials containing aggregates, binders, fillers, cement and additives, and are bonded through the hydration of calcium

aluminate phases which are present in the cement. Before going into the temperature effect on the castable, a brief review of hydration of cement is required.

High alumina cement contains normally three phases such as CA, CA_2 and $C_{12}A_7$. Up on contact with water, rapid dissolution of Ca_{2+} and $Al(OH)_4$- in to water, takes place at surface of cement grains. Then Calcium alumina hydrate later is formed on the anhydrous CA grains. In course of time, rupture of layer occurred after which hydration proceeds with faster rate. The phases formed during hydration at different temperatures are shown in Table A2. When micro silica is present ,it will react with C_2AH and form C_2ASH_8 (gehlenite hydrate) between 30 to 60°C. The presence of microsilica retards the hydration of CA and CA_2 phases.

Table A2. Phases formed during hydration of calcium aluminate cement (76)

Phase formed	Reaction of Formation	Temperature Range (C)
CA H10	CA + 10 H -→ CAH_{10}	< 21.4
C_2A H8	2 CA + 11 H -→ C_2AH8 + AH_3 (gel)	21.4 <T> 35
C_3A H6	3 CA + 12H --→ C_3AH6 + 2 AH_3	>35

C--- CaO; A----Al_2O_3; H--- H_2O ; S--- SiO_2

In addition with reactive alumina will also influence the hydration of HA cement. In fact it would accelerate the hydration process due to the presence of soluble sodium in the alumina which in turn changes the concentration of solution.

The effect of temperature on the cement phase is shown in Figure A14. In addition with several phases formation are possible in the fine matrix position which depends on the temperature. Above 1000°C, the alumina and magnesia will react and form in-situ spinel which has expansive in nature. One more thing is that at high temperature there is a possibility of reaction between the fibre and matrix which may change the interface characteristics. This has been confirmed by the M. Schmucker et al, who have studied the effect of temperature induced fibre /matrix interactions in alumina silicate ceramic matrix composites and found that the damage tolerance capacity of composite is reduced above 1300°C [78].

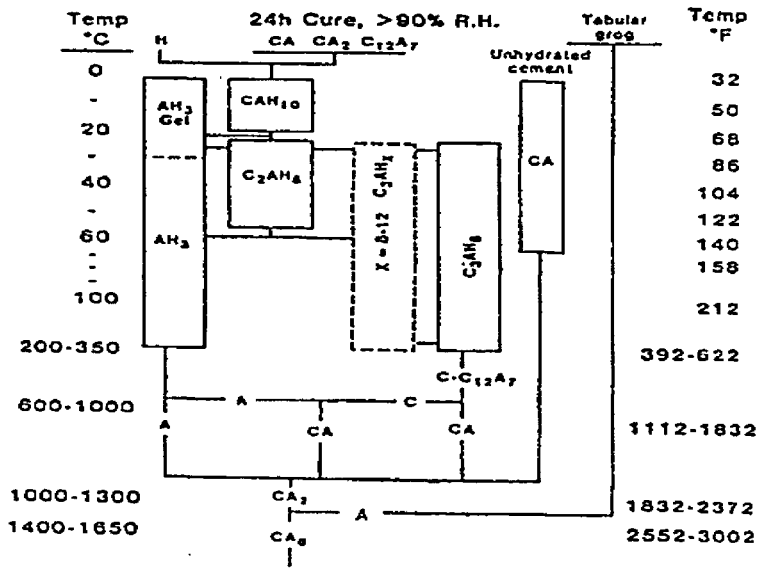

Figure A14. Shows the dehydration of calcium aluminate cement with respect to temperature. [77]

9.1 Steel fibres in castable

Addition of steel fibres to castable has several impacts on properties. It was first studied by David et al, [67] in the year 1971 and their findings are that the use of 2 vol % of fibres resulted in enhancement of Alumina based castable's cold modulus of rupture value from 80 to 120 % when measured from 110 to 1100°C. Beyond 1100°C, there is a decline in MOR value due to the reaction of castable with fibre and also observed improvement in ultimate strength and equivalent fracture strain. With regard to Hot Modulus of Rupture the fibre addition enhances the value almost three fold at 1000°C and beyond this temperature the addition has no effect on either MOR or in load deflection curve and the fracture stress remains same as that of plain castable.Thermal shock resistance of the same castables are found to be improved remarkably. The fibre reinforced castable retained 70% of its dried strength at 1000°C where as plain castable retained 50 %. Stephen et al [54] et, al studied fibre effects in 94 % alumina and 50 % alumina castable. Addition of fibres up to 4 wt % reduced the hot modulus of rupture value of both the castable in the temperature range 800-1100°C but considerable improvement in work of fracture is observed. Study of varying fibre content with hot modulus of rupture at 900°C depicted a indirect relation between hot modulus of rupture value and fibre content.

A review paper by Kenji Anan [68] revealed more information on the influence of chemistry and shape of steel on permanent linear change, oxidation rate, hot modulus of rupture and load-deflection curve. It has been shown that oxidation rate has a direct

relation with chemistry and amount of fibres. Certain type of fibres performed exceedingly well with low oxidation rate even at 1400°C where as others showed high. The reason quoted for such behavioural difference is due to difference in chemistry of fibres. Permanent linear change value also has found to be influenced by the oxidation rate and shape of the fibres. The influence of shape on the load –deflection curve has also been studied [68] and very clearly proved that dog-bone shape exhibiting higher value of toughness compared to other type of fibre like straight ,wavy type.

Interfacial character plays an important role in deciding the mechanical property. A study by T. Cutard et al, [69] clearly indicates that fibre addition has peak stress broadening effect in the load-deflection curve. In their study sample were fired at three different temperatures 110, 500 and 900°C and the pull out test was conducted at room as well at high temperature. The room temperature test results indicates that peak stress value found to be shown declining trend in accordance with firing temperature due to reduction in interfacial shear stress. While subjecting the sample to firing temperature, two types of modifications are observed one with radial crack and another with fibre –matrix decohesion region. Radial crack results from thermal stress that has been developed due to thermal expansion mismatch between fibre and matrix. Such a stress, which is tensile in nature, increases with firing temperature. Radial cracks will form when the thermal stress value exceeds the tensile strength of matrix. Scanning electron microscopic study shows the presence of decohesion region at the interface. In addition with, adhesion regions are also observed locally at the interface. This

decohesion region is found to be responsible for the non-zero value of peak stress at high temperature.

The same group conducted test by the holding the sample at different temperatures (110, 500 and 1100° C). The peak stress value at 500°C was found to be higher than that at room temperature. The reason for such behaviour is due to fritting pressure which developed between the fibre and matrix. One more important finding is the influence of angle of inclination of fibres on the pull out load. As the angle of inclination of fibre increases with respect to pull out direction, it takes more pull out load due to additional frictional stress that developed at the entry point of non-embedded part of fibre into matrix. When the angle exceeds above 45°, the net pull out load decreases.

APPENDIX B

Rheology Curves For The AMC Castables Tested

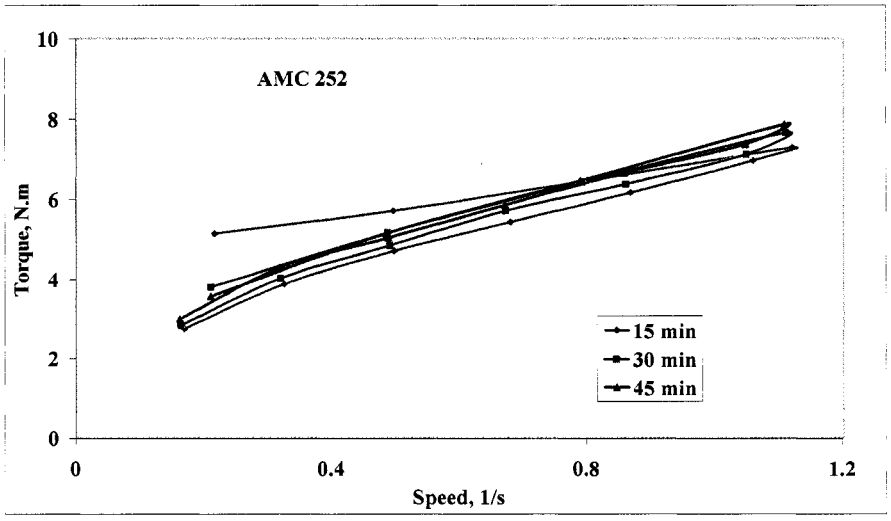

Figure B1. Torque Vs. Speed w.r.t time for AMC castable containing 25 mm length carbon steel fibre with 2 wt % fibre loading.

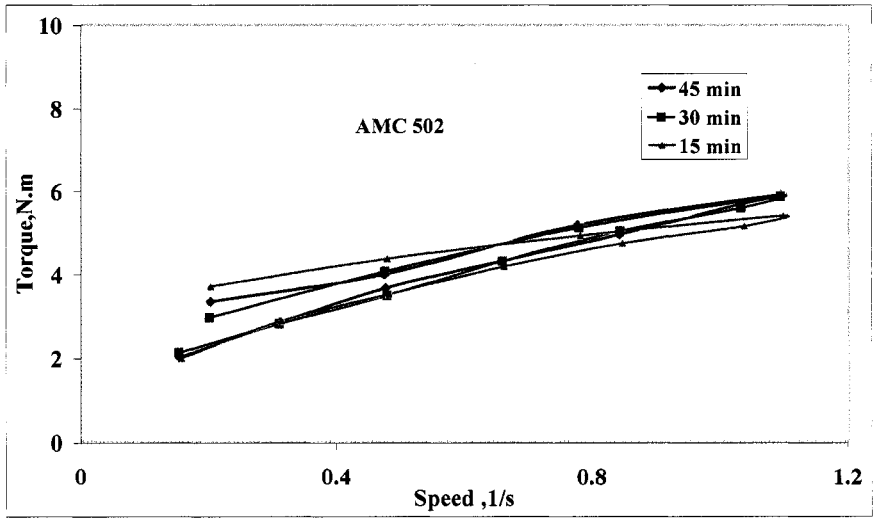

Figure B2. Torque Vs. Speed w.r.t time for AMC castable containing 50 mm carbon carbon steel fibre with 2 wt % loading .

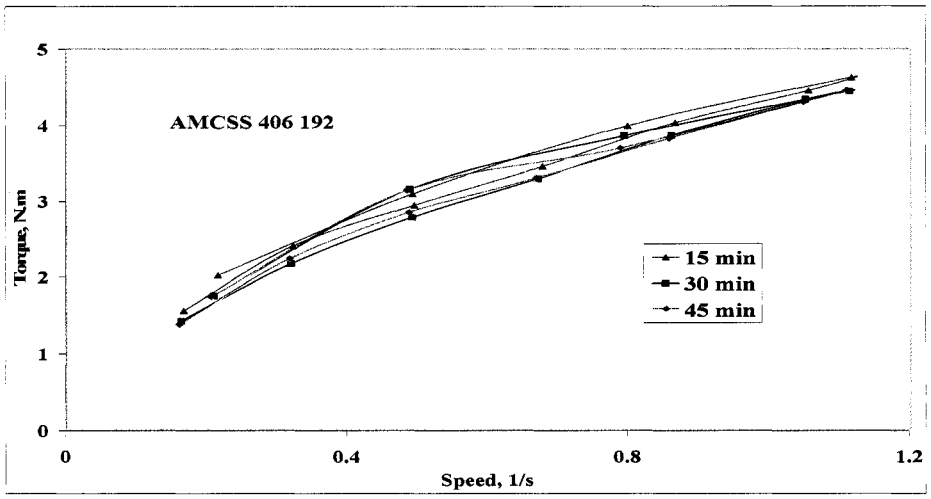

Figure B3. Torque Vs. Speed w.r.t time for AMC castable containing 19 mm length of stainless steel fibre with 2 wt % loading .

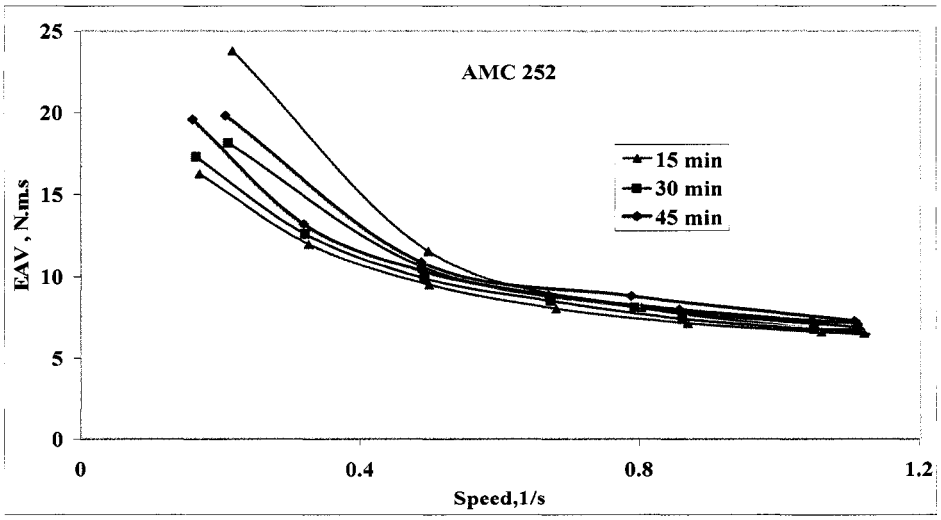

Figure B4. EAV Vs. Speed curve w.r.t time for AMC castable containing 25 mm length of carbon steel fibre with 2 wt % loading.

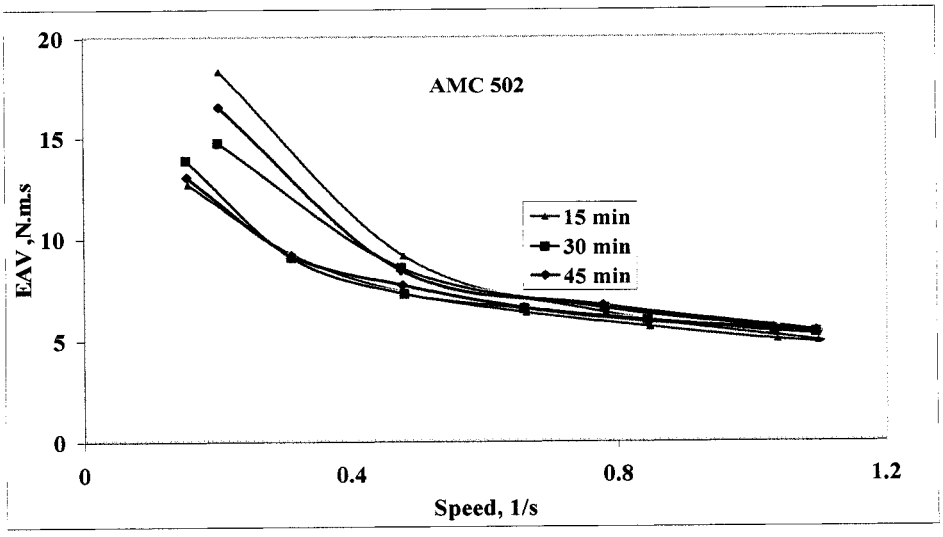

Figure B5. EAV Vs. Speed curve w.r.t time for AMC castable containing 50 mm length of carbon steel fibre with 2 wt % fibre loading.

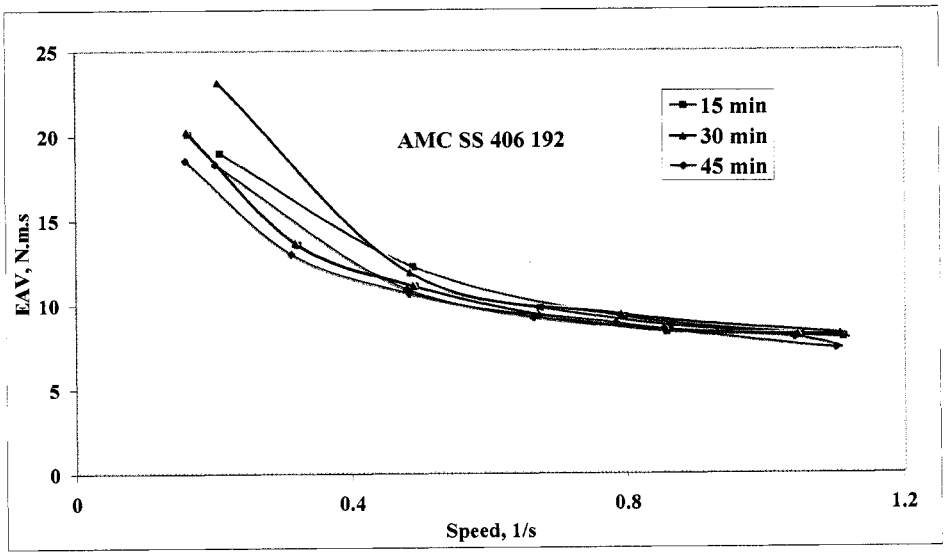

Figure B6. EAV Vs. Speed curve w.r.t. time for AMC castable containing 19 mm length of stainless steel fibre with 2 wt % fibre loading.

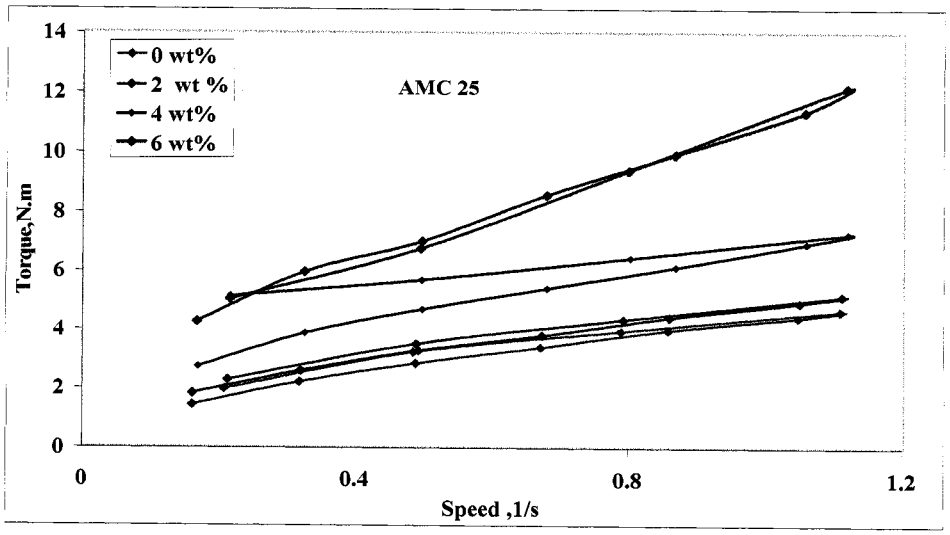

Figure B7. Torque Vs. Speed curve for AMC castable containing 25 mm length of carbon steel fibre at different fibre loading (0, 2, 4, 6 wt %).

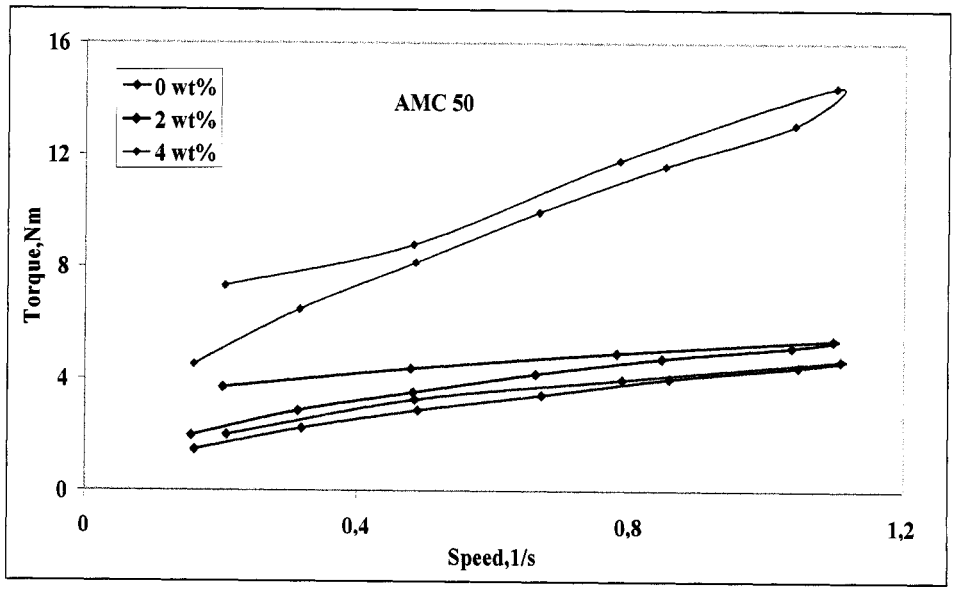

Figure B8. Torque Vs. Speed curve for AMC castable containing 50 mm length of carbon steel fibre at different fibre loading (0, 2, 4 wt %).

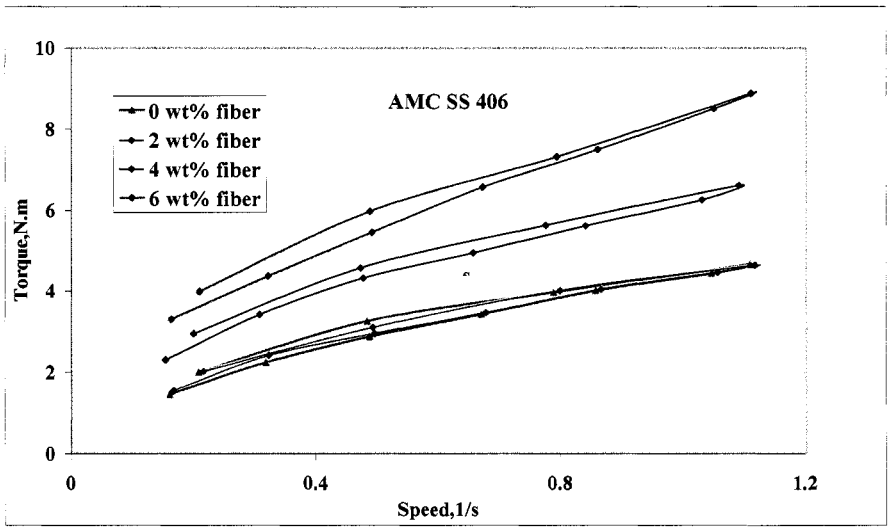

Figure B9. Torque Vs. Speed curve for AMC castable containing 19 mm length of stainless steel fibre at different fibre loading (0, 2, 4, 6 wt %).

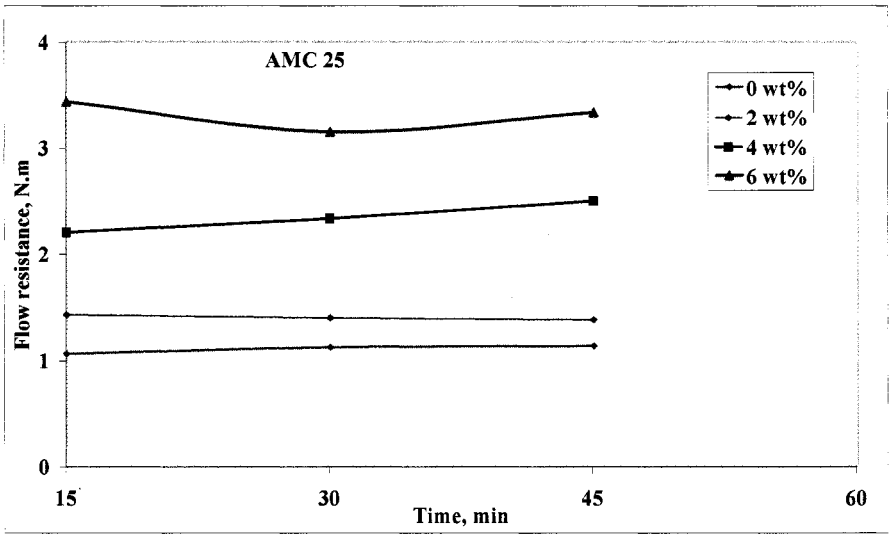

Figure B10. Flow resistance Vs Time curve for AMC castable containing 25 mm length of carbon steel fibre at different loadings(0, 2, 4, 6 wt %).

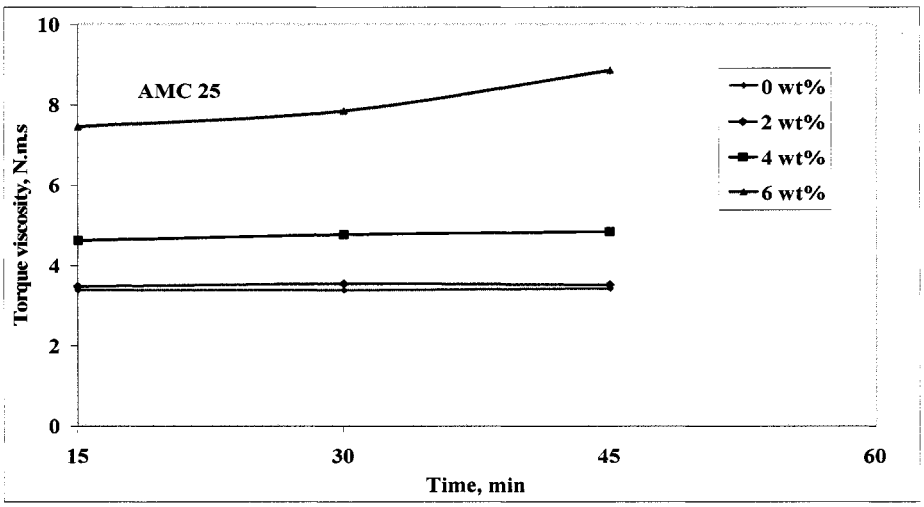

Figure B11. Torque viscosity Vs Time curve for AMC castable containing 25 mm length of carbon steel fibre different loadings (0, 2, 4, 6 wt %).

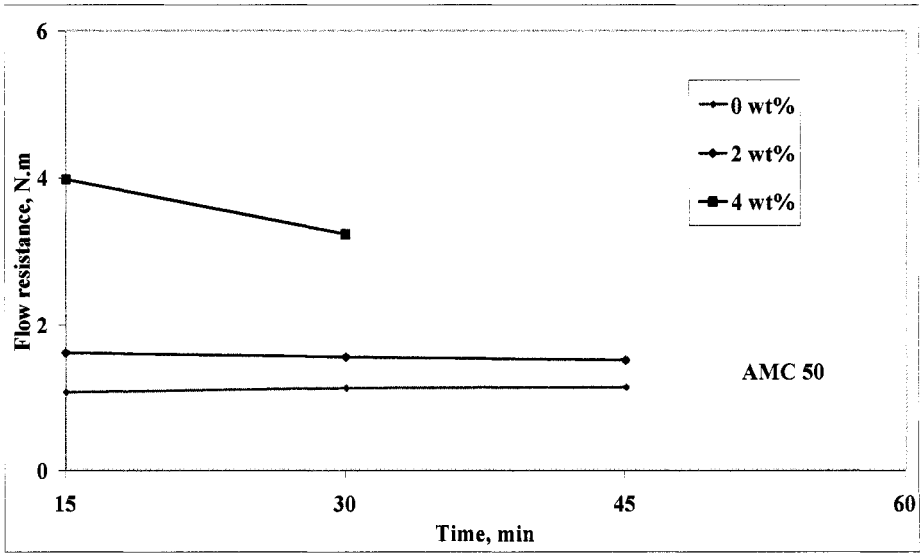

Figure B12. Flow resistance Vs Time curve for AMC castable containing 50 mm length of carbon steel fibre at different fibre loadings (0, 2, 4 wt %)

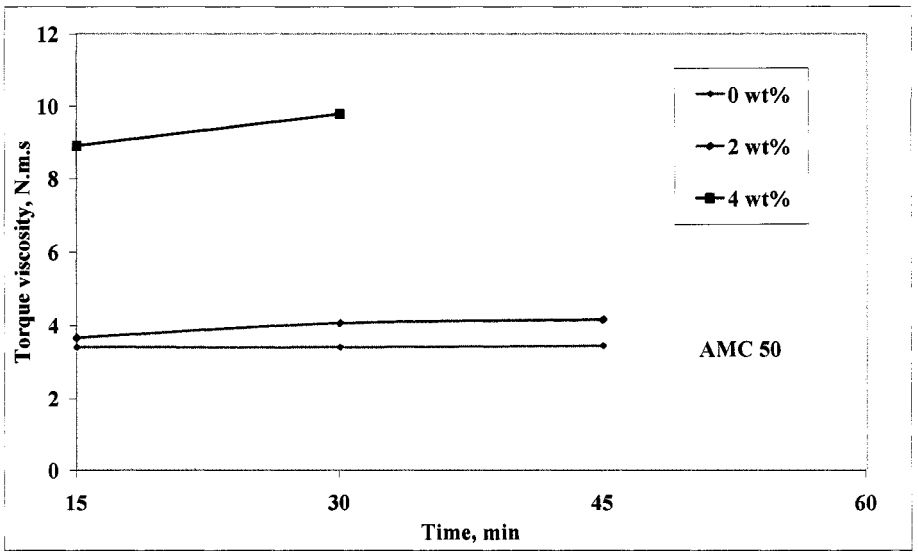

Figure B13. Torque viscosity Vs Time curve for AMC castable containing 50 mm length of carbon steel fibre at different loadings (0, 2, 4, 6 wt %).

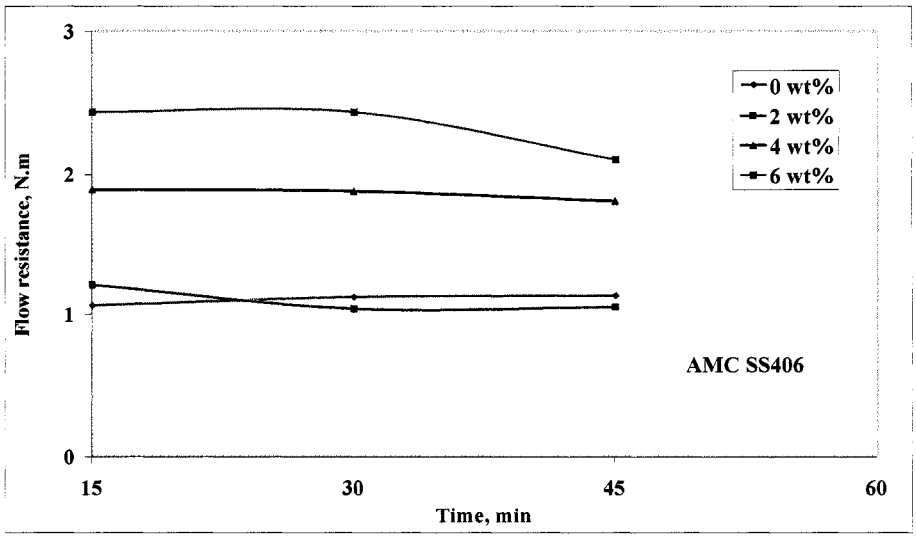

Figure B14. Flow resistance Vs Time for AMC castable containing 19 mm length of stainless steel fibre at different fibre loadings (0, 2, 4, 6 wt %).

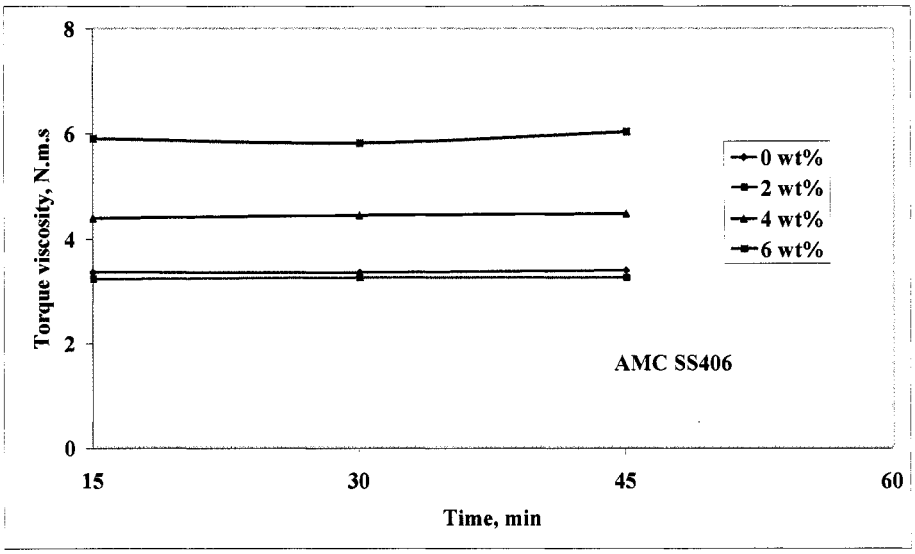

Figure B15. Torque viscosity Vs Time curve for AMC castable containing 19 mm stainless steel fibre at different loadings (0, 2, 4, 6 wt %).

APPENDIX C

Force- Extension Curves For The AMC Castables Tested

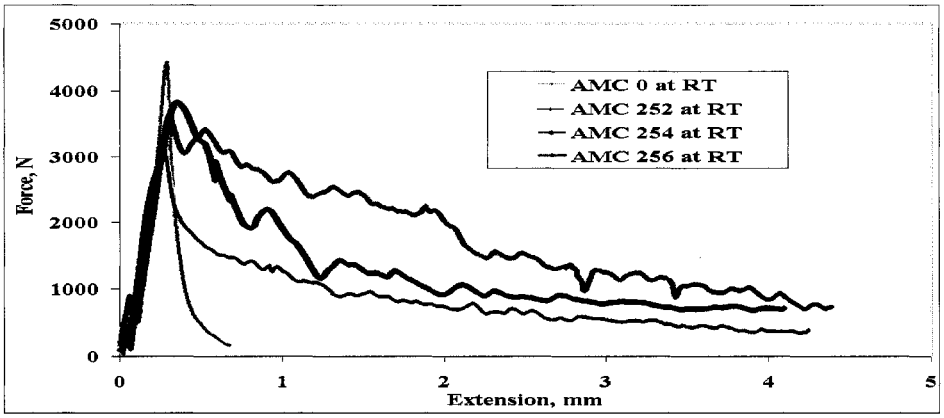

Figure C1. Comparison of force-extension curves of 25 mm length of carbon steel fibre reinforced AMC castables with fibre loadings (0, 4, 6, wt %) at room temperature.

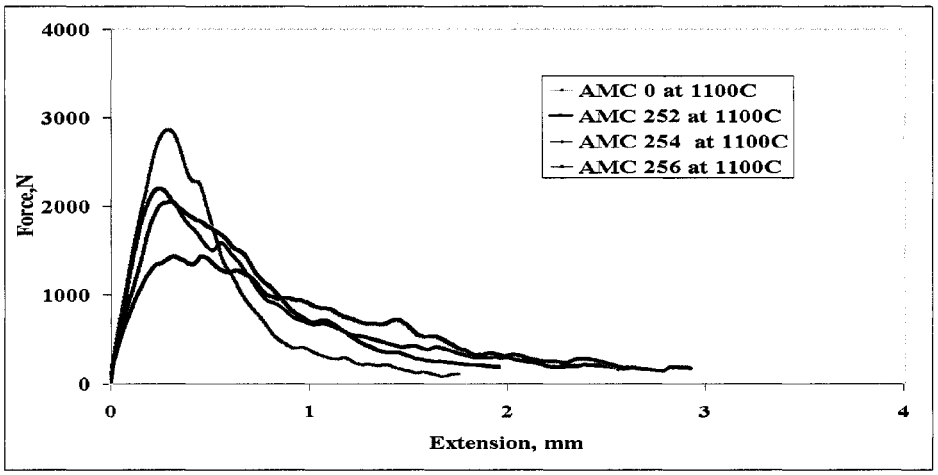

Figure C2. Comparison of force-extension curves of 25 mm length of carbon steel fibre reinforced AMC castables with fibre loadings (0, 2, 4, 6 wt %) at 1100°C.

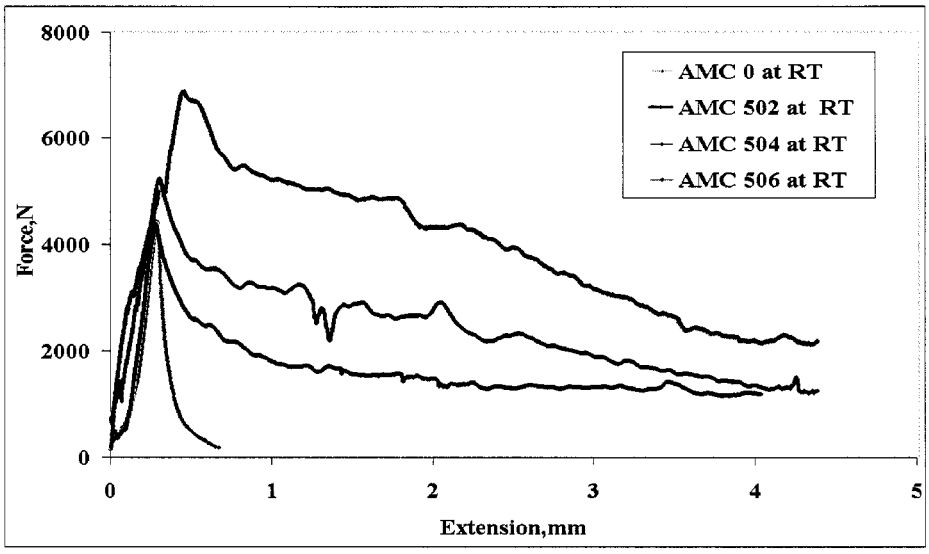

Figure C3. Comparison of force-extension curves of 50 mm length of carbon steel fibre reinforced AMC castables with fibre loadings (0, 2, 4, 6 wt %) at room temperature.

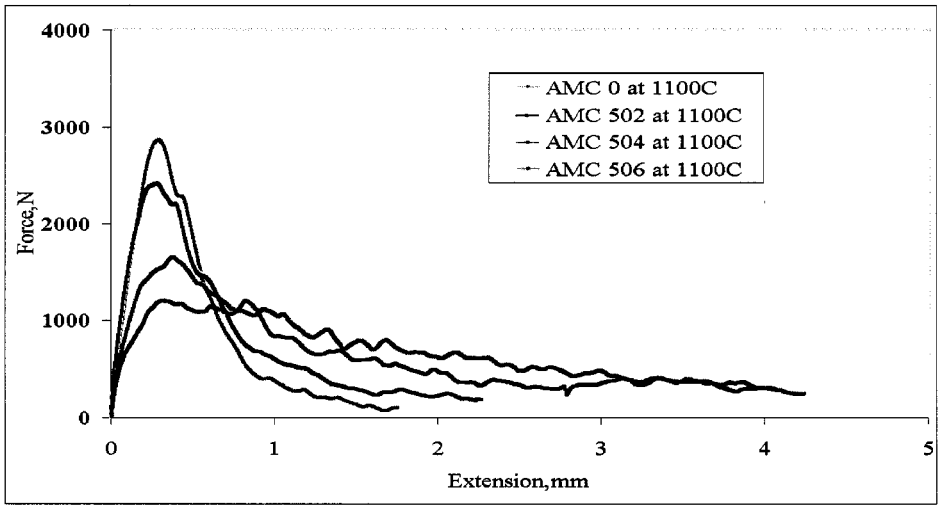

Figure C4. Comparison of force-extension curves of 50 mm length of carbon steel fibre reinforced AMC castables with fibre loadings (0, 2, 4, 6 wt %) at 1100°C.

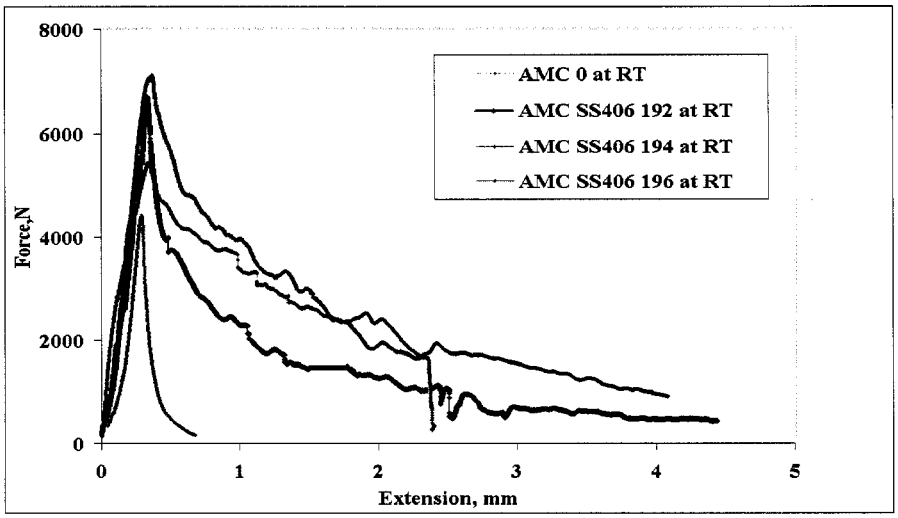

Figure C5. Comparison of force-extension curves for 19 mm length of stainless steel fibre reinforced AMC castables with fibre loadings (0,2, 4, 6 wt %) at room temperature.

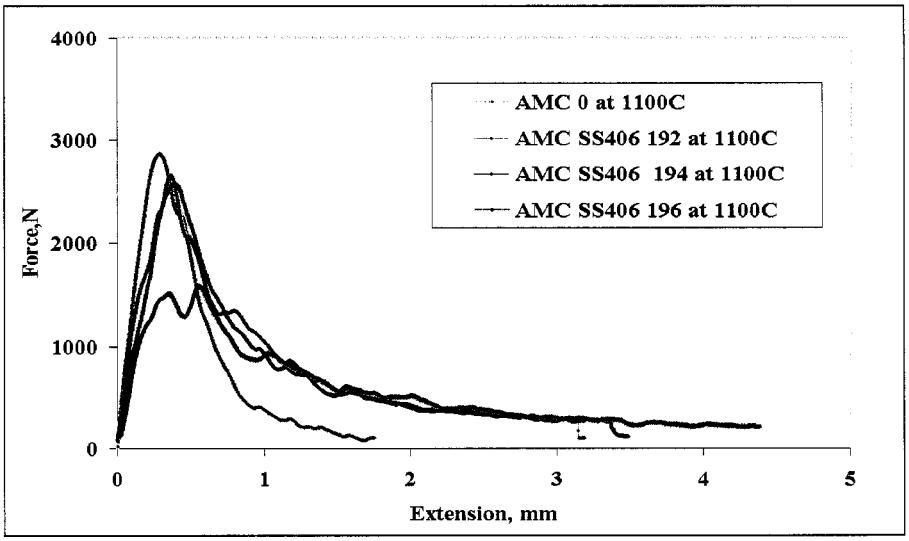

Figure C6. Comparison of force-extension curves for 19 mm length of stainless steel fibre reinforced AMC castables with fibre loadings (0,2,4,6 wt %) at 1100°C.

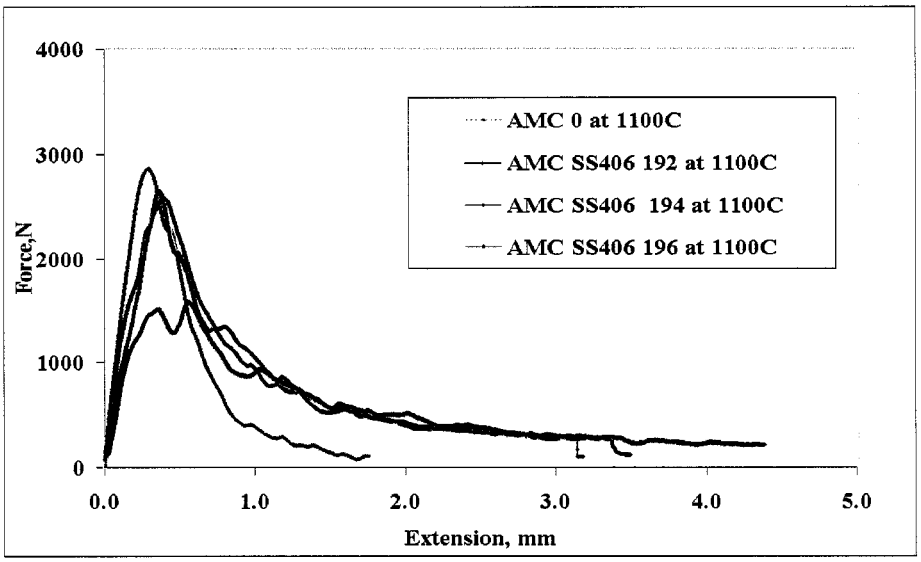

Figure C7. Comparison of force-extension curves for 2 wt % carbon steel fibre reinforced AMC castables with different length levels (19, 25, 50 mm) at room temperature.

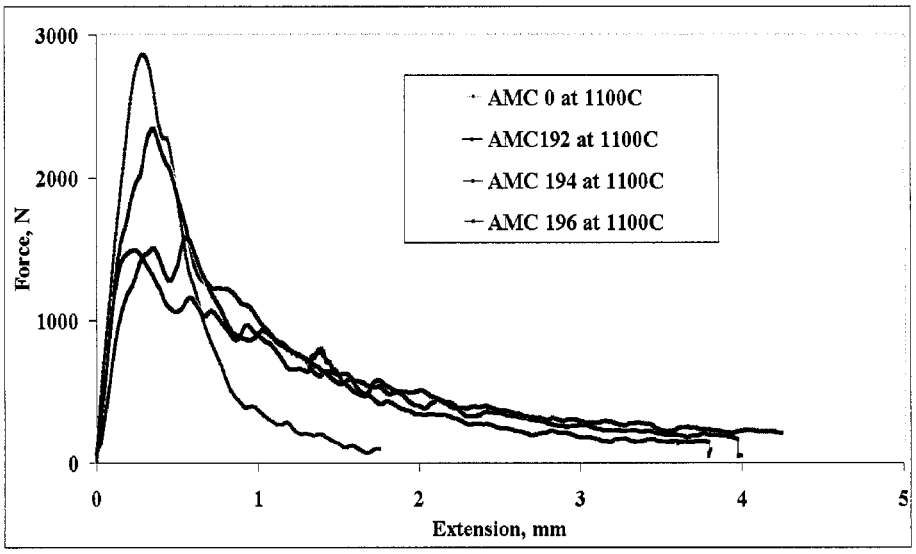

Figure C8. Comparison of force-extension curves for 2 wt % carbon steel fibre reinforced AMC castables with different length levels (19, 25, 50 mm) at 1100°C.

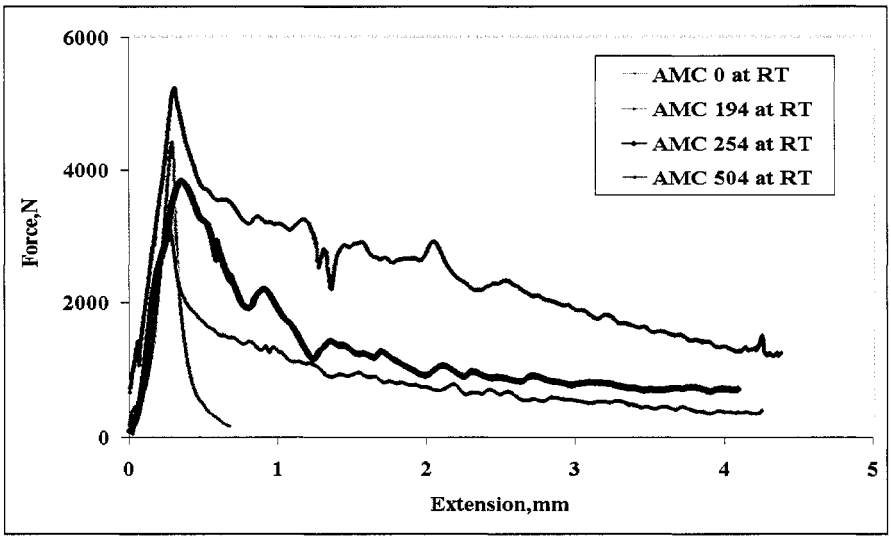

Figure C9. Comparison of 4 wt % of carbon steel fibre reinforced AMC castables with different length levels (19, 25,50 mm) at room temperature.

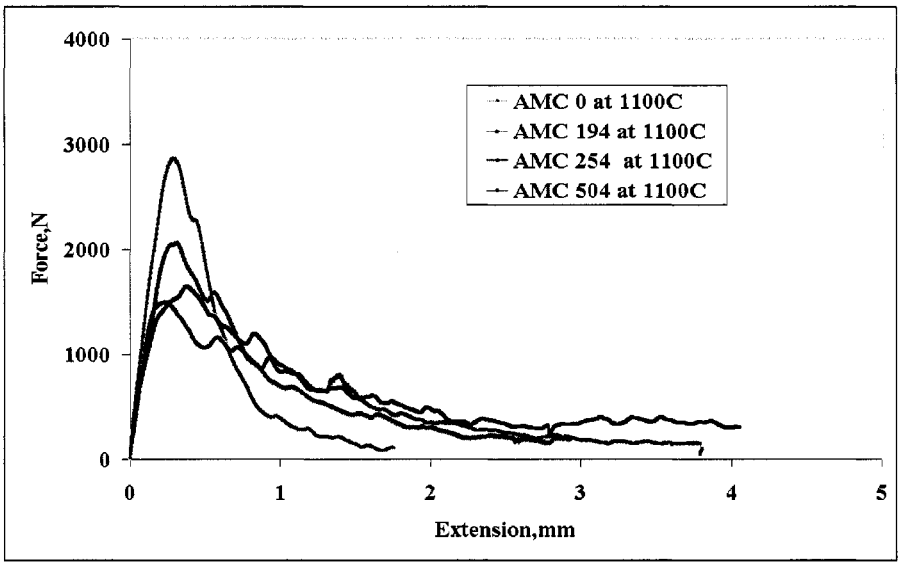

Figure C10. Comparison of 4 wt % of carbon steel fibre reinforced AMC castables with different length levels (19, 25, 50 mm) at 1100°C.

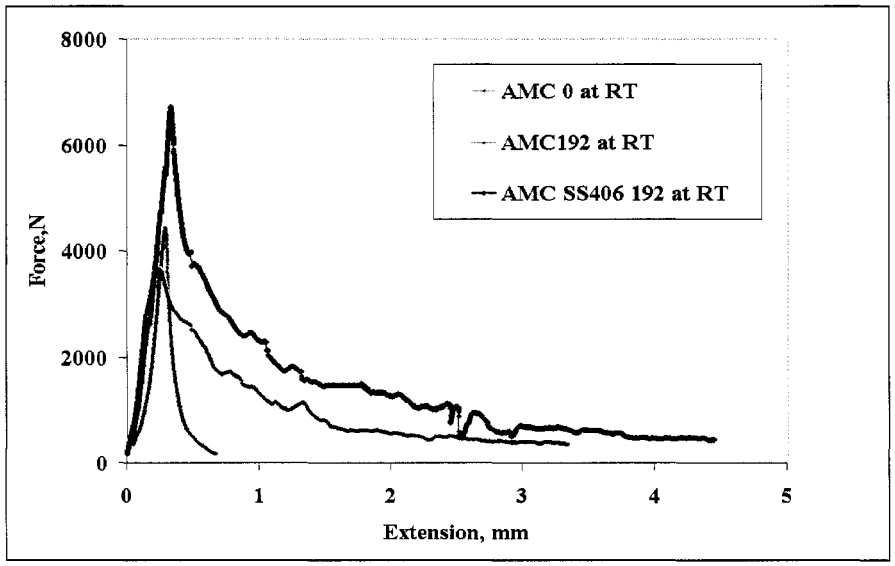

Figure C11. Comparison of 2 wt % of carbon and stainless steel fibre reinforced AMC castables with 19 mm length level at room temperature.

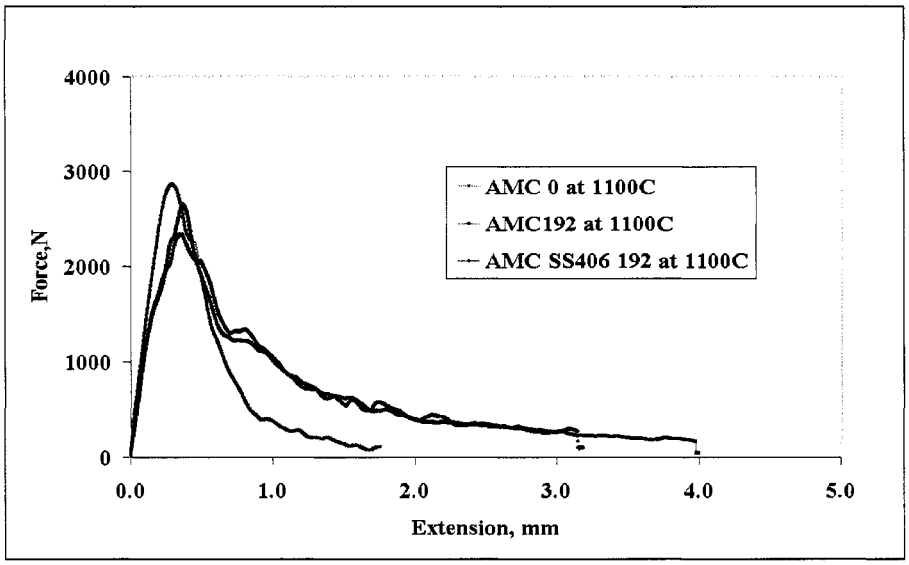

Figure C12. Comparison of 2 wt % of carbon and stainless steel fibre reinforced AMC castables with 19 mm length level at 1100°C.

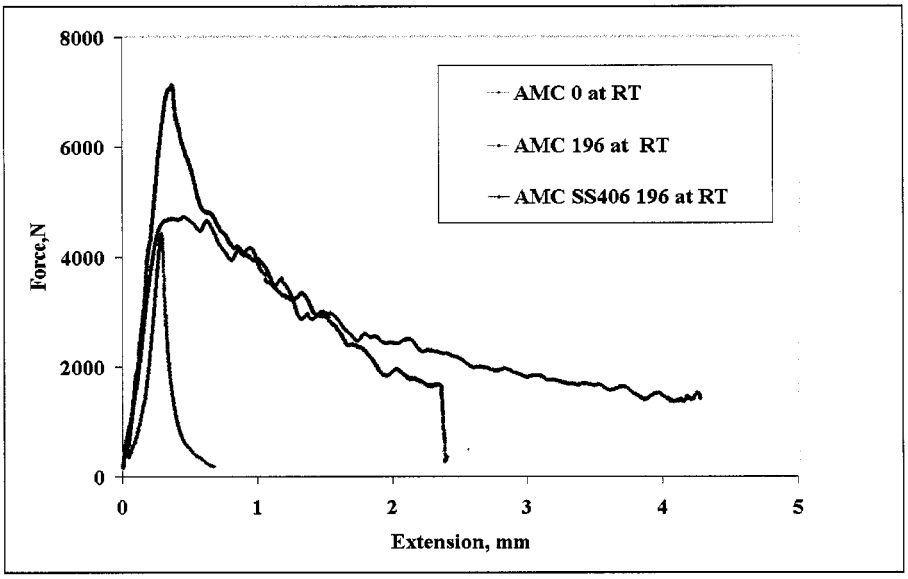

Figure C13 Comparison of 4 wt % of carbon and stainless steel fibre reinforced AMC castables with 19 mm length level at room temperature.

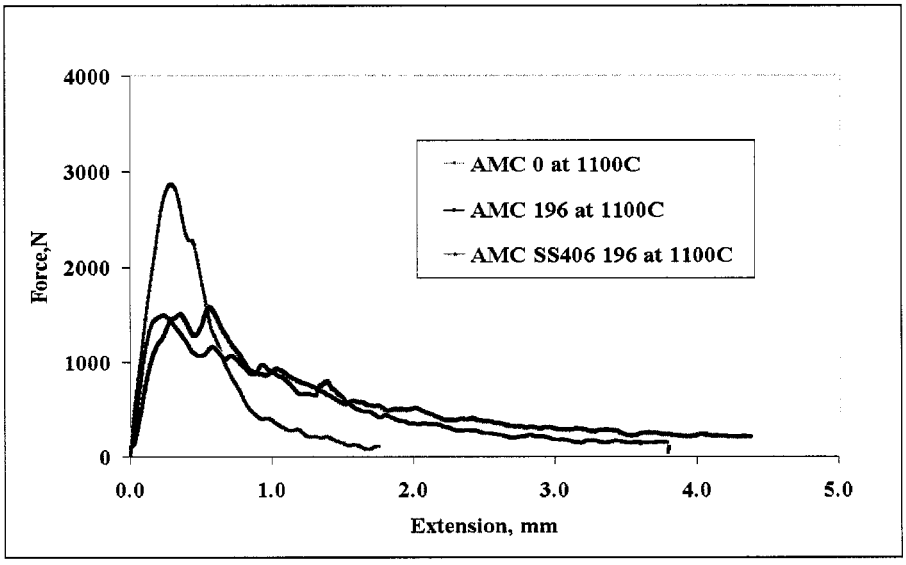

Figure C14. Comparison of 6 wt % of carbon and stainless steel fibre reinforced AMC castables with 19 mm length level at 1100°C.

APPENDIX D

Other Test Results For AMC Without And With Fibre Additions

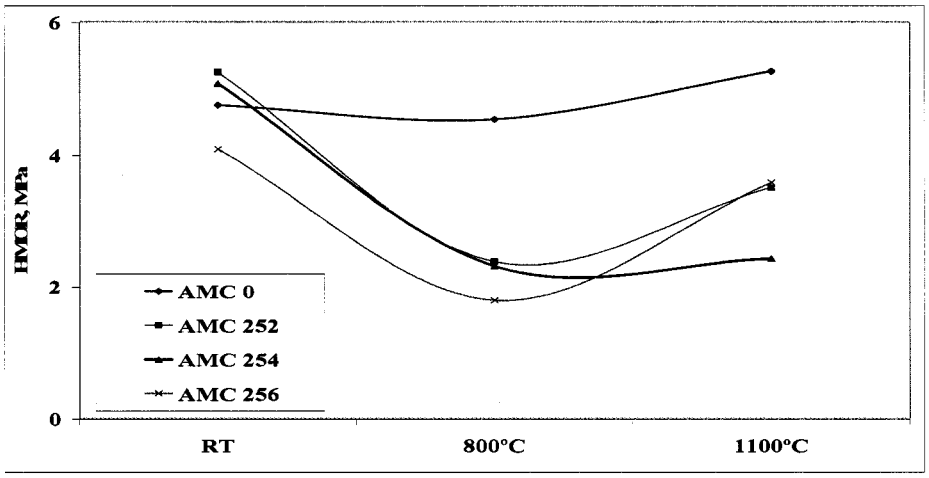

Figure D1. Variation of modulus of rupture w.r.t. temperature for 25 mm carbon steel fibre reinforced AMC castables at different fibre loadings (0, 2, 4, 6 wt %).

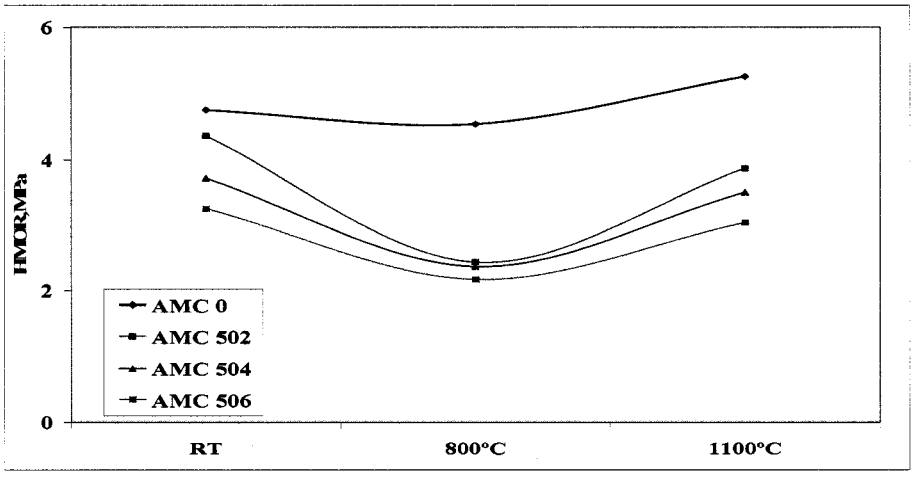

Figure D2. Variation of modulus of rupture w.r.t. temperature for 50 mm carbon steel fibre reinforced AMC castables at different fibre loadings (0, 2, 4, 6 wt %).

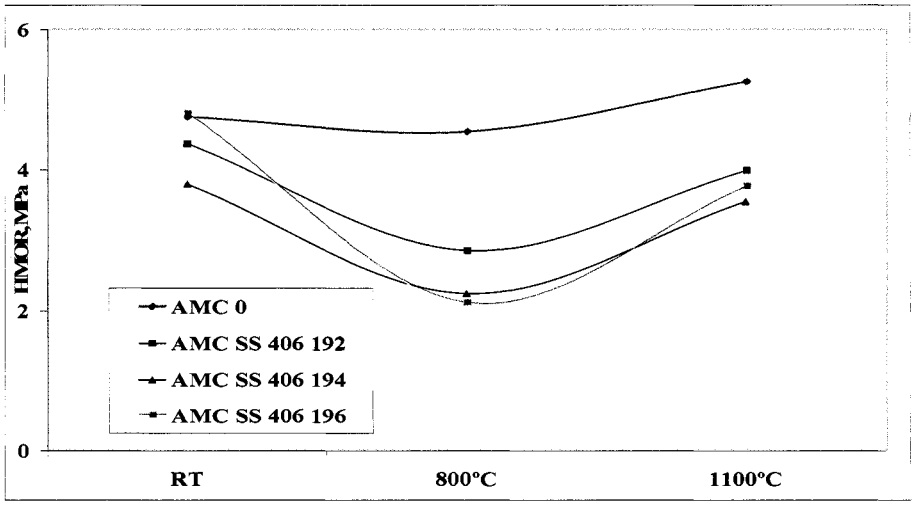

Figure D3. Variation of modulus of rupture w.r.t.temperature for 19 mm length of stainless steel fibre reinforced AMC castables at different fibre loadings (0,2, 4, 6 wt %).

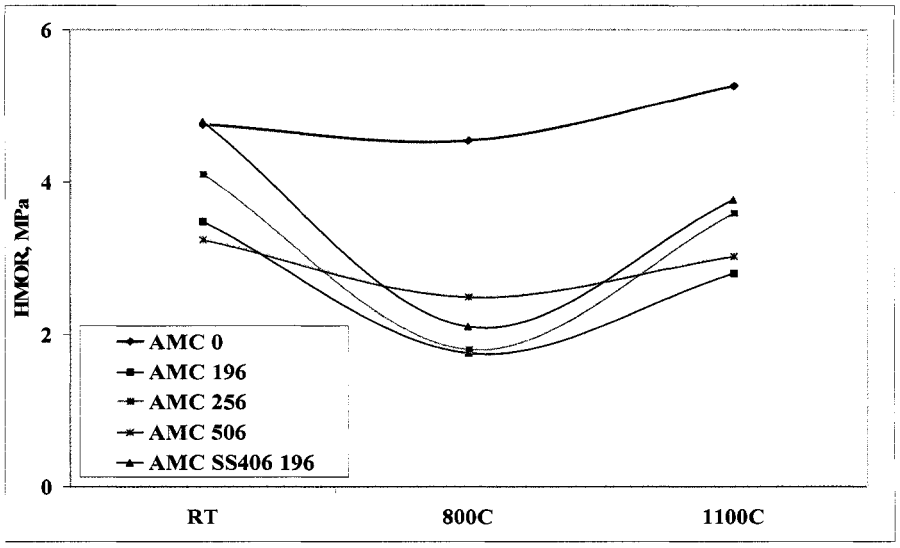

Figure D4. Variation of modulus of rupture w.r.t. temperature for 6 wt % of carbon steel fibre reinforced AMC castables with different length levels (19, 25, 50 mm).

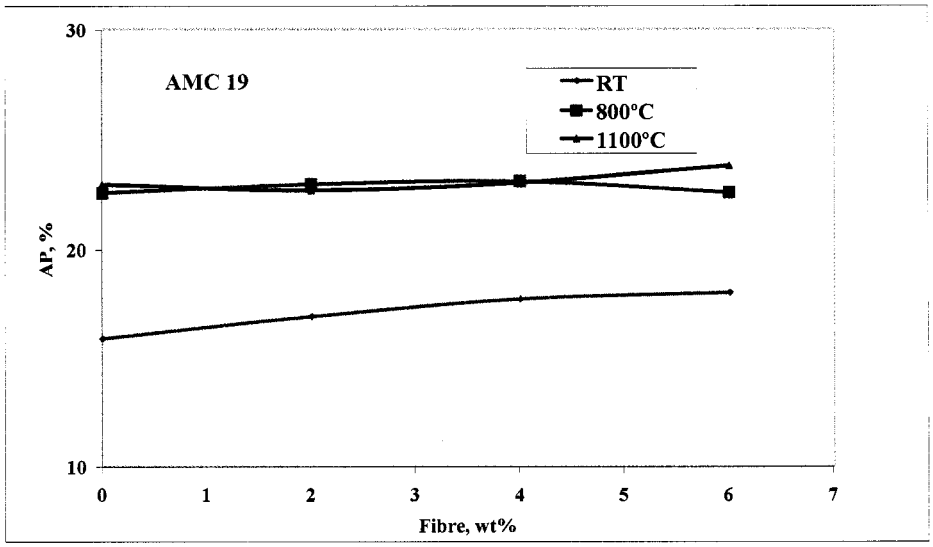

Figure D5. Variation of apparent porosity w.r.t. fibre loadings for 19 mm length of carbon steel fibre reinforced castables at different temperatures.

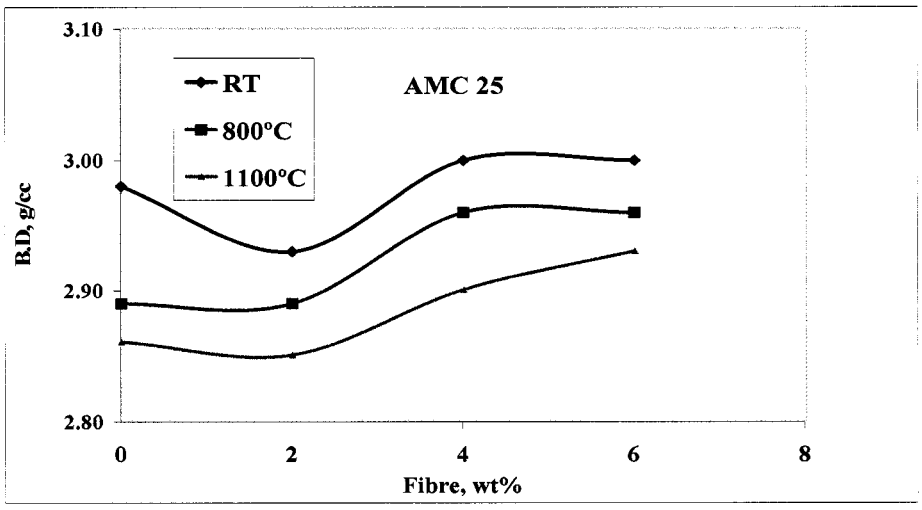

Figure D6. Variation of apparent porosity w.r.t. fibre loadings for 25 mm length of carbon steel fibre reinforced castables at different temperatures.

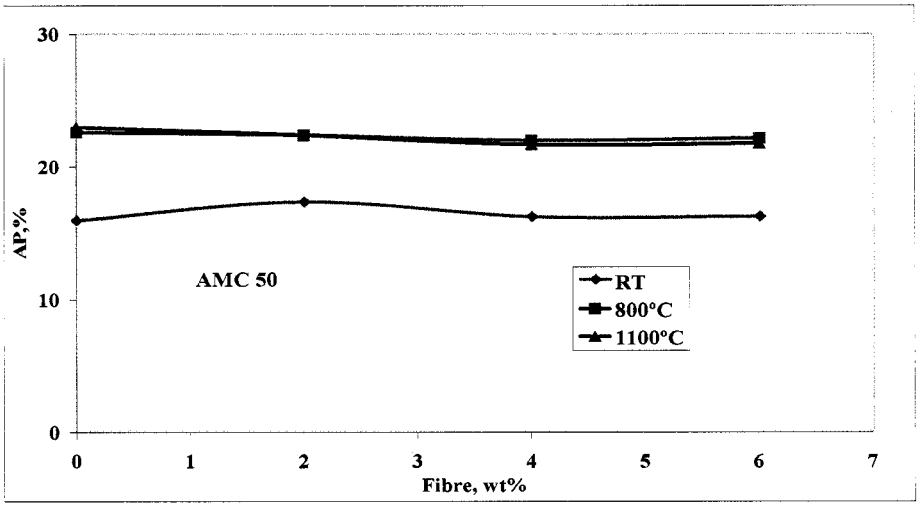

Figure D7. Variation of bulk density w.r.t.fibre loadings for 50 mm length of carbon fibre reinforced AMC castables at different temperatures.

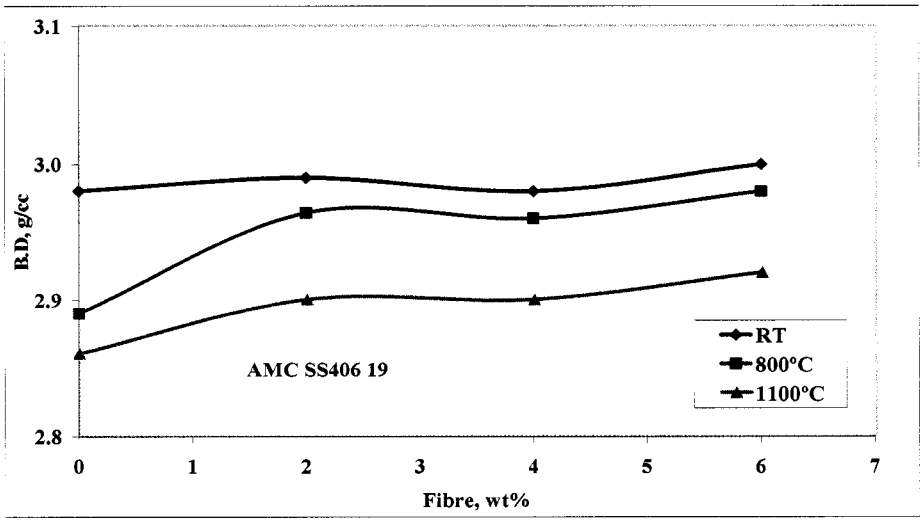

Figure D8. Variation of bulk density w.r.t. fibre loadings for 19 mm length of stainless steel fibre reinforced AMC castable at different temperatures.

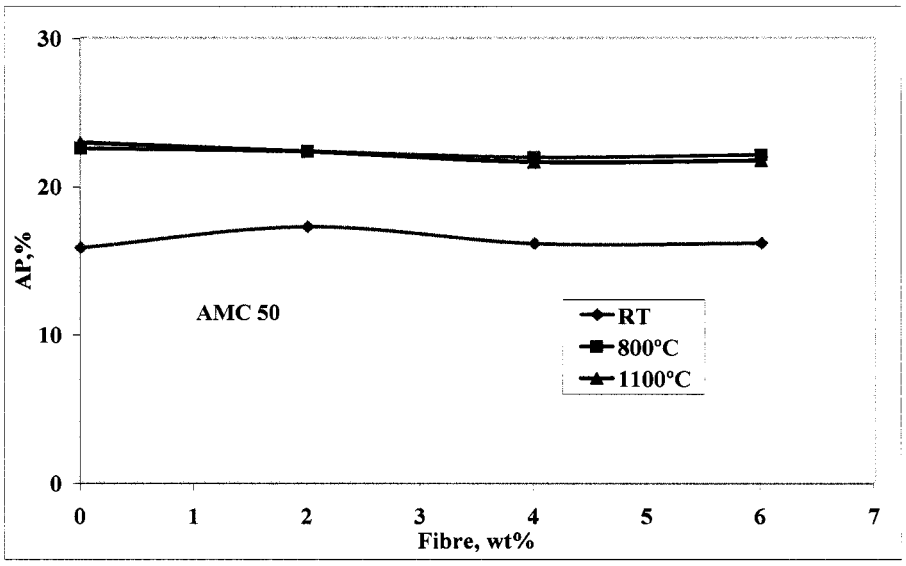

Figure D9. Variation of apparent porosity w.r.t fibre loading for 50 mm length carbon steel fibre reinforced AMC castables at different temperatures.

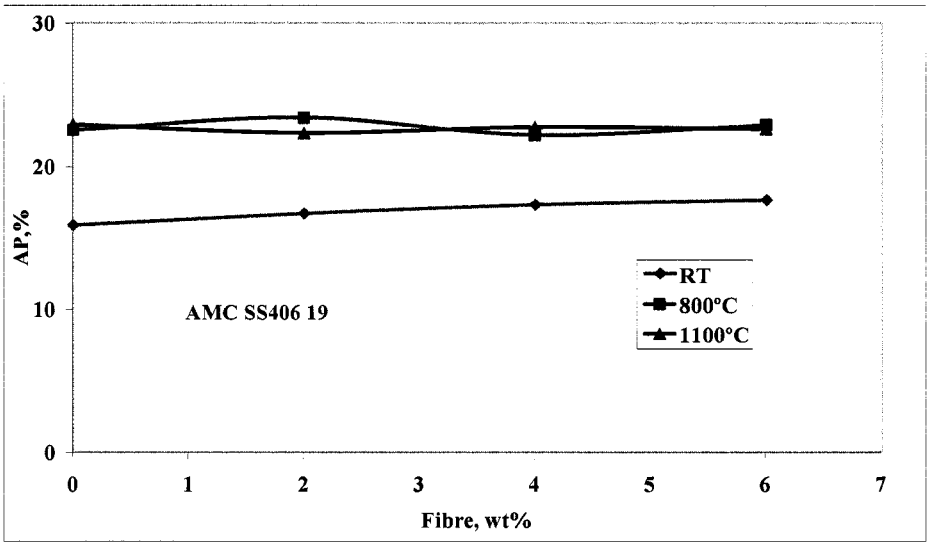

Figure D10. Variation of apparent porosity w.r.t fibre loading for 19 mm length of stainless steel fibre reinforced AMC at different temperatures.

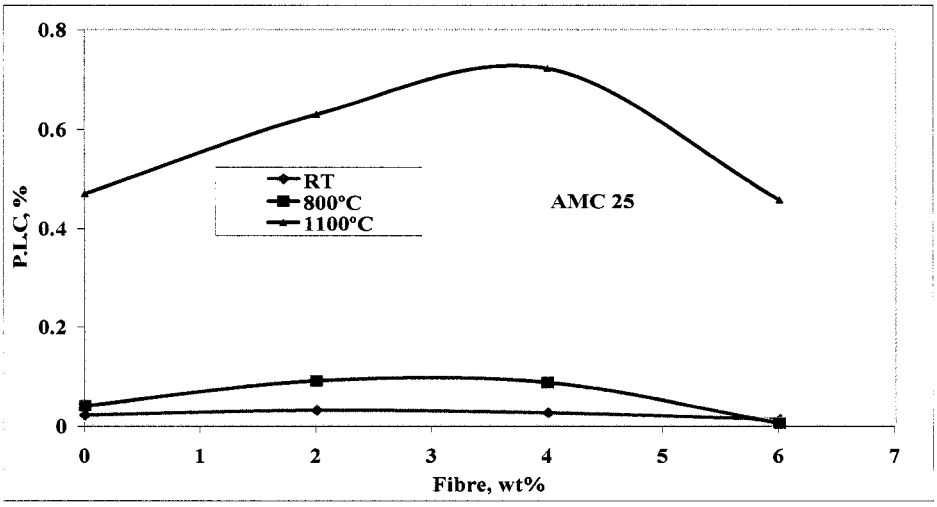

Figure D11. Variation of permeanat linear change w.r.t. fibre loadings (0,2, 4, 6 wt %) for 25 mm carbon steel fibre reinforced AMC castables at different temperatures.

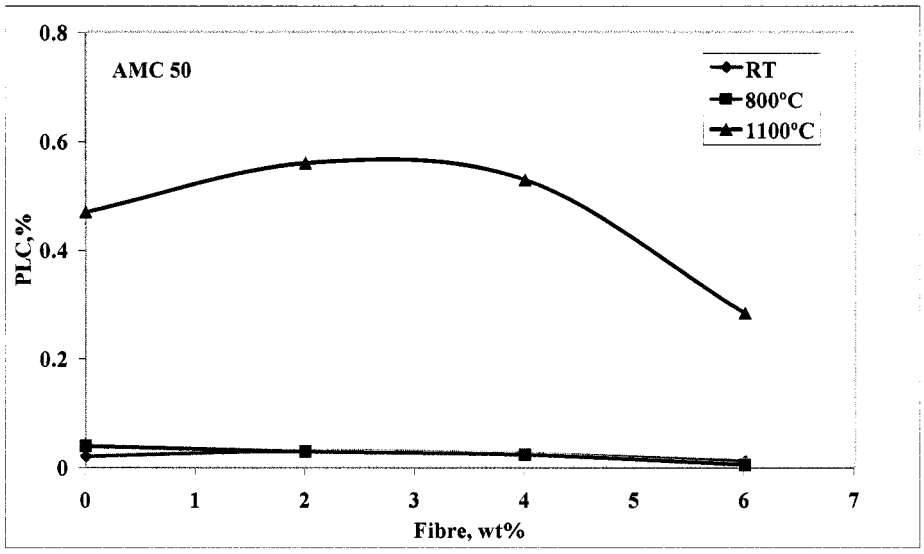

Figure D12. Variation of permeanat linear change w.r.t.fibre loadings (0, 2, 4, 6 wt %) for 50 mm carbon steel fibre reinforced AMC castables at different temperatures.

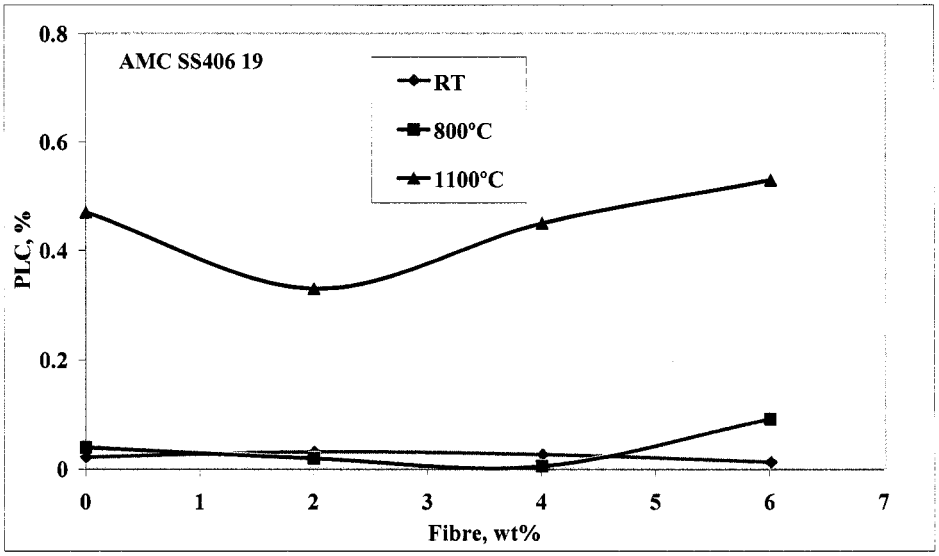

Figure D13. Variation of permanent linear change w.r.t. fibre loadings (0, 2, 4, 6 wt %) for 19 mm length of stainless steel fibre reinforced AMC castables at different temperatures.